The Silent Majority

Jets and Radio Cores from Weakly Active Black Holes

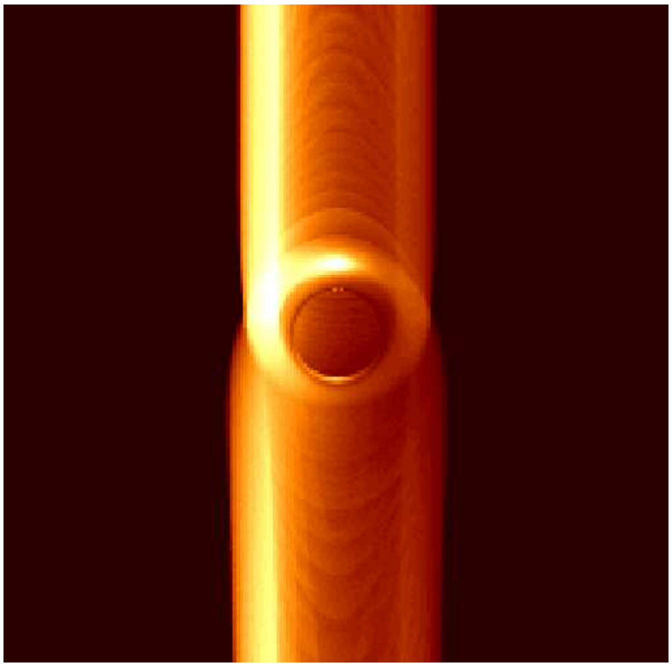

Heino Falcke

The Silent Majority

Jets and Radio Cores from Weakly Active Black Holes

Die schweigende Mehrheit

Jets und Radiokerne von schwach-aktiven schwarzen Löchern

Habilitationsschrift
zur
Erlangung
der
Venia Legendi
der
Hohen Mathematisch-Naturwissenschaftlichen Fakultät
der
Rheinischen Friedrich-Wilhelms-Universität Bonn

vorgelegt von

Dr. rer. nat. Heino Falcke

aus Köln

Bonn, im März 2000

This whole way of thinking and acting rests on the assumption that reality is reliable, not that disasters, and failures, and evil things will never happen, but that the world in which they happen ultimately makes sense. It is not just 'buzzing, booming confusion' but springs from the will of a creator whose purposes are trustworthy and whose ultimate aim is glorious however dark and mysterious the way to it.

(John Habgod in "Can Scientists Believe?", Ed. Sir Nevill Mott, 1991)

Abstract

They are weak, they are small, and they are often overlooked, but they are numerous and an ubiquitous sign of accreting black holes: compact radio cores and jets in radio-weak AGN. Here I summarize our work concerning these radio cores and jets in recent years, specifically focusing on the large population of low-luminosity and radio-quiet AGN. Special attention is given to Sgr A*, the supermassive black hole candidate at the Galactic Center, whose radio properties are reviewed in detail. This source exhibits a submm-bump, possibly from an ultra-compact region around the black hole, has unusually high circular but very low linear polarization and is variable at cm-waves where it shows phases of quasi-periodic oscillation. Particularly the compact submm emission is of great interest since it should allow imaging of the event horizon of the black hole in the not too distant future. A jet model is proposed which explains the basic feature of Sgr A*: its slightly inverted radio spectrum, the submm-bump, the lack of extended emission, and the X-ray emission. This model is also applied to famous sources like M81, NGC4258, and GRS1915+105 based on the argument that radio cores are jets whose emission can be scaled with the accretion power over many orders of magnitude. This scaling is corroborated by the detection of many Sgr A*-like radio cores in nearby Low-Luminosity AGN (LLAGN), many of which show jet structures on the VLBI (Very Long Baseline Interferometry) scale. These cores confirm an AGN origin of at least half of the known low-luminosity AGN classified as LINERs and dwarf-Seyferts. It is argued that in fact most of the compact radio emission in LLAGN is produced by a compact radio jet and not an Advection Dominated Accretion Flow (ADAF). Finally, we extend our view to compact radio cores and jets in radio-'quiet' AGN such as Seyferts and radio-quiet quasars. Hubble Space Telescope (HST) and Very Large Array (VLA) images show that jets can have a significant impact on their environment even in these sources. It is also suggested that basically all AGN contain relativistic jets. This idea is strengthened by the first detection of superluminal expansion in a spiral galaxy with a Seyfert nucleus. In general one can say that compact radio cores are a genuine feature of AGN, allowing one to precisely pinpoint black holes in many galaxies.

Foreword

This review was written to fulfill the requirements for the "Habilitation"-procedure at the University of Bonn. It summarizes a big part of the research I have conducted over the recent years, focusing on compact radio cores and jets. While I try to review what has been done in the field where possible, this work is strongly biased towards my own contributions. It therefore will not represent the final wisdom but can just be a progress report that can help to stimulate new research and perhaps sometimes different answers. Naturally, in a rapidly evolving and highly competitive field like astronomy and astrophysics many of the results presented here have already been published in refereed journals and conference proceedings, but some results are still unpublished and new. By collating this material in one, hopefully homogeneous, publication this review can perhaps provide a more comprehensive overview over the questions and answers related to the given topic than a set of individual publications could. The list of original publications used as the basis for this work is given in the bibliography at the end. It is certainly necessary, at this point, to thank all my collaborators who contributed to many of the results presented here and are listed as co-authors on the individual publications. In every case it was a pleasure to work together with them. I think we are truly blessed to have such an open and international scientific community today which is connected through personal contacts and electronic communications. Most of my research would not have been possible without it, or at least would have taken much longer to complete.

Heino Falcke, March 2000

Contents

Chapter 1

Introduction

1.1 The Vocal Minority

One of the main subjects for radio astronomers has been the study of extragalactic radio jets. When observed at a higher resolution, many of the first radio sources discovered in the early years of radio astronomy later turned out to be powerful, collimated plasma flows of relativistic plasma (called jets) which were ejected from the nucleus of giant elliptical galaxies. These structures can reach sizes of several million light years and hence extend well beyond their host galaxies into the vastness of intergalactic space. This relative isolation is ideal for studying the physics of astrophysical plasma flows in great detail (see e.g., Bridle & Perley 1984; Bridle et al. 1994; Klein et al. 1994; Marti et al. 1997) and allows us to make some estimates of the properties of the IGM (inter-galactic medium, e.g., Subrahmanyan & Saripalli 1993).

An even more important aspect of radio jets, however, is that they are the largest and most visible sign – literally the "smoking gun" – of Active Galactic Nuclei (AGN). The standard model of an AGN consists of a supermassive black hole at the center of a galaxy that accretes matter via an accretion disk (von Weizsäcker 1948; Lüst 1952; Shakura & Sunyaev 1973; Lynden-Bell & Pringle 1974). The inflow of matter in the potential well leads to an enormous energy production that is released through infrared (IR), optical, ultra-violet (UV), and X-ray emission. In a fraction of sources one also sees very strong γ-ray and TeV emission. Some of the energy is also funneled into a relativistic radio jet along the rotation axis of the disk (Fig. 1.1). It was, in fact, the strong radio emission from these jets which first led to the discovery of quasars (3C273, Hazard, Mackey, & Shimmins 1963; Schmidt 1963).

Jets have therefore been studied with great interest over many years and in this time a huge zoo of different jet species has emerged. The main characteristics of radio jets are the size (compact, i.e. parsec to kiloparsec scale, or extended, i.e. tens to hundreds of kiloparsecs), and the spectral index (flat or steep) of the radio sources. Steep radio spectra ($\alpha < -0.5$, $S_\nu \propto \nu^\alpha$) are due to optically thin

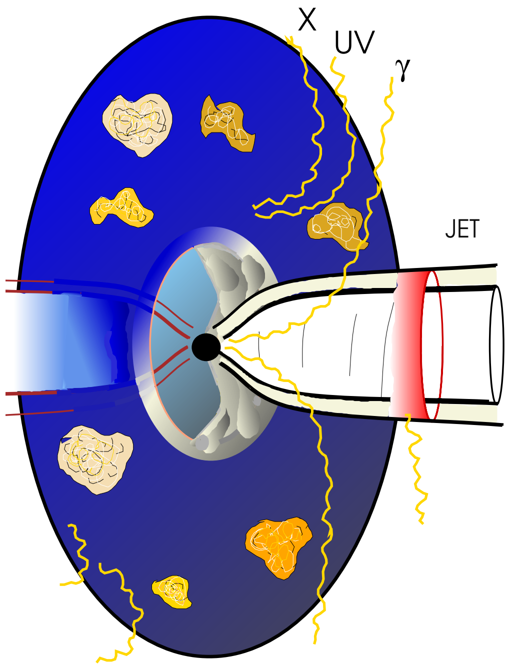

Figure 1.1: Schematic view of an AGN. An accretion disk rotates around a central black hole and ejects a relativistic magneto-hydrodynamic jet along its rotation axis. Jet and disk produce emission across the entire electromagnetic spectrum from radio to TeV photons. Surrounding ISM (interstellar medium) clouds are ionized by strong UV flux from the disk and produce the visible emission-lines in the optical spectra (Figure courtesy of Silke Britzen, MPG Jahrbuch 1995).

synchrotron emission from large, extended radio sources, while flat radio spectra can be produced if the source is very compact and the spectrum is dominated by radiation from a number of optically thick synchrotron components.

A typical powerful radio galaxy – a so called Fanaroff & Riley (1974) type II radio galaxy (short FR II) – consists of two steep-spectrum, extended lobes connected by very faint (if visible at all), well-collimated plasma beams, and a compact flat-spectrum core (which will be discussed in more detail later). FR II jets are produced by the most powerful AGN, have the largest kinetic powers of any jets observed (i.e. Rawlings & Saunders 1991), and attain the absolute largest sizes observed (see Fig. 1.2). Probably due to their huge powers FR II jets can plow with relativistic speeds through the ambient medium, self-shielded by a huge cocoon (Begelman & Cioffi 1989), until they slow down and terminate in a massive shock – the hot spots. It is speculated that these termination shocks are the site of intense acceleration of electrons and protons (e.g., Biermann & Strittmatter 1987), possibly responsible for some of the ultra-high energy cosmic rays observed at earth (Rachen & Biermann 1993). Behind the shock the jet material disperses and at least a part of it flows back toward the galaxy it was ejected from. This can be

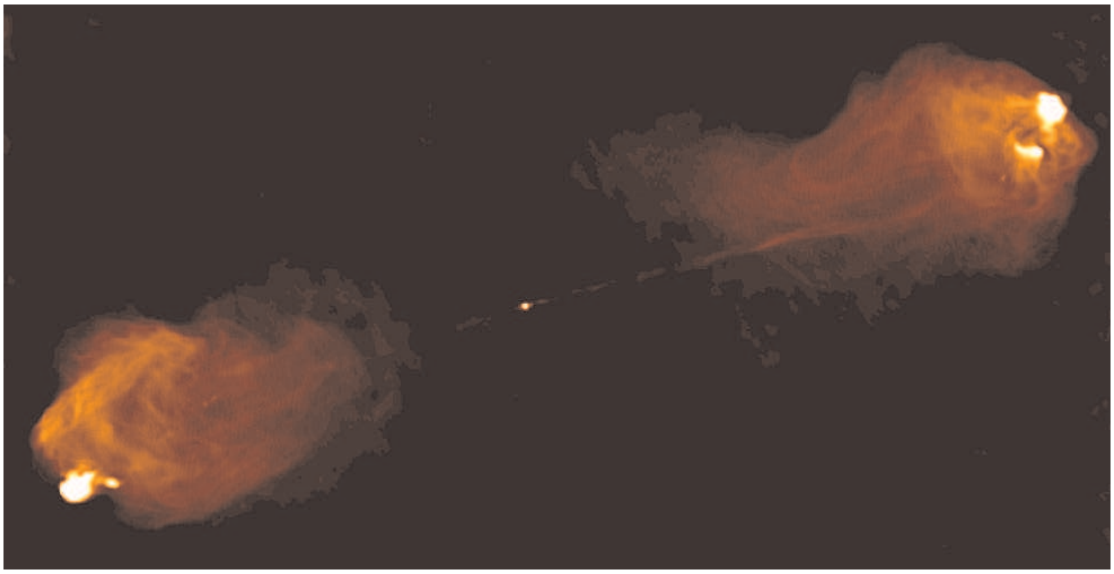

Figure 1.2: VLA image of the bright FR II radio galaxy Cygnus A (from R. Perley et al. 1984, VLA/NRAO). One can see the bright lobes connected by well-collimated jets emerging from a compact radio core at the center. The jets expand over more than 600,000 lightyears.

seen on many of the beautiful high dynamic-range VLA maps made in recent years (e.g., Black et al. 1992; Leahy et al. 1997).

Such beautiful structures, however, are not the rule but rather the exception: at lower powers the jet morphology seems to change and FR II radio galaxies suddenly turn into FR Is, where instead of a well-collimated pencil-like beam with a well-defined terminus, the jet has a larger opening angle, entrains material from the interstellar medium (ISM) (de Young 1993; Bicknell 1994), becomes bright, and then slowly fades along the way (Fig. 1.3). Clearly, in those cases the jet is no longer independent of its environment but interacts with the ISM of the host galaxy. Initially one was only able to see the effects of this interaction on the radio jet itself, but now we can also see the other side of this coin in X-ray observations, which indicate how the radio plasma pushes against gas in the galaxy (e.g., Böhringer et al. 1993; Holloway et al. 1996; Clark et al. 1997).

Not always, however, are we so fortunate to see all details of the extended jets. If, for example, those jets happen to be seen under a very small aspect angle with respect to the line of sight, relativistic effects will become very important. Since the jet has velocities close to the speed of light in the nucleus, the emission from the flat-spectrum radio core will be boosted by the relativistic Doppler effect and for small inclination angles will become so bright that it dominates the entire radio emission, overwhelming even the bright extended lobes (even though they still can be found in high-dynamic range observations, e.g., Kollgaard et al. 1992). These galaxies appear as compact, core-dominated flat-spectrum radio galaxies or quasars, sometimes called Blazars. If observed at very high resolution Blazars often

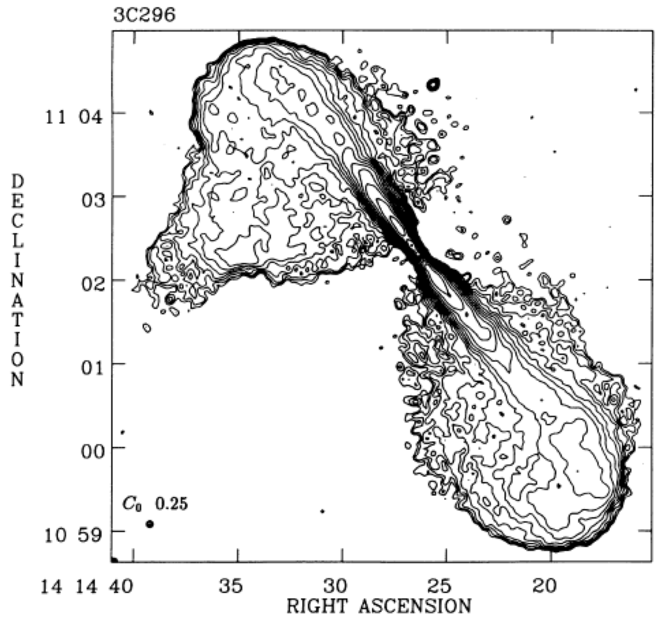

Figure 1.3: VLA map at 1.4 GHz obtained with the VLA of the FR I radio galaxy 3C296 (from Leahy & Perley 1991). In contrast to FR II radio galaxies the jet is de-collimated very close to the nucleus and is not able to produce hotspots at its terminus.

show superluminal motion (an optical illusion caused by the relativistic motion of bright features in the jet) which is accompanied by strong flux variability down to scales of less than a day (Wagner & Witzel 1995; Zensus 1997). In addition one finds luminous high-energy emission, such as X-ray and γ-emission ($\gtrsim 10$ TeV, Aharonian et al. 1999; Zweerink et al. 1997), most certainly produced by scattering processes (e-γ, p-γ, or p-p) from relativistic particles within the jet (Mannheim & Biermann 1992; Dermer & Schlickeiser 1993). In fact, for some sources most of the observed luminosity is seen in γ-rays (e.g., von Montigny et al. 1995).

The radio cores of Blazars are not only interesting because of their astrophysics, but they are also used as beacons for a global coordinate reference frame. Because of their compact bright radio emission and cosmological distances, implying no significant proper motion, their positions can be measured with radio-interferometers to milli-arcsecond precisions. This not only allows extremely precise astrometry on the sky, but it also can be used to determine fundamental parameters of the earth orientation and even measure continental drifts on earth (see Robertson 1991).

However, not all compact radio galaxies are Blazars. Some galaxies show steep radio spectra (at least at high frequencies), yet, instead of penetrating deep into the inter-galactic medium (IGM) as FR Is and FR IIs do, they are stuck inside their host galaxies. The currently favored idea is that these galaxies are very young and still need to plow their way out through the ISM (see Owsianik & Conway 1998). These sources are called CSS (compact steep-spectrum) or GPS (Gigahertz-peaked spectrum) sources (see O'Dea 1998 for a recent review). Looking with

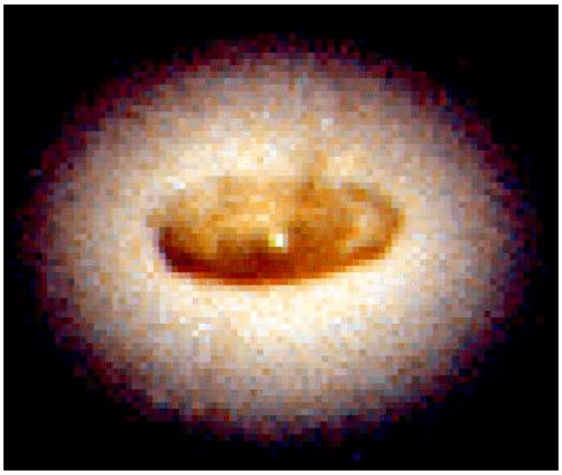

Figure 1.4: HST image of the galaxy NGC 4261 showing a dark disk surrounding a bright nucleus (Ferrarese et al. 1996). A black hole is suspected at the center producing a low-luminosity AGN, a weak sibling of a quasar, surrounded by a dusty disk.

higher resolution one can resolve the jets and find extended lobes on scales of several kpc (for CSS) down to hundreds of parsecs (GPS, needs Very Long Baseline Interferometry) – at least some of them must be the predecessors of the large FR I and FR II radio galaxies.

The main reason why all these radio galaxies and radio-loud quasars have been studied in such detail so far is their large radio fluxes of 100 mJy up to several tens of Jansky, which makes them easily accessible with current technology. On the other hand, it was noted early on that the majority of quasars and AGN in the universe are *not* radio-loud (Strittmatter et al. 1980; Kellermann et al. 1989) and have in fact a rather low radio flux, despite having very similar optical properties compared to radio-loud quasars. Moreover, classical radio galaxies and radio-loud quasars are among the most luminous AGN we know, corresponding to black holes with the largest masses and the largest accretion rates. Hence, when we discuss the properties of relativistic jets in AGN, we usually tend to think exclusively about a relatively small but vocal group of sources. Is this the whole universe, or just the tip of the iceberg? Most likely there are many more, weaker black holes and jets in the universe.

1.2 The Silent Majority

The evidence for supermassive black holes in the nuclei of most galaxies has become much stronger recently. Some of the best cases are the Milky Way (Eckart & Genzel 1997), NGC 4258 (Miyoshi et al. 1995), and a number of other nearby galaxies (Faber et al. 1997; Richstone et al. 1998; Magorrian et al. 1998) where convincing dynamical evidence for black holes exists. Hence, the basic powerhouse for an AGN – the black hole – is built into almost every galaxy, but compared to quasars and radio galaxies there is a huge range in power output between the

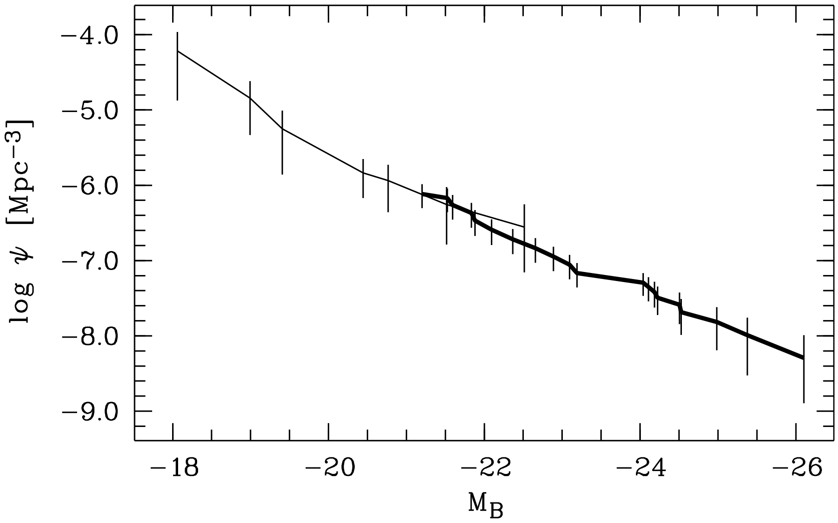

Figure 1.5: Local luminosity function (number density as a function of absolute magnitude) of $z < 0.3$ quasars and Seyferts. The number of AGN decreases with a power-law index of $\alpha \simeq -2.2$ as the luminosity increases (from Köhler et al. 1997).

most luminous quasars and barely active galaxies like the Milky Way.

For example in a spectroscopic survey of 486 nearby bright galaxies, Ho, Filippenko, & Sargent (1997) found that a large fraction of these galaxies have optical emission-line spectra. Roughly one third of the galaxies surveyed showed spectra usually attributed to active galactic nuclei. The energy output of these systems, is $10^{-6} - 10^{-3}$ times lower than in typical quasars (Ho 1999). Consequently, these galaxies are called low-luminosity AGN (LLAGN, see Fig. 1.4). The large fraction of LLAGN already indicates that the number of AGN increases with decreasing luminosity. This is, in fact, exactly what has been found already in studies of the luminosity function of quasars and Seyfert galaxies, namely a power-law distribution of AGN as a function of luminosity with an index $\alpha \simeq -2.2$ (e.g., Köhler et al. 1997, see Fig. 1.5). As in real life, the majority of the entire population is rather quiet. To get a complete view of the astrophysics of AGN and black holes one therefore needs to look at this silent majority as well.

The question of how the central engines in quasars and low-luminosity AGN are related to each other and why they appear so different despite being powered by the same type of object is therefore of major interest. For many nearby galaxies with low luminosity nuclear emission-lines, it is not even clear whether they are powered by an AGN or by star formation. This is especially true for Low Ionization Nuclear Emission Region (LINER) galaxies (Heckman 1980; Heckman et al. 1983), some of which can be explained in terms of aging starbursts (e.g., Filippenko & Terlevich 1992; Alonso-Herrero et al. 2000).

One of the best ways to probe the very inner parts of these engines is to study the compact radio sources found in many AGN. Indeed, despite their low optical luminosity, quite a few nearby galaxies have such radio sources in their nuclei, prominent cases being the Milky Way (Sgr A*), and the galaxies M 104 and M 81 (Bietenholz et al. 1996). These radio sources resemble the cores of radio-loud quasars, showing a very high brightness temperature and a flat to inverted radio spectrum that extends up to sub-millimeter (submm) wavelengths.

1.3 Radio Cores, Jets, and Accretion

What are these compact radio cores and how are they related to the AGN? Early on in the discussion about the existence of black holes, Lynden-Bell & Rees (1971) suggested that they would be accompanied by compact radio nuclei, detectable by Very Long Baseline Interferometry (VLBI), and predicted such a source for the Galactic Center. Indeed, this source (Sgr A*) was then discovered by Balick & Brown (1974) and it became clear in later years that compact radio cores are indeed good evidence for the existence of an AGN or a black holes in a galaxy. For luminous radio galaxies and radio-loud quasars the basic nature of these compact radio nuclei has been clarified in the meantime through extensive and detailed VLBI observations (see Zensus 1997 for a review) as being the inner regions of relativistic jets emanating from the nucleus.

Despite this progress, a number of important questions remain when looking back at the initial discussion. First of all, it is unclear whether there indeed is a direct link between compact radio cores and AGN, i.e. whether compact radio cores and jets are just an accidental by-product of black hole activity or a necessary consequence. Secondly, for the lesser studied, low-luminosity AGN the jet nature of compact radio nuclei has not yet been established beyond any doubt, leaving the question open whether in fact a compact radio core in a low-luminosity AGN is the same as in a high-luminosity AGN, i.e. a quasar.

The latter was exactly the claim made by (Falcke & Biermann 1995), stimulated by the seminal paper from Rawlings & Saunders (1991), where it was proposed that accretion disks and jets form symbiotic systems. A scaling law was was proposed which connects high-power and lower-power accretion disks and their associated radio jets (cores). The scaling law was based on the assumption of an equipartition between the energy released and radiated away through dissipation processes in the accretion disk and the power put into the formation of magnetically driven radio jets.

The question whether this scaling law holds all the way down to LLAGN, as later claimed in Falcke & Biermann (1996), also has some very interesting implications for the current discussion of accretion flows. Since the early papers on the observational appearance of black holes (e.g., Shakura & Sunyaev 1973), it was assumed that luminous, thermal emission at optical, UV, or X-ray wavelengths was the primary sign for the presence of an accreting black hole. It was argued that any matter falling onto the black hole would likely form an accretion disk, if there was any residual angular momentum, and hence would need to dissipate its potential energy into heat by viscous processes allowing it to transport angular momentum outwards while matter is falling inwards (α-disk). This idea was used successfully to explain the "big blue bump" in quasars (e.g., Sun & Malkan 1989).

However, the view that the α-disk can be extended to much lower powers has been challenged (Narayan & Yi 1994; Narayan & Yi 1995a; Narayan & Yi 1995b) and it was argued that accretion disks will turn into Advection Dominated Accretion Flows (ADAFs) if the accretion rate onto the black hole is sufficiently sub-Eddington (see Meyer-Hofmeister & Meyer 2000). Narayan, Yi, & Mahadevan (1995) and Narayan, Yi, & Mahadevan (1996) applied this idea to the Galactic Center (see also Rees 1982 and Melia 1994), trying to explain the compact radio source Sgr A* and its faintness at other wavelengths. Lasota et al. (1996) used the ADAF model to explain the broad-band spectrum of the nearby LLAGN and LINER galaxy NGC 4258 which is famous for its megamaser emission from a molecular disk (Miyoshi et al. 1995, see Fig. 2.5).

An integral part of these ADAF models is the prediction of very compact radio emission associated with the innermost part of the accretion flow, providing an alternative explanation to the jet model for compact radio nuclei in LLAGN. While initially the predicted, highly inverted radio spectra of the ADAF model, did not fit the observed characteristics of these radio cores very well, Mahadevan (1998) presented a more recent version of this model that was at least[1] able to account for the correct radio spectrum of Sgr A*. Still, di Matteo et al. (1999) found a number of serious constraints for ADAF models – at least for compact radio nuclei in elliptical galaxies, casting some doubt on the applicability of the ADAF model to compact radio cores in general. Hence, the question now is whether indeed the radio emission from compact nuclei in sub-Eddington accretion systems can be used as an argument for the existence and necessity of ADAFs, or whether they are equally well, or even better explained, in a scaled down AGN jet model.

The purpose of this work is therefore to describe a comprehensive study of the radio emission from AGN operating at powers less than those of typical quasars and to clarify their nature. Specifically we will test the applicability of the standard AGN jet model to low-power black holes.

By going to lower powers we want to understand how universal the central engine really is. Are radio cores in LLAGN different from those in quasars? How important is the formation of jets at lower power and in radio-weak objects? Are there classes of sources where no jet is found? What happens with the jets in quasars if the power of the engine becomes less and less? Will the jets die completely, implying that accretion near the Eddington limit is required for the jet formation, or will the jet just become proportionally weaker, implying that jet formation is an integral part of accretion physics and independent of the exact nature of the accretion disk itself?

[1] It was never shown that also the size predicted by this model is within the observationally allowed constraints.

1.4 Outline

In the next chapter, we will describe the jet-disk symbiosis model of Falcke & Biermann (1995) and Falcke (1996a). Then we will apply these solutions to some specific sources which are of particular interest and check the basic predictions of the model.

In the subsequent chapters we will explore the applicability of the model to a wider range of sources. In Chapter 3 we will review in great detail the observational constraints on one of the most famous and best studied radio cores – Sgr A*, the supermassive black hole candidate at the Galactic Center. We present a detailed model of its emission characteristics within the frame work of the radio core model described in Chapter 2. This source is of particular interest because general-relativistic ray tracing calculations, presented at the end of this chapter, suggest that in the near future the radio core could lead to the first detection and imaging of the event horizon of a black hole.

In Chapter 4 we will extend our view again and present a search for Sgr A*-like radio cores in low-luminosity AGN. This will show that Sgr A*'s are a rather common phenomenon in the universe. Finally, Chapter 5 discusses the evidence we have that the radio cores in radio-quiet AGN, such as radio-quiet quasars and Seyferts which make up the majority of luminous AGN, can be explained in a very similar fashion. We will present the first conclusive evidence for the existence of relativistic jets in Seyfert galaxies. Hubble Space Telescope (HST) observations will show that, even after jets have been slowed-down significantly, in Seyferts they can significantly effect their environment – despite being radio-quiet. In general, we will see that in fact the majority of accreting black holes at the various levels of accretion rates, despite being relatively silent in the radio regime, can have quite active jets.

Given this finding, and with the ever-increasing sensitivity in radio astronomy, one can foresee that these radio cores will become more and more important as tracers of supermassive black holes in galaxies near and far.

Chapter 2

The Jet-Disk Symbiosis Model

2.1 The Universal Engine – a *Simple* Ansatz

If the central engine of an AGN is indeed associated with a black hole, it has the unpleasant property of being so small that it is almost inaccessible by observational means and hence open to wild theoretical speculations. Currently there is no way to prove or disprove that all central engines are completely different or absolutely identical and one is forced to choose a basic Ansatz for the nature of the engine. This allows one to draw further conclusions and test them against observational data.

Strangely, in Astronomy the burden of proof is usually on those who postulate a simpler solution (like the unified schemes) while Occam's Razor should force one to start with the simplest theory until experimentally disproven. Consequently, our Ansatz for the nature of the central engines in AGN should be that they are all very similar and governed by a few parameters only, until forced to introduce more parameters or a completely new theory. Such a simple engine is a black hole accreting matter within an accretion disk and producing a jet at the black hole/disk boundary layer, flowing out along the rotation axis. As the escape speed from a black hole is relativistic, those jets would have to be relativistic as well. Since the jets are produced by the disk, one expects a strong coupling between jet and disk. Since most of the power in an accretion disk is released close to the center, the jet can be very powerful, and finally, because "a black hole has no hair", there are not many parameters that can vary from one engine to another. The main parameter of the engine is therefore expected to be the accretion rate[1]. This "simple Ansatz" also implies that jets are a natural companion to accretion disks, and both are necessary and symbiotic features in the accretion process onto the compact central object (Falcke & Biermann 1995).

While this postulate sounds simple and almost trivial at first sight it faces severe opposition if applied to individual sources, i.e. there is a trend to "personalize"

[1]The spin of the black hole could be a secondary parameter, e.g., explaining the radio-loudness

models for each and every new source and source class[2]. In the following we will therefore try to go in the opposite direction and describe a heterogeneous set of sources with just one model, based on the principles discussed above.

2.2 Radio Cores

Jets in AGN are coherent structures with spatial scales from a few AU up to several megaparsecs. Therefore we should be able to investigate basic parameters of a jet at different scales and get similar answers. For example, we can use the large, extended lobes of radio jets in FR II radio galaxies to estimate their total power, e.g., by calculating their minimum energy content from synchrotron theory or from their interaction with hot, X-ray emitting gas and dividing by the life time of the sources (e.g., derived from spectral aging). The derived powers (which are often *lower* limits) are very high – up to 10^{45-47} erg/sec (Rawlings & Saunders 1991) and thus larger than the total power output of a typical galaxy. The only reasonable place where such enormous amounts of energy can be released is deep in the potential well of a supermassive black hole.

Even though at these larger distances the jet pressure has decreased enough so that pressure balance between jet and external medium is reached, it is believed that the implied adiabatic losses are largely avoided by a constant re-collimation (Sanders 1983) of the jets: the side-ways lateral expansion leads to a re-collimation shock which in turn will focus the kinetic energy of the jet back into the forward direction. Otherwise one would have to account for expansion factors of $\gtrsim 10^6$ between launch and termination of powerful jets. For a relativistic plasma where adiabatic losses scale as $r^{-2/3}$ this would translate into an energy loss of four orders of magnitude and require the jets to start with enormous initial powers of 10^{49-51} erg/sec, corresponding to accretion rates of $10^{2-4} M_\odot$/yr and Eddington luminosities for black holes with a mass of $10^{10-12} M_\odot$. From all what we know today, this seems to be too high and one must conclude, that most of the way, the jet does not suffer adiabatic losses.

The argument based on hotspots still has the problem that it depends on parameters characterizing the external medium the jet is interacting with. If we go to low-power jets we will find that most of them (e.g., in FR I radio galaxies, Seyferts) do not even have hotspots that would provide one with a well-defined, isolated dissipation region to determine basic jet parameters easily. Fortunately, every jet should also have an "inflationary phase" close to the nucleus, after leaving the nozzle where the energy density in powerful jets can be $1 - 100$ erg/cm^3 and above, compared to 10^{-12} erg/cm^3 in the local ISM. This is the region, where flat spectrum radio cores are produced and which we will use in the following to make more quantitative statements. The advantage of radio cores is that they are

[2]This sometimes leads to the strange effect that a model is not quoted and applied because it has the 'wrong' source name in the title, thus forcing theorists to publish the same model over and over again for different source names.

largely independent of external conditions and therefore should be visible in basically all types of sources that produce relativistic jets. Their independence comes for a price, since less interaction often means less shocks, less energy dissipation, and less radio emission. Hence, compact radio cores are much more difficult to observe than extended lobes and jets, but modern radio astronomy is now sensitive enough to do just this.

2.3 Jet-Disk Coupling

In order to quantify the radio emission we expect from a radio jet close to the nucleus we will make a few simple assumptions and resort to the simple Ansatz made above, assuming that every jet is coupled to an accretion disk. A coupled jet-disk system has to obey the same conservation laws as all other physical systems, i.e. at least energy and mass conservation (other conservation laws we do not use yet). We can express those constraints by specifying that the total jet power $Q_{\rm jet}$ of the two oppositely directed beams is a fraction $2q_{\rm j} < 1$ of the accretion power $Q_{\rm disk} = \dot{M}_{\rm disk}c^2$, the jet mass loss is a fraction $2q_{\rm m} < 1$ of the disk accretion rate $\dot{M}_{\rm disk}$, and the disk luminosity is a fraction $q_{\rm l} < 1$ of $Q_{\rm disk}$ ($q_{\rm l} = 0.05 - 0.3$ depending on the spin of the black hole). The dimensionless jet power $q_{\rm j}$ and mass loss rate $q_{\rm m}$ are coupled by the relativistic Bernoulli equation (Falcke & Biermann 1995, see Eq. 2.11) for a jet/disk-system. For a large range in parameter space the total jet energy is dominated by the kinetic energy such that one has $\gamma_{\rm j}q_{\rm m} \simeq q_{\rm j}$, in case the jet reaches its maximum sound speed, $c/\sqrt{3}$, the internal energy becomes of equal importance and one has $2\gamma_{\rm j}q_{\rm m} \simeq q_{\rm j}$ ('maximal jet'). The internal energy is assumed to be dominated by the magnetic field, turbulence, and relativistic particles. We will constrain the discussion here to the most efficient type of jet where we have equipartition between the relativistic particles and the magnetic field and also have equipartition between the internal and kinetic energy (i.e. bulk motion) – one can show (see Falcke & Biermann 1995) that other, less efficient models would fail to explain the highly efficient radio-loud quasars.
Knowing the jet energetics, we can describe the longitudinal structure of the jet by assuming a constant jet velocity (beyond a certain point) and free expansion according to the maximal sound speed ($c_{\rm s} \lesssim c/\sqrt{3}$). For such a jet, the equations become very simple. The magnetic field is given by

$$B_{\rm j} = 0.3\,G\;Z_{\rm pc}^{-1}\sqrt{q_{\rm j/l}L_{46}} \tag{2.1}$$

and the particle number density is

$$n = 11\,{\rm cm}^{-3}L_{46}q_{\rm j/l}Z_{\rm pc}^{-2} \tag{2.2}$$

(in the jet rest frame). Here $Z_{\rm pc}$ is the distance from the origin in parsec (pc), L_{46} is the disk luminosity in 10^{46} erg/sec, $2q_{\rm j/l} = 2q_{\rm j}/q_{\rm l} = Q_{\rm jet}/L_{\rm disk}$ is the ratio between jet power (two cones) and disk luminosity which is of the order 0.1–1

(FMB95) and $\gamma_{\rm j,5} = \gamma_{\rm j}/5$ ($\beta_{\rm j} \simeq 1$). If one calculates the synchrotron spectrum of such a jet, one obtains locally a self-absorbed spectrum that peaks at

$$\nu_{\rm ssa} = 20\,{\rm GHz}\,\mathcal{D}\frac{\left(q_{\rm j/l}L_{46}\right)^{2/3}}{Z_{\rm pc}}\left(\frac{\gamma_{\rm e,100}}{\gamma_{\rm j,5}\sin i}\right)^{1/3}. \tag{2.3}$$

Integration over the whole jet yields a flat spectrum with a monochromatic luminosity of

$$L_\nu = 1.3\cdot 10^{33}\,\frac{\rm erg}{\rm s\,Hz}\,\left(q_{\rm j/l}L_{46}\right)^{17/12}\mathcal{D}^{13/6}\sin i^{1/6}\gamma_{\rm e,100}^{5/6}\gamma_{\rm j,5}^{11/6}, \tag{2.4}$$

where $\gamma_{\rm e,100}$ is the minimum *electron* Lorentz factor divided by 100, and $\mathcal{D}$ is the *bulk* jet Doppler factor. At a redshift of 0.5 this luminosity corresponds to an un-boosted flux of $\sim$ 100 mJy. The brightness temperature of the jet is

$$T_{\rm b} = 1.2\cdot 10^{11}\,{\rm K}\,\mathcal{D}^{4/5}\left(\frac{{\gamma_{\rm e,100}}^2 q_{\rm j/l}L_{46}}{\gamma_{\rm j,5}^2\beta_{\rm j}}\right)^{1/12}\sin i^{5/6} \tag{2.5}$$

which is almost independent of all parameters except the Doppler factor. An important factor that governs the synchrotron emissivity is, of course, the relativistic electron distribution, for which we have assumed a power-law distribution with index $p = 2$ and a ratio 100 between maximum and minimum electron Lorentz factor. As we are discussing here the most efficient jet model we also assume that all electrons are accelerated (i.e. $x_{\rm e} = 1$ in Falcke & Biermann 1995), hence the only remaining parameter is the minimum Lorentz factor of the electron distribution $\gamma_{\rm e,100}$ determining the total electron energy content. In order to reach the magnetic field equipartition value, which is close to the kinetic jet power governed by the protons, we have to require $\gamma_{e,100} \sim 1$. It cannot be higher because otherwise the power in electrons would exceed the total jet power, and it cannot be much lower because we would not reach equipartition. Such a high, low-energy cut-off in the electron energy distribution was suggested already by Wardle (1977) and Celotti & Fabian (1993) for other reasons and could for example be produced in hadronic processes (e.g., Biermann, Strom, & Falcke 1995)[3].

If radio-interferometric techniques were not yet developed today, and we would have been asked to predict what kind of jet sources we would expect to see, we would have needed only very few considerations:

a) *'total equipartition' everywhere*, i.e. equipartition between the luminosity radiated by the disk and expelled by a jet, equipartition between internal energy and kinetic energy, and equipartition between relativistic particles and magnetic field

[3]Only recently, Wardle et al. (1998) argued for lower electron Lorentz factors based on circular polarization observations, but their result depends quite strongly on the exact shape of the electron distribution and whether or not a second population of low-energy electrons is present in these astrophysical plasmas. Therefore a conclusive answer to how the low-energy electron distribution looks like cannot be given and we have to live with some assumptions.

b) *relativistic speed*, because, if the jet is produced close to the black hole, relativistic escape speeds are required,

c) *disk luminosity* (UV-bump), which is a measurable quantity.

Thus, using $L_{\rm disk} \sim 10^{46}$ erg/sec (typical optical/UV-luminosity) and $\gamma_{\rm j} \sim 5$ (a few times the escape speed from a black hole), we could have predicted pc-scale radio cores at cm-wavelengths, with brightness temperatures of 10^{11} K and fluxes of 100 mJy and more. But of course, nobody would have believed us, as those assumptions are obviously too simplified ...

2.4 UV/Radio Correlation

Now, we will have to validate some of our assumptions and test the jet-disk coupling derived above. To stay on safe grounds we will in this section concentrate on the well-studied quasars. For these sources we have to estimate the disk luminosity as precisely as possible and compare it to their radio cores. The best studied quasar sample so far is the PG quasar sample (Schmidt & Green 1983). For most sources in this sample Sun & Malkan (1989), using optical and IUE data, fitted the UV bump with accretion-disk models and a few more were available in the archive (Falcke, Malkan, & Biermann 1995). There are also excellent photometric (Neugebauer et al. 1987) and spectroscopic data (Boroson & Green 1992) available. Unlike the broadband UV-bump fits, which give $L_{\rm disk}$ directly, emission-lines and continuum colors do not give a direct estimate for the bolometric UV luminosity and $L_{\rm disk}$. We will need to calibrate those values to obtain an equivalent UV bump luminosity using the sources which have a complete set of data available. This yields

$$\lg(L_{\rm disk}/{\rm erg\ s^{-1}}) = 2.85 + \lg(L_{\rm [OIII]}/{\rm erg\ s^{-1}}), \tag{2.6}$$

$$\lg(L_{\rm disk}/{\rm erg\ s^{-1}}) = 2.1 + \lg(L_{\rm H\beta}/{\rm erg\ s^{-1}}), \tag{2.7}$$

$$\lg(L_{\rm disk}/{\rm erg\ s^{-1}}) = -0.4 M_{\rm b} + 35.90. \tag{2.8}$$

Here $L_{\rm [OIII]}$ and $L_{\rm H\beta}$ are the luminosities in the [OIII]λ5007 and Hβ (broad) emission-lines, $M_{\rm b}$ is the absolute blue continuum magnitude as used by Boroson & Green (1992). The scatter in this relation, ~ 0.5 in the log, is shown in Falcke, Malkan, & Biermann (1995).

With these correlations one should be able to estimate the "disk luminosity" for almost any quasar. If several indicators are available, we can combine them (assigning appropriate weights) to get the final estimate. This provides us with a fairly reliable estimate of $L_{\rm disk}$ and reduces the scatter in the radio-optical correlations considerably. It also reduces the effects of the orientation dependence of some lines (e.g., [OIII]). In the next step, we can compare those disk luminosities with VLA radio cores (Kellermann et al. 1989; Miller, Rawlings, & Saunders 1993) and the total radio emission of quasars. In addition to the optically selected sample in Falcke, Malkan, & Biermann (1995) we have now also included quasars from the southern 2 Jansky sample (Morganti, Killeen, & Tadhunter 1993; Tadhunter et al. 1993) which are predominantly flat-spectrum quasars, and steep-spectrum, lobe dominated quasars from Bridle et al. (1994), Akujor et al. (1994), and Reid et al. (1995) which had emission-lines readily available (Steiner 1981; Jackson & Browne 1991; Wills et al. 1993). Thus, the number of radio-loud quasars is increased considerably – the results are shown in Figure 2.1 & 2.2.

In Figure 2.1 we can see that the total radio emission of radio-loud quasars with typical undisturbed FR II-type radio structure correlates very well with their UV emission, while the radio-emission of CSS and GPS sources does not. This emphasizes that the interaction of the compact jets in CSS and GPS sources with the ISM of the host galaxy significantly affects, i.e. increases, the radio emissivity. Moreover, flat-spectrum radio-loud quasars also spoil the correlation since their total radio flux is still dominated by the relativistically boosted core, pointing towards the observer and outshining emission from the extended jet. This makes a simple derivation of jet powers based on the radio flux at one frequency alone subject to large uncertainties, unless one concentrates on isotropically radiating jets in 'isolation'. Interestingly, radio-quiet quasars show a relatively good correlation between radio and UV luminosity (see also Baum & Heckman 1989). This is a first indication already that also in this radio-quiet AGN the radio emission is directly linked to the central engine.

Figure 2.2, demonstrates that the *cores* of these quasars show the distribution expected within the jet-disk model, assuming one has relativistic jets in radio-loud *and* radio-quiet quasars operating at two basic levels of efficiency (see Falcke & Biermann 1995 for a discussion of what these basic levels could be). In contrast to the total emission, this is true for the cores of CSS and GPS sources as well, meaning that at the scales where the cores are produced jet-ISM interactions are not so important. The spread in the radio luminosity distribution is dominated by relativistic boosting and random inclination angles. As expected, flat spectrum radio-loud quasars, with the exception of a few radio-intermediate quasars discussed in Chap. 5, are found at the highest radio luminosities expected for jets with small inclination angles. This spread can be translated into characteristic bulk Lorentz factors for the jets, yielding a range between $\gamma_{\rm j} = 3 - 10$.

Being aware that the discussion of basic cosmological parameters continues to evolve (e.g., Perlmutter et al. 1999; Priester, Hoell, & van de Bruck 1996) we have in these figures still used the parameters from the original publication for a then standard cosmology with $H_0 = 50$ km sec^{-1} Mpc^{-1}, $q_0 = 0.5$, and $\Lambda = 0$. Different cosmologies would show different behaviors in such a plot at high-redshifts and luminosities. Once more radio data and optical data for high-z quasars is available and the basic parameters of these radio cores are better understood, constraining cosmological parameters with radio cores might therefore not be impossible (see also Gurvits, Kellermann, & Frey 1999 and Taylor & Vermeulen 1997). On the

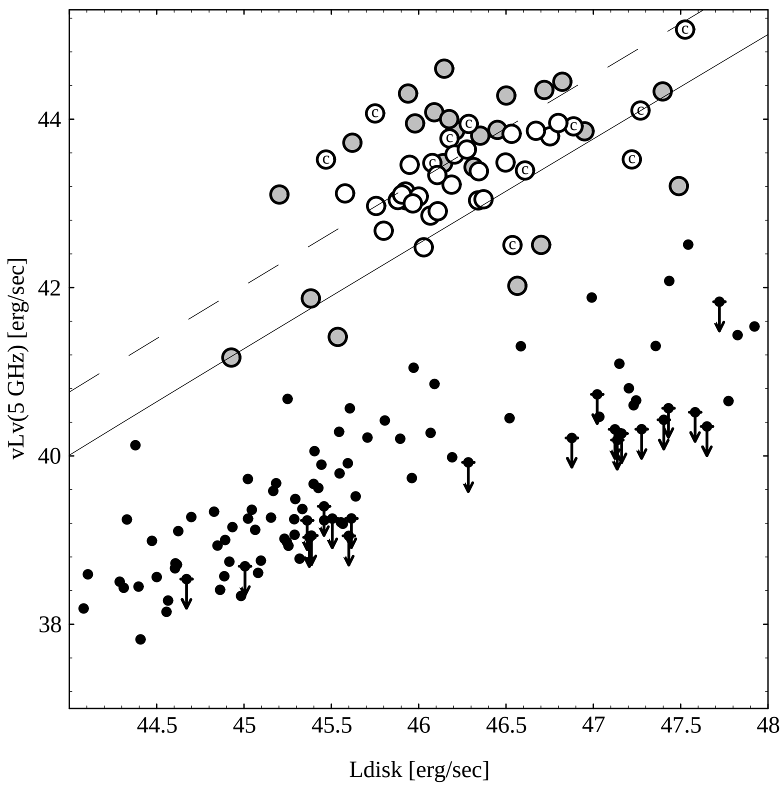

Figure 2.1: Total radio luminosity vs. disk (UV-bump) luminosity for quasars (including a complete optical and a radio-selected sample). The shaded circles are core-dominated, flat-spectrum sources, open circles are steep-spectrum (FR II type) sources, circles labeled 'c' are Compact Steep-Spectrum (CSS) sources and filled points are radio-quiet (diffuse or unresolved) sources. Only undisturbed radio-loud FR II type and radio-quiet sources show a tight correlation. Flat-spectrum sources are boosted to the upper end of the distribution except six radio-intermediate quasars which might be boosted radio-quiet quasars (see Chap. 5). The total emission of CSS source does not show a tight correlation with disk luminosity. The solid line is the (oversimplified) model for the lobes from Falcke & Biermann (1995, see also Falcke, Malkan, & Biermann 1995).

other hand it is not yet completely clear how well such a method can compete with current supernova studies.

One can extend this kind of plot also to lower luminosities – even down to X-ray binaries. Already Hjellming & Johnston (1988) had suggested that the radio emission of some of these sources could be explained as jet emission. Of course, for these stellar-mass systems the peak in the spectral energy distribution is shifted from the UV to the X-rays, as predicted by accretion disk theory. Hence, $L_{\rm disk}$ is no longer given by the UV luminosity but by the X-ray luminosity. This extension to lower mass and lower mass accretion rates was done in Falcke & Biermann (1996). The respective figure is shown here as Fig. 2.3. It shows that basically all astrophysical radio cores roughly fall along the lines predicted by the simple jet-disk symbiosis model.

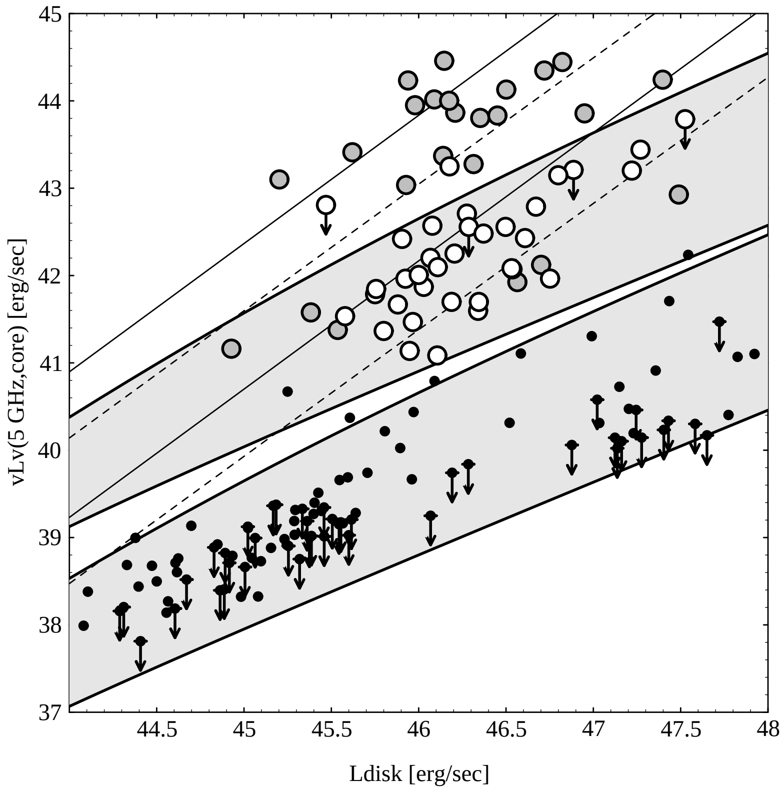

Figure 2.2: The same as Fig. 2.1 (CSS are not explicitly marked), but now the radio core flux is plotted. The shaded bands represent the radio-loud and radio-quiet jet models where the width is determined by relativistic boosting. The jet velocity evolves with luminosity as $\gamma_{\rm j}\beta_{\rm j} \propto L^{0.1}$, as discussed in Falcke, Malkan, Biermann (1995). The dashed lines represent the expected level of emission for sources just within the boosting cone (i.e. inclination $i = 1/\gamma$) and the isolated solid lines represent emission for $i = 0°$ inclination – corresponding to the maximally boosted flux. The position of flat-spectrum and steep-spectrum sources and the radio-loud/radio-quiet separation can be naturally accounted for with the coupled jet-disk model.

There are some notable exception though. Some FR I radio galaxies, for example, seem to be somewhat above the line in cases where relativistic boosting is not a dominant factor. This could mean that these galaxies are underluminous in thermal emission or over-luminous in non-thermal radio emission (see Falcke, Gopal-Krishna, & Biermann 1995 for further discussion). In any case, even those galaxies probably do not deviate by many orders of magnitude from the general trend. The spread induced by AGN being either radio-loud or radio-quiet and by relativistic boosting is much larger.
This kind of plot certainly has its limitations if it comes to individual sources, however, it helps to obtain a broad[4] perspective and to place sources and source classes in a proper context and relation.

[4]The term “global perspective” I would have liked to use in this context seems unfitting given the “universal” scale of the problem discussed here.

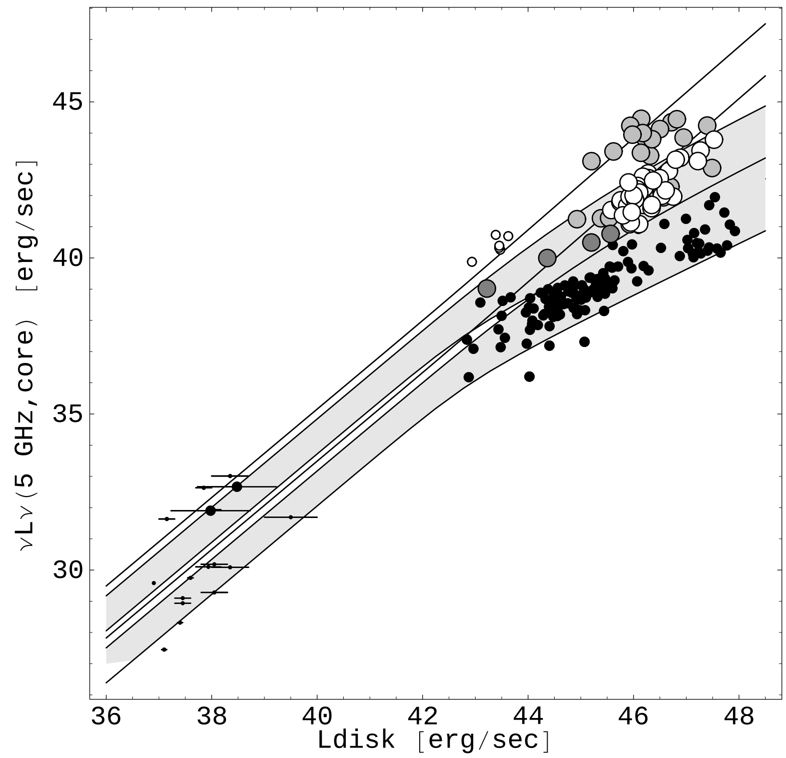

Figure 2.3: The same as Fig. 2.2. The shaded bands, representing the radio-loud and radio-quiet jet models are extrapolated to much lower jet powers while keeping the bulk Lorentz factors fixed at $\gamma_{\rm j} = 2$. To simplify the display, upper limits of the radio-quiet quasars are no longer displayed as such. Small open circles represent radio cores of FR I galaxies from Rawlings & Saunders (1991). At the lower end of the radio-quiet quasar distribution radio cores of Seyfert galaxies from the CfA sample (Kukula et al. 1995) are added. Finally, at the lowest accretion rates we display radio cores of X-ray binaries as discussed in Falcke & Biermann (1996). Radio cores obviously decrease in luminosity as the accretion disk luminosity decreases, roughly along the lines predicted by the jet-disk symbiosis model. The gap at intermediate accretion luminosities implicitly predicts the presence of radio cores in low-luminosity AGN. It is worth noting that the predicted relation is not linear (see Eq. 2.4) and hence is not a simple consequence of a luminosity-luminosity plot.

For example, the plot published in Falcke & Biermann (1996) was a direct prediction of where radio cores at even lower-luminosities, i.e. in LLAGN, are expected if the basic theme of the jet-disk symbiosis holds. These cores are now being discussed in the subsequent sections.

2.5 Radio Cores in LLAGN: Free Jet with Pressure Gradient

Radio cores in quasars are quite well-studied and therefore one can tolerate a number of free parameters in the jet model which are constrained by additional observations. One of these parameter is the jet speed which is generally believed to be in the range $\gamma_{\rm jet} \sim 5-10$ based on the observation of superluminal motion (e.g., Zensus 1997). In LLAGN the situation is different and we have no direct evidence whether they are highly-, moderately-, or sub-relativistic. It is therefore useful to find a self-consistent description of the velocity field in these radio cores mainly based on first-principles. One possibly important inconsistency of the basic jet model outlined above, which is based on (Blandford & Königl 1979), is that it ignores the effects of any pressure gradients along the jet. In the following we show that a self-consistent treatment of the Blandford & Königl (1979) model implies a weak acceleration of the bulk jet flow due to its longitudinal pressure gradient. This cannot only naturally explain why the radio spectra of some LLAGN radio cores are slightly inverted (e.g., Sgr A* & M81; see Duschl & Lesch 1994; Reuter & Lesch 1996; Falcke et al. 1998) rather than just flat, it also provides one with a natural velocity field for the jet, taking away $\gamma_{\rm jet}$ as a free parameter.

2.5.1 Longitudinal Velocity Profile

As in Falcke & Biermann (1995), we shall describe the jet core within the framework of relativistic gas dynamics of a relativistic gas with adiabatic index $\Gamma = 4/3$. We consider only the supersonic regime and impose as boundary condition, that the jet expands freely with its initial sound speed $\beta_{\rm s}$ without any lateral gradients behind the jet nozzle. This leads to the familiar conical jet with $B^2/4\pi \propto z^{-2}$ (Blandford & Königl 1979), where adiabatic losses due to lateral expansion need not be considered. For a confined jet scenario at larger scales the adiabatic losses could, however, be quite severe with energy densities scaling as $z^{-2\Gamma}$ during phases of adiabatic expansion unless reconfinement is important (Sanders 1983).

Nonetheless, even in a simple, free jet at least some work due to expansion will be done, because there is always a longitudinal pressure gradient, which will accelerate the jet along its axis. This acceleration is described by the z-component of the modified, relativistic Euler equation (e.g., Pomraning 1973, Eq. 9.171) in cylindrical coordinates where we set $\partial/\partial r = 0$ and $\partial/\partial\theta = 0$

$$\gamma_{\rm j}\beta_{\rm j}\frac{\partial}{\partial z}\left(\gamma_{\rm j}\beta_{\rm j}\frac{\omega}{n}\right) = -\frac{\partial}{\partial z}P. \tag{2.9}$$

Here, $\omega = m_{\rm p}nc^2+U_{\rm j}+P_{\rm j}$ is the enthalpy density of the jet, $U_{\rm j}$ is the internal energy density, n is the particle density, and $P_{\rm j} = (\Gamma-1)U_{\rm j}$ is the pressure in the jet (all in the local rest frame). For 'maximal jets' – the radiatively most efficient type of jet (Falcke & Biermann 1995) – to be discussed here, we demand the equivalence of internal energy and kinetic (or better rest mass) energy $U_{\rm j} \simeq m_{\rm p} n c^2$, hence $\omega = (1+\Gamma)U_{\rm j}$ and $\omega/n = (1+\Gamma)m_{\rm p}c^2 = {\rm const}$ at the sonic point $z = z_0$. In a free jet with conical shape the energy density evolves as $U_{\rm j} \propto (\gamma_{\rm j}\beta_{\rm j})^{-\Gamma} z^{-2}$ and we do not consider any loss mechanisms other than adiabatic losses due to the longitudinal expansion. Using the relations mentioned above, the Euler equation becomes

$$\frac{\partial \gamma_{\rm j}\beta_{\rm j}}{\partial z}\left(\frac{\left(\frac{\Gamma+\xi}{\Gamma-1}\right)(\gamma_{\rm j}\beta_{\rm j})^2 - \Gamma}{\gamma_{\rm j}\beta_{\rm j}}\right) = \frac{2}{z} \tag{2.10}$$

with $\xi = \left(\gamma_{\rm j}\beta_{\rm j}/(\Gamma(\Gamma-1)/(\Gamma+1))\right)^{1-\Gamma}$. For $\xi \sim 1$ this is analogous to the well known Euler equation for an isothermal, pressure driven wind, with the wind speed replaced by the proper jet speed. The sound speed is fixed by the required equivalence between internal and rest mass energy density at a value $\beta_{\rm s} = \sqrt{(\Gamma-1)/(\Gamma+1)} \sim 0.4$.

The asymptotic solution of Eq. 2.10 for $\xi = $const and $z \rightarrow \infty$ is $\gamma_{\rm j}\beta_{\rm j} \propto 2\sqrt{\ln z}$. If we ignore terms of the order $\ln \gamma_{\rm j}\beta_{\rm j}$ we could approximate the solution by $\gamma_{\rm j}\beta_{\rm j} \simeq \sqrt{\frac{\Gamma-1}{\Gamma+1}\left(\Gamma + 4\ln(z/z_0)\right)}$. For the following calculations we will, however, use the exact, numerical solution to Eq. 2.10 ($\xi \neq$const), but the deviation from the approximate, asymptotic solution is rather small.

2.5.2 Plasma Properties

The basic ideas how to derive the synchrotron emissivity and the basic properties of a jet in a coupled jet-disk system have been described extensively in (Falcke & Biermann 1995). The power $Q_{\rm j} = q_{\rm j}\dot{M}_{\rm disk}c^2 = q_{\rm j/l}L_{\rm disk}$ of *one* jet cone is a fixed fraction of the disk luminosity, relativistic particles and magnetic field B are in equipartition within a factor $k_{\rm e+p}$ – which we hereafter set to one, and the energy fluxes are conserved along the conical jet (for a moment we will ignore the adiabatic losses). Mass conservation requires that the mass loss in the jet $\dot{M}_{\rm jet}$ is smaller than the mass accretion rate in the disk $\dot{M}_{\rm disk}$, thus $q_{\rm m} = \dot{M}_{\rm jet}/\dot{M}_{\rm disk} < 1$, while mass and energy of the jet are coupled by the relativistic Bernoulli equation for a jet/disk-system (Falcke, Mannheim, & Biermann 1993).

$$\gamma_{\rm j} q_{\rm m}\left(1 + \beta_{\rm s}^2/(\Gamma-1)\right) = q_{\rm j}. \tag{2.11}$$

Here we will make use of the same logic and notation but with three changes with respect to Falcke & Biermann (1995), namely (1) applying the velocity law Eq. 2.10, (2) neglecting the energy contents in turbulence, and (3) considering only a quasi mono-energetic energy distribution for the electrons at a Lorentz factor $\gamma_{\rm e}$ (usually $\gtrsim 100$). The latter is indicated by the steep submm-to-IR cut-off found in Sgr A* (Zylka et al. 1995; Serabyn et al. 1997; Falcke et al. 1998) – and probably also M81* (Reuter & Lesch 1996) – which is different from typical Blazar spectra and precludes an initial electron power-law distribution (see Fig. 3.11).

The semi-opening angle of the jet is $\phi = \arcsin(\gamma_\mathrm{s}\beta_\mathrm{s}/\gamma_\mathrm{j}\beta_\mathrm{j})$, and the magnetic field in the co-moving frame of a maximal jet with the given sound speed, $L_\mathrm{disk} = L_{41.5}10^{41.5}$ erg/sec, $q_\mathrm{j/l} = 0.5q_{0.5}$, and $z_{16} = z/10^{16}$cm becomes (see Eq. 19 in Falcke & Biermann 1995)

$$B = 0.6\,\mathrm{G}\,\sqrt{\beta_\mathrm{j} L_{41.5} q_{0.5}}\, z_{16}^{-1}. \tag{2.12}$$

The number of relativistic electrons that are to be in equipartition with the magnetic field are a fraction $x_\mathrm{e} = n_\mathrm{e}/n$ of the total particle number density, and the energy density ratio between relativistic protons and electrons is $(\mu_\mathrm{p/e} - 1)$. From the energy equation $\gamma_\mathrm{j}\omega\gamma_\mathrm{j}\beta_\mathrm{j} c\pi r^2 = q_\mathrm{j/l} L_\mathrm{disk}$ we find that the characteristic Lorentz factor and electron density required to achieve equipartition are

$$\begin{aligned} \gamma_\mathrm{e} &= m/\left(4\Gamma m_\mathrm{e}\mu_\mathrm{p/e}x_\mathrm{e}\right) = 344/\left(\mu_\mathrm{p/e}x_\mathrm{e}\right) && (2.13)\\ n_\mathrm{e} &= 45\,\mathrm{cm}^{-3}\,\beta_\mathrm{j} L_{41.5} q_{0.5} x_\mathrm{e} z_{16}^{-2}. && (2.14) \end{aligned}$$

Finally, to incorporate adiabatic losses we now have to make the following transitions with respect to the equations in Falcke & Biermann (1995)

$$\begin{aligned} &\gamma_\mathrm{j}\beta_\mathrm{j} \to \gamma_\mathrm{j}\beta_\mathrm{j}(z), \quad \gamma_\mathrm{e} \to \gamma_\mathrm{e}\cdot\left(\gamma_\mathrm{j}\beta_\mathrm{j}(z)/\gamma_\mathrm{j}\beta_\mathrm{j}(z_0)\right)^{1/3}\\ &B \to B\cdot\left(\gamma_\mathrm{j}\beta_\mathrm{j}(z)/\gamma_\mathrm{j}\beta_\mathrm{j}(z_0)\right)^{1/6}. \end{aligned} \tag{2.15}$$

2.5.3 Synchrotron Emission

The local spectrum of the jet will be $F_\nu \propto \nu^{1/3}$ between the synchrotron self-absorption frequency $\nu_\mathrm{ssa}(z)$ and the characteristic frequency $\nu_\mathrm{c}(z) = 3e\gamma_\mathrm{e}^2 \sin\alpha_\mathrm{e} B(z)/4\pi m_\mathrm{e} c$ (here we will use an average pitch angle $\alpha_\mathrm{e} = 60°$). For the maximal jet using Equations 2.12, 2.13, 2.14 and 2.15, we have in the observers frame

$$\nu_\mathrm{c}(z) = 100\,\mathrm{GHz}\,\mathcal{D}\sqrt{L_{41.5}q_{0.5}}/\left(\sqrt{\beta_\mathrm{j}}\gamma_\mathrm{j} x_\mathrm{e}^2 \mu_\mathrm{p/e} z_{16}\right) \tag{2.16}$$

with the Doppler factor $\mathcal{D} = 1/\gamma_\mathrm{j}\left(1 - \beta_\mathrm{j}\cos i\right)$ for an inclination i of the jet axis to the line of sight.

To find the local synchrotron self-absorption frequency ν_ssa we have to solve the approximate equation $\tau = n_\mathrm{e}\sigma_\mathrm{sync}(\nu)\cdot 2r_\mathrm{j}/\sin i = 1$ and transform into the observers frame. The jet radius is $r_\mathrm{j} \sim \phi z$ and the synchrotron self-absorption cross section for a mono-energetic electron distribution is given by $\sigma_\mathrm{sync} = 4.9\cdot10^{-13}\,\mathrm{cm}^2\,(B/\mathrm{G})^{2/3}\gamma_\mathrm{e}^{-5/3}(\nu/\mathrm{GHz})^{-5/3}$, yielding

$$\nu_\mathrm{ssa} = 3.3\,\mathrm{GHz}\,\mathcal{D}\frac{\beta_\mathrm{j}^{1/5} L_{41.5}^{4/5} q_{0.5}^{4/5} x_\mathrm{e}^{8/5}\mu_\mathrm{p/e}}{\gamma_\mathrm{j}^{3/5}(\mathcal{D}\sin i)^{3/5} z_{16}}. \tag{2.17}$$

If we now use the velocity profile Eq. 2.10 we can invert Eq. 2.16 to find the size of the jet as a function of observed frequency. For the asymptotic regime $z \gg z_0$, ν_c is approximated for a fixed inclination angle to within a few per-cent by a power law in z, such that

$$z_{\rm c} = (z_{\rm c,0}/\sin i)(\mu_{\rm p/e}x_{\rm e})^{-2\xi}\left(q_{0.5}L_{41.5}\right)^{\xi/2} z_{13.7}^{1-\xi}\nu_{10.3}^{-\xi} \quad (2.18)$$

where the parameters are $z_{13.7} = z_0/3$ AU, $\nu_{10.3} = \nu/22$ GHz, $\xi = (0.99, 0.95, 0.9, 0.89, 0.88)$ and $z_{\rm c,0} = (500, 1200, 1100, 900, 700)$ AU for $i = (5°, 20°, 40°, 60°, 80°)$.
The total spectrum of the jet is obtained by integrating the synchrotron emissivity $\epsilon_{\rm sync}$ along the jet: $F_\nu = (4\pi D^2)^{-1}\int_{z(\nu_{\rm ssa})}^{z(\nu_{\rm c})} \epsilon_{\rm sync}\pi r^2 {\rm d}z$, which can again be approximated using power laws:

$$\begin{aligned} F_\nu &= 745\,{\rm mJy}(q_{0.5}L_{41.5})^{1.46}\mu_{\rm p/e}^{.17}x_{\rm e}^{1.17}z_{13.7}^{0.08}\nu_{10.3}^{0.08} \\ &\quad -337\,{\rm mJy}(q_{0.5}L_{41.5})^{1.54}\mu_{\rm p/e}^{.92}x_{\rm e}^{2.1}z_{13.7}^{0.08}\nu_{10.3}^{0.08}, & (2.19) \\ F_\nu &= 247\,{\rm mJy}(q_{0.5}L_{41.5})^{1.42}\mu_{\rm p/e}^{.33}x_{\rm e}^{1.33}z_{13.7}^{0.16}\nu_{10.3}^{0.16} \\ &\quad -143\,{\rm mJy}(q_{0.5}L_{41.5})^{1.48}\mu_{\rm p/e}^{.85}x_{\rm e}^{1.95}z_{13.7}^{0.15}\nu_{10.3}^{0.15}, & (2.20) \\ F_\nu &= 106\,{\rm mJy}(q_{0.5}L_{41.5})^{1.40}\mu_{\rm p/e}^{.40}x_{\rm e}^{1.40}z_{13.7}^{0.20}\nu_{10.3}^{0.20} \\ &\quad -71\,{\rm mJy}(q_{0.5}L_{41.5})^{1.45}\mu_{\rm p/e}^{.81}x_{\rm e}^{1.89}z_{13.7}^{0.19}\nu_{10.3}^{0.19}, & (2.21) \end{aligned}$$

for $D = 3.25$ Mpc (using as an example the distance of M81 which contains a 200 mJy radio core), and $i = (20°, 40°, 60°)$ respectively. This means that the resulting spectrum is no longer flat but tends to be inverted with $\alpha \sim 0.15 - 0.27$ for $i = 30° - 90°$. The spectral index, like the size index, is a function of the inclination angle of the jet and tends to become flatter for smaller i.

2.6 Weeding Out Parameters

Unfortunately, the equations given above are not easy to handle since the power-law indices are a function of the inclination angle. We therefore derive here an approximate formula for the spectra and sizes predicted by such a model.
We note here once more that Eq. 2.19 has two inherent constraints. First of all, by definition $\mu_{\rm p/e}$ cannot be smaller than unity since it is defined as the ratio between the energy densities in protons and electrons plus one. For the sake of simplicity only, we will now ignore the relativistic proton content and set $\mu_{\rm p/e} = 1$, so that we can substitute the relativistic electron fraction $x_{\rm e}$ with

$$x_{\rm e} = m_{\rm p}/\left(4\Gamma m_{\rm e}\gamma_{\rm e}\right) = 344/\gamma_{\rm e}. \quad (2.22)$$

Secondly, one cannot increase $\gamma_{\rm e}$ indefinitely since at some point the flux would become negative, i.e. the jet would become completely self-absorbed and the simplifications would break down[5]. Moreover, the equations are difficult to handle

[5]This is avoided when using numerical calculations as presented in Chap. 3.8

because of this sum, since for large changes in $Q_{\rm jet}$ the sum also would become negative. Hence, we formally introduce an arbitrary scaling relation

$$\gamma_{\rm e} = \gamma_{\rm e,0} \left(\frac{Q_{\rm jet}}{10^{39}{\rm erg/sec}}\right)^{0.09} \tag{2.23}$$

which allows us to simplify the equations further. The physical meaning is that electrons are pushed to somewhat higher energy with increasing $Q_{\rm jet}$ to keep them in the optically thin part. A mechanism which indeed could lead to such an effect is the 'synchrotron boiler' (Ghisellini, Guilbert, & Svensson 1988) that describes the evolution of low-energy electrons in a self-absorbed system, but it is not clear whether this formally introduced relation here has any significance in the real world and therefore we will ignore it in the discussion of our results.

To further simplify the equations we have rounded the exponents typically to the 2nd digit after the decimal and factorized the equations. Even for the most strongly varying parameters, like $L_{\rm disk}$ which can vary over 6 orders of magnitude, the resulting error will be only some ten percent. Moreover, the exponents in the equations, which are a function of the inclination angle i of the jet, were fitted by 2nd and 3rd order polynomials in i to an accuracy of much better than a few percent over a large range of angles.

All these simplifications lead to the following expressions for the observed flux density and angular size of a radio core observed at a frequency ν as a function of jet power. For a source at a distance D, with black hole mass $M_\bullet$, size of nozzle region $Z_{\rm nozz}$ (in $R_{\rm g} = GM_\bullet/c^2$), jet power $Q_{\rm jet}$, inclination angle i, and characteristic electron Lorentz factor $\gamma_{\rm e}$ (see Eq. 2.23) the observed flux density spectrum is given as

$$\begin{aligned} S_\nu &= 10^{2.06\cdot\xi_0}\ {\rm m}Jy\ \left(\frac{Q_{\rm jet}}{10^{39}{\rm erg/sec}}\right)^{1.27\cdot\xi_1} \\ &\cdot \left(\frac{D}{10{\rm kpc}}\right)^{-2} \left(\frac{\nu}{8.5{\rm GHz}}\right)^{0.20\cdot\xi_2} \left(\frac{M_\bullet}{33M_\odot}\frac{Z_{\rm nozz}}{10R_{\rm g}}\right)^{0.20\cdot\xi_2} \\ &\cdot \left(3.9\cdot\xi_3\left(\frac{\gamma_{\rm e,0}}{200}\right)^{-1.4\cdot\xi_4} - 2.9\cdot\xi_5\left(\frac{\gamma_{\rm e,0}}{200}\right)^{-1.89\cdot\xi_6}\right), \end{aligned} \tag{2.24}$$

with the correction factors ξ_{0-6} depending on the inclination angle i (in radians):

$$\xi_0 = 2.38 - 1.90\,i + 0.520\,i^2 \tag{2.25}$$
$$\xi_1 = 1.12 - 0.19\,i + 0.067\,i^2 \tag{2.26}$$
$$\xi_2 = -0.155 + 1.79\,i - 0.634\,i^2 \tag{2.27}$$
$$\xi_3 = 0.33 + 0.60\,i + 0.045\,i^2 \tag{2.28}$$
$$\xi_4 = 0.68 + 0.50\,i - 0.177\,i^2 \tag{2.29}$$
$$\xi_5 = 0.09 + 0.80\,i + 0.103\,i^2 \tag{2.30}$$
$$\xi_6 = 1.19 - 0.29\,i + 0.101\,i^2. \tag{2.31}$$

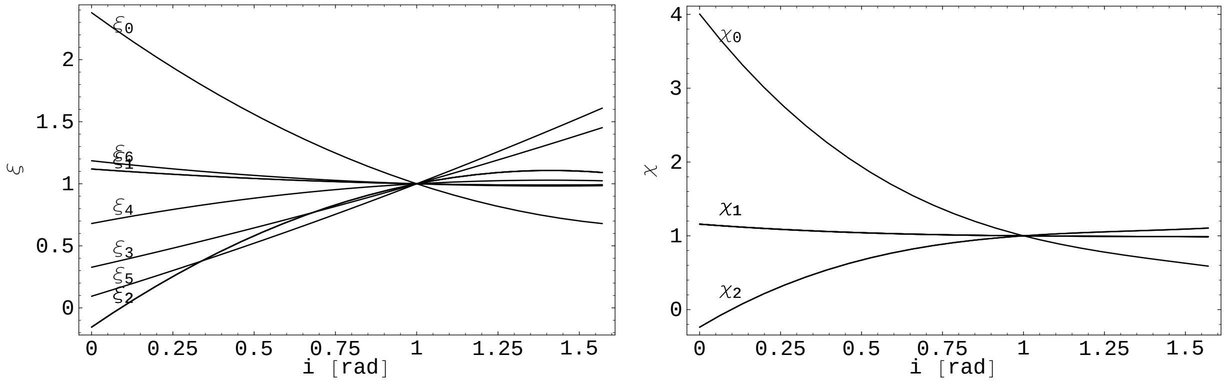

Figure 2.4: Correction factors ξ and χ for the exponents and factors in Eqs. 2.24 & 2.32 as a function of inclination angle i in radians, where $i = 0$ corresponds to face-on orientation. Note, however, that for $i \lesssim 10°$ most approximations fail.

Likewise, the characteristic angular size scale of the emission region is given by

$$\begin{aligned}
\Phi_{\rm jet} &= 1.36 \cdot \chi_0 \,\text{mas} \sin i \\
&\cdot \left(\frac{\gamma_{\rm e,0}}{200}\right)^{1.77\cdot\chi_1} \left(\frac{D}{10\text{kpc}}\right)^{-1} \left(\frac{\nu}{8.5\text{GHz}}\right)^{-0.89\cdot\chi_1} \\
&\cdot \left(\frac{Q_{\rm jet}}{10^{39}\text{erg/sec}}\right)^{0.60\cdot\chi_1} \left(\frac{M_\bullet}{33 M_\odot}\frac{Z_{\rm nozz}}{10 R_{\rm g}}\right)^{0.11\cdot\chi_2}, \qquad (2.32)
\end{aligned}$$

with the correction factors

$$\chi_0 = 4.01 - 5.65\, i + 3.40\, i^2 - 0.76\, i^3 \qquad (2.33)$$
$$\chi_1 = 1.16 - 0.34\, i + 0.24\, i^2 - 0.059\, i^3 \qquad (2.34)$$
$$\chi_2 = -0.238 + 2.63\, i - 1.85\, i^2 + 0.459\, i^3, \qquad (2.35)$$

where again the inclination angle i is in radians. We point out that in this model the characteristic size scale of the core region is actually equivalent to the offset of the radio core from the black hole. This does not exclude the existence of emission in components further down the jet, which might be caused by shocks or other processes.
The equations are now scaled to the typical values for Galactic jet sources like GRS1915+105 and the correction factors are normalized to an inclination angle of 1 rad ($\sim 57°$). We note that the approximations fail at small inclination angles where the accretion disk is seen face on and the jet points towards the observer (i.e. $i \lesssim 10°$). The benefits of these equations now are that they can be used to quickly compare observed radio core properties with the model predictions, especially since we have reduced the number of free parameters to the absolute minimum.

2.7 Application to Individual Sources

Application of these simplified equations to real radio cores is straight forward, the basic input parameters being the jet power, the characteristic electron energy, the inclination to the line of sight, the observed frequency, the distance, the black hole mass, and the relative size of the nozzle region. The latter two enter only weakly and hence need to be known only to an order of magnitude.
A few systems are so well studied that most of these parameters (especially i, D, & $M_\bullet$) can be fixed with some confidence and where size and flux of their cores at a certain frequency are well known through VLBI observations. Even though this may be a subjective criterion, one can argue that the radio cores in M81, NGC 4258, and GRS 1915+105 are, for various reasons, perhaps the best studied and best constrained examples of low-power radio cores. Following the convention in Falcke (1996a) and (Melia 1992b) and in analogy to Sgr A*, we will identify the radio cores in these sources by adding an asterisks to their host galaxy or source name to clearly distinguish them from their hosts.
We have listed the sources and their parameters in Table 2.1. The observed quantities we have used as input parameters for the model are given in Columns 2-7. Since in all cases, we have only two unknowns left (jet power and characteristic electron energy) to describe the two observed quantities of the radio cores (flux and size) we were able to solve the model equations for each source completely and determine $Q_{\rm jet}$ and $\gamma_{\rm e}$ directly from the observations. These results and the predicted spectral indices for the radio spectrum are given in the three right-most columns of Table 2.1. For comparison with the jet power, we also listed the accretion disk luminosity of each system in Column 8. In the following we will briefly discuss the data and the modeling of each source. A detailed discussion within this model of the famous radio core Sgr A* in the Galactic Center is given in Chapter 3.

2.7.1 NGC 4258

The VLBI observations of megamaser emission has led to the detection of a molecular disk in NGC 4258 (Miyoshi et al. 1995) which can be used to determine the inclination angle $i = 82^\circ$ of the system, the black hole mass $M_\bullet = 3.5 \cdot 10^7 M_\odot$, and the distance $D = 7.3 \pm 0.3$ Mpc (Herrnstein et al. 1997; Herrnstein et al. 1999) almost directly from the observations. The variable central VLA radio core (Turner & Ho 1994), here called NGC 4258*, has a flux of roughly 3 mJy and was interpreted by Lasota et al. (1996) as emission from an advection dominated accretion flow while Falcke (1997) suggested a scaled down AGN jet origin. The latter picture was confirmed by Herrnstein et al. (1997) and Herrnstein et al. (1998) who discovered a nuclear jet in NGC 4258 offset by 0.35 to 0.46 milli-arcsecond from the dynamical center (see Fig. 2.5). Herrnstein et al. (1997) suggested that this offset could be interpreted within the framework of the Blandford & Königl (1979) model as being due to self-absorption in the inner jet cone. The search for

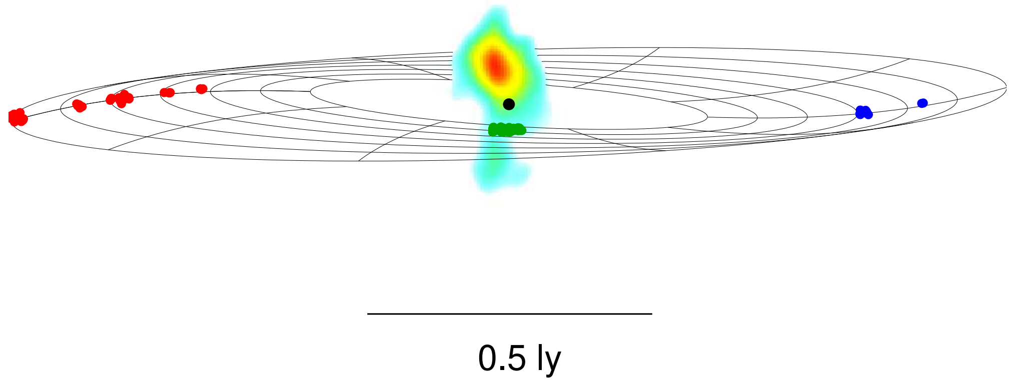

Figure 2.5: VLBI results for the LLAGN NGC4258 (from Herrnstein et al. 1998). The compact radio core is resolved by continuum VLBI into a jet-like structure, slightly offset from the center. The red and blue points mark the position of the red- and blue-shifted H_2O megamaser lines in the molecular disk. Their velocity and position are modeled by a warped disk shown as a mesh.

radio emission directly at the dynamical center remained unsuccessful (Herrnstein et al. 1998) and required a revision of the Lasota et al. (1996) ADAF model (Gammie, Narayan, & Blandford 1999).

For our purposes NGC 4258* is an ideal system because all crucial parameters, especially the inclination angle, seem to be fixed. Using an average radio flux of 3 mJy at 22 GHz and the offset of the core from the dynamical center as the characteristic size scale of the system we find a jet power of $10^{41.7}$ for the nuclear jet, a characteristic electron Lorentz factor of $\sim$ 630, and predict an average spectral index $\alpha = 0.22$ ($S_\nu \propto \nu^\alpha$). The jet-power of the nuclear jet is consistent with the large scale emission-line jet in NGC 4258, since its kinetic power is also of the order 10^{42} erg/sec – as derived from the mass ($2 \cdot 10^6 M_\odot$) and velocity ($\sim$ 2000 km/sec) of the emission-line gas (Cecil et al. 1995). Moreover, this is also in line with the estimated nuclear accretion disk luminosity of $\sim 10^{42}$ erg/sec (Stüwe, Schulz, & Hühnermann 1992; Wilkes et al. 1995; see also discussions in Herrnstein et al. 1997 and Gammie, Narayan, & Blandford 1999). Hence, all the activity in NGC 4258 can be described in a consistent way by a low-luminosity jet/disk-system and an accretion rate of the order $10^{-4} M_\odot$/yr. One caveat exists, however, because the interpretation of the offset of the core from the dynamical center as the characteristic scale of the model (and not the self-absorption size which is smaller) actually implies that also the core size is of similar order. If it were smaller, e.g., 0.1 milli-arcsecond, this would reduce the relatively high value for γ_e to around 200 without significantly reducing the required jet power. A difference between offset and actual core size would occur if the jet were collimated more in the inner region than assumed in our model (i.e. were narrower than the Mach cone).

2.7.2 GRS 1915+105

Mirabel & Rodriguez (1994) discovered a compact radio jet in the Galactic X-ray source GRS 1915+105 with apparent superluminal motions, for which they were able to determine the jet speed ($0.92c$) and the inclination angle ($\sim 70°$) of the system. Moreover, in recent papers (Fender et al. 1997; Pooley & Fender 1997; Mirabel et al. 1998; Eikenberry et al. 1998) an intriguing correlation between radio outbursts and X-ray flares was found and hence a symbiotic jet/disk-system as proposed earlier (Falcke & Biermann 1996) seems to be a good description for GRS 1915+105. The parameters $L_{\rm disk} \sim 10^{39}$ erg/sec and $M_\bullet \sim 33 M_\odot$ are discussed in the literature (e.g., Mirabel et al. 1997; Morgan, Remillard, & Greiner 1997) for this source, but we point out that the mass determination is extremely uncertain, yet is also not really critical for the modeling.
Dhawan, Mirabel, & Rodriguez (1998) observed the central radio core in a relatively quiescent phase finding an intrinsic source size of ~ 2 milli-arcsecond (major axis) at 15 GHz and fluxes around 40 mJy (flat spectrum). For these parameters the jet model gives a jet power of $10^{39.1}$ erg/sec and a $\gamma_{\rm e}$ of ~ 400. In addition, the predicted scaling of the core size ($\propto \nu^{-0.9}$) is consistent with the observed one (roughly $\propto \nu^{-1}$, taking out the scatter broadening). The observed time delay of ~ 4 min between outburst peaks at 3.5 and and 2cm (Pooley & Fender 1997) can be explained as the delay it takes for each outburst to reach the optically thin regime ($\tau \simeq 1$) at the angular distance $\Phi_{\rm s}$ where the outburst first becomes visible. For the parameters given here and in Table 2.1 we get[6] $\Phi_{\rm s} = 0.035$ milli-arcsecond and the time delay between 2 and 3.5 cm is predicted by the model to be of order 3 mins. The velocity of the jet in the model grows asymptotically as determined by Eq. 2.10, yielding $\beta = 0.92$ at $10^4 R_{\rm g}$ and $\beta = 0.96$ at the scale of a few milli-arcseconds, where the radio emission is coming from. Considering that Eq. 2.10 is a no-fit asymptotical description of the velocity field in the jet this is a reasonably good prediction. Apparently, the pressure gradient effect must be at work at least to some degree here. However, it has to be pointed out that recently Fender et al. (1999) claim that the velocity is not as well constrained as initially thought. On the other hand Mirabel & Rodriguez (1994) found tentatively that – in addition to their advance speed – the blobs may also expand with $0.2c$ at larger scales, thus perhaps finding direct evidence for a relativistic "sound speed" which is needed for the pressure gradient effect to be important. All in all the model seems to give a remarkable good description of GRS 1915+105 as well.

2.7.3 M81*

For the nearby galaxy and LLAGN (Ho, Filippenko, & Sargent 1996) M81* Bietenholz et al. (1996) and Bietenholz, Bartel, & Rupen (1999) presented some

[6] This is smaller than Φ where the spectrum should peak. In the light curve the actual peak of an outburst could appear somewhere between those scales if the duration of the outburst were smaller than the travel time between $\Phi_{\rm s}$ and Φ.

Table 2.1. PARAMETERS OF WELL-STUDIED JET-DISK SOURCES

Source	D	i	$\nu_{\rm obs}$ [GHz]	S_ν [mJy]	size [mas]	$M_\bullet$ [$M_\odot$]	$L_{\rm disk}$ [erg/sec]	$Q_{\rm jet}$ [erg/sec]	lg $\gamma_{\rm e}$	α
GRS 1915+105*	12 kpc	70°	15	40	2	(33)	10^{39}	$10^{39.1}$	2.6	0.21
NGC 4258*	7.3 Mpc	82°	22	3	0.35	$3.5 \cdot 10^7$	(10^{42})	$10^{41.7}$	2.8	0.22
M81*	3.25 Mpc	35°	8.5	100	0.5	(10^6)	$10^{41.5}$	$10^{41.8}$	2.4	0.14

Parameters for compact radio cores in various sources. Columns 2-7 are observationally determined input parameters: distance D, inclination angle i of disk axis and jet to the line of sight, observing frequency $\nu_{\rm obs}$, flux density of radio core S_ν, size of radio core, and black hole mass $M_\bullet$. The inferred disk luminosity $L_{\rm disk}$ is not an input parameter here and given in column 8 for comparison only. Uncertain values are given in brackets, but since the black hole masses do not enter strongly the uncertainties in the black hole mass for M81 and GRS 1915 are actually irrelevant. Columns 9-11 are output parameters of the radio core model: jet power $Q_{\rm jet}$, characteristic electron Lorentz factor $\gamma_{\rm e}$, and average spectral index α ($S_\nu \propto \nu^\alpha$) in the radio.

new measurements confirming that indeed it has a core-jet structure as predicted in Falcke (1996a). The average flux and size of M81* at 8.5 GHz was ~ 120 mJy and ~ 0.5 milli-arcsecond. Falcke (1996a) concluded that a range of inclinations between $30-40°$ fitted the radio observations best and this was confirmed by the detection of a nuclear emission-line disk in M81 with similar inclination (Devereux, Ford, & Jacoby 1997). The jet power derived from our model of M81* with these parameters is $10^{41.8}$ erg/sec and $\gamma_{\rm e}=250$. For comparison, (Ho, Filippenko, & Sargent 1996) give a bolometric nuclear luminosity for M81 of $10^{41.5}$ erg/sec.

2.8 Implications

2.8.1 Model Fitting

The results of the model fitting in the previous section has a number of interesting consequences and caveats. The fact that all radio cores can be fitted with one simple model is already important, since the sources discussed here are so well constrained that by far not all combinations of size and flux could be fitted by the model. What is, however, more striking is the fact that the parameters required to explain sizes and fluxes are very similar. Firstly, in all sources the typical Lorentz factor of the electrons is of the order of a few hundred. Given the extreme simplicity of the model and the extensive use of equipartition assumptions (departing from which would be reflected in a change of $\gamma_{\rm e}$ as well) this similarity points to a relatively similar internal structure of the radio cores. Secondly, all sources have jet-powers very close to or larger than the luminosity of their thermal radiation, i.e. the suspected accretion disk luminosity. Since the model was constructed such that the radiative efficiency is maximal, applying more realistic models – for exam-

ple by including protons or using different equipartition factors, velocity fields, or electron distributions – will therefore in almost all cases only lead to an increased demand for jet power in these sources.
The model fits perhaps most convincingly the jet in GRS 1915+105, where it not only reproduces core size and flux very well, but apparently also predicts radio time delay and jet velocity reasonably well. The latter indicates that perhaps the pressure gradient in the jet of GRS 1915+105 is mainly responsible for reaching its asymptotical velocity – unless higher velocities are found in future observations.

2.8.2 Limitations

We note that for determining $Q_{\rm jet}$ from the jet model, the flux and to some degree the inclination angle (especially for small i) are most important, while $\gamma_{\rm e}$ is mainly determined by the size of the core. Consequently, the latter seems to be the most uncertain part since it is often ambiguous how to define the core and its characteristic size, especially when the resolution is of the order of the core size. Moreover, we have introduced $\gamma_{\rm e}$ mainly to easily reflect the possibility of a low-energy cut-off or break in the spectrum. This has the positive effect that cores can be larger than their size purely given by the $\tau = 1$ surface (which is particularly useful in GRS 1915+105 and NGC 4258), however, it also means that the core size may depend sensitively on the evolution of the electron distribution which we have ignored almost completely. Hence, the predictive power of this model for radio core sizes is very limited and only good to an order of magnitude, so that we will not base our interpretation heavily on the sizes. It should also be noted that the jet model used here has been trimmed towards LLAGN to achieve the greatest possible degree of simplification with the assumption that their velocity field can be described by Eq. 2.10. We know that this does not apply to quasars where the bulk Lorentz factor of the jets seems to be larger and the fully parameterized equations (e.g., as in Falcke & Biermann 1995) have to be used.
However, taking all this into consideration we can give yet a more simplified formula where we have fixed $\gamma_{\rm e}$ at an intermediate value of 300 and which can be used to very roughly estimate the jet power of a LLAGN from its flux and presumed inclination angle alone:

$$Q_{\rm jet} = 10^{37.6}\,{\rm erg/sec}\;\frac{0.024^{\frac{\xi_0}{\xi_1}}\,1.56^{\frac{\xi_4}{\xi_1}}}{0.024\cdot 1.56}\,\frac{\left(\frac{D}{10{\rm kpc}}\right)^{\frac{1.6}{\xi_1}}\left(\frac{S_\nu}{\rm mJy}\right)^{\frac{0.79}{\xi_1}}}{\left(\frac{M_\bullet}{33M_\odot}\right)^{\frac{0.15\,\xi_2}{\xi_1}}\left(\frac{\nu}{8.5{\rm GHz}}\right)^{\frac{0.15\,\xi_2}{\xi_1}}\xi_3^{\;\frac{0.79}{\xi_1}}} \tag{2.36}$$

2.8.3 Jet-Disk Symbiosis

The main result of this work, however, is that in three very different sources, with very different sizes and fluxes, we can explain the central core with a single model by just scaling the jet power with the accretion rate. This works because the three selected sources, GRS 1915+105, NGC 4258, and M81*, all have some very

important ingredients in common. All three have clear evidence for a massive black hole, signs of (large or small scale) accretion disks, jet structures in their radio cores, and a good determination of the inclination angle (important for the fitting of individual sources). In GRS 1915+105 there is even direct evidence for a coupling between jet and disk from the X-ray and radio light curves (Eikenberry et al. 1998). The high jet power we derive for the radio core in a relatively quiescent phase is quite consistent with but lower than the power derived for the major outbursts (e.g., Mirabel et al. 1998).
In hindsight this high power in the radio cores justifies the assumptions we have made earlier that jet and disk can be considered symbiotic systems and that – at least in a few systems – the assumption of $Q_{\rm jet}/L_{\rm disk} \sim 1$ (or even larger) seems appropriate. This also strengthens the picture that the jets are produced in the inner region of an accretion disk, where a major fraction of the dissipated energy is channeled into the jet (Falcke & Biermann 1995; Donea & Biermann 1996). As a consequence, modeling of accretion disks and X-ray light curves in jet systems like GRS 1915+105 clearly requires taking the jet into account.

2.8.4 Accretion Disks and ADAFs

Another consequence from those radio cores is their amazing scale invariance. It seems that we can use the very same model for a stellar mass black hole which is accreting near its Eddington limit (GRS 1915+105) as well as for a supermassive black hole which is presumably accreting at an extreme sub-Eddington rate (M81, NGC 4258). Moreover, a very similar model was successfully applied to a quasar sample earlier (Falcke, Malkan, & Biermann 1995), i.e. supermassive black holes near the Eddington limit. That would suggest that certain properties of an accretion disk/flow, namely jet production, is very insensitive towards changes in accretion rate or black hole mass, and that the 'common engine' mechanism of black hole accretion and jet formation, suggested by Rawlings & Saunders (1991), may include a much larger range of AGN than only quasars and radio galaxies.
If this is so, it has to be asked whether indeed every accretion flow necessarily has to make a transition from a thin α-disk to an ADAF when turning sub-Eddington (Meyer-Hofmeister & Meyer 2000). In order to maintain this proposition one then needs to explain how the accretion disk structure can change so drastically without affecting its innermost region, where jets presumably are being produced.
If one asks what the arguments for ADAFs in low-power AGN really are, the observational evidence remains thin. For NGC 4258 it is quite obvious now that the radio core cannot serve to support an ADAF emission model. Quite contrary the derived jet power is consistent with a low accretion rate, which in turn is consistent with the low luminosity of the nucleus and, of course, a thin disk is directly seen at least at larger radii. With the radio emission gone the ADAF spectral energy distribution, extending over many orders of magnitude, merely serves to explain a single X-ray data point. Hence, it is currently not obvious that an ADAF is really needed to explain this source at all.

The same seems to be true for M81, which is equally sub-Eddington as NGC 4258. Here the situation is even worse, since Ishisaki et al. (1996) also claim the detection of a broad iron Fe-K line suggesting that probably the inner disk cannot be as hot as required in an ADAF model. As similar broad line has been tentatively claimed also for NGC 4258 by Cannizzo et al. (1998). In any case the two galaxies serve as a general warning to view the existence of a compact radio core in low-luminosity AGN as prima facie evidence for an ADAF – a jet origin may be a more natural explanation here and in other cases.
Of course, one could ask whether indeed the interpretation of $L_{\rm disk}$ as emission from an accretion disk is correct in in each and every case. Mannheim, Schulte, & Rachen (1995), for example, argue that some of the ionizing emission can be produced in the base of the jet. Moreover, already Heckman (1980) pointed to the possibility of producing some of the optical line emission, used here to gauge the accretion disk luminosity, by shock excitation. The latter could then also be related to the jet who might be driving these shocks into the ISM. So, while the radio core emission in the cases discussed here is most likely not produced by an ADAF, the latter are not entirely excluded either (see also discussion in Chap. 4).
A much more detailed discussion of the properties of a specific compact radio core, Sgr A*, where the jet-versus-ADAF discussion also plays an important role, is presented in the next chapter.

Chapter 3

The Galactic Center – Sgr A*

Sgr A* is the unique 1 Jy flat spectrum radio point source located at the center of the Galaxy. Within the Sgr A complex (see Mezger, Duschl, & Zylka 1996 for a review) it is surrounded by a thermal radio source Sgr A West and embedded in the non-thermal "hypernova" shell Sgr A East. The presence of this compact source was first predicted by Lynden-Bell & Rees (1971) and later indeed found with radio interferometry (Balick & Brown 1974). Due to its unusual appearance it has long been speculated that this source is powered by a supermassive black hole. Its mass was believed to be around $M_\bullet \sim 2\cdot 10^6 M_\odot$ (e.g., Genzel & Townes 1987). In recent years high-resolution imaging (Eckart et al. 1993) and spectroscopy (Haller et al. 1996) in the near-infrared (NIR) have made this case much stronger and the detection of proper motions of stars around the Galactic Center has solidified this case even further (Eckart & Genzel 1996; Ghez et al. 1998) yielding an enclosed mass of $2.6\cdot 10^6 M_{\rm sun}$. The latest development in this direction is that first signs of acceleration in the star's motion have been found and that the determination of entire orbits will be possible soon (Ghez, Morris, & Becklin 2000). This will make the mass determination yet more precise. Moreover, since the relative position of the radio source Sgr A* in the NIR frame has now been well determined (Menten et al. 1997) one can also now state that Sgr A* is in the dynamical center of the central star cluster of the Galaxy within $0\farcs1$ (Ghez et al. 1998). The constraints from the first accelerations found in the stellar proper motions mentioned above seem to have pushed this limit even further, indicating that the center of mass is within 10 milli-acrsecond of Sgr A*. Corroborating evidence that this radio source is associated with the large amount of dark matter comes from the fact that, in great contrast to the surrounding stars, Sgr A* does not show any random proper motion down to a limit of 20 km/sec (Reid et al. 1999; Backer & Sramek 1999), while it does show the apparent proper motion on the sky expected from the sun's rotation around the Galactic Center. The lower limit placed on the mass of Sgr A* from these observations is around 1000 $M_{\rm sun}$ – much larger than any stellar object or remnant we know of in the Galaxy.
The enormous increase in observational data obtained for Sgr A* in recent years has enabled us to develop, compare, and constrain a variety of models for the emis-

sion characteristics of this source. Because of its relative proximity and further observational input to come Sgr A* may therefore become one of the best laboratories for studying supermassive black hole candidates and basic AGN physics. Hence it is worth to dedicate a separate chapter to this radio source and briefly summarize what its radio properties are and how we can model its emission.

3.1 The Size of Sgr A*

A problem in determining the size of Sgr A* is that its true structure is washed out by scattering in the interstellar medium (Davies, Walsh, & Booth 1976; van Langevelde et al. 1992; Yusef-Zadeh et al. 1994; Lo et al. 1998) leading to a λ^2 dependence of the apparent size of Sgr A* as a function of observed wavelength. Nevertheless, the mm-to-submm size of Sgr A* is constrained at least within one order of magnitude. From the absence of refractive scintillation Gwinn et al. (1991) have argued that Sgr A* must be larger than 10^{12} cm at $\lambda1.3$ and $\lambda0.8$mm. Krichbaum et al. (1993) obtained a source size for Sgr A* of $9.5 \cdot 10^{13}$cm at 43 GHz with VLBI – well above the expected scattering size as extrapolated from lower frequencies. This claim was challenged by Rogers et al. (1994) who only got $2 \cdot 10^{13}$ cm at 86 GHz consistent with the scattering size. Krichbaum et al. (1993) also found an additional weak component and a somewhat elongated source structure at 43 GHz not seen by Backer et al. (1993). A possibility to reconcile the results could be source variability and elongation of the internal structure which would lead to different sizes if observed with differently oriented baselines. The problems of interpreting elongated source structures in Sgr A* with insufficient baseline coverage was discussed recently by Doeleman et al. (1999). The most recent results are by Bower & Backer (1998) who find a source size of $6 \cdot 10^{13}$ cm at 43 GHz (λ7mm) – a mere 2 σ above the scattering size, while Lo et al. (1998) infer an elongated source in North-South direction with a size of $5.5 \times 1.5 \cdot 10^{13}$ cm. The latter result is a 4 σ deviation from the scattering size and would either confirm the basic results of Krichbaum et al. (1993) of a jet-like structure or suffer the same problems as the earlier observations. Finally, observations at 86 (λ3mm) and 215 GHz (λ1.4mm) (Krichbaum et al. 1998) demonstrate that Sgr A* is compact at a scale at or below 10^{13} cm at the highest frequencies, i.e. 17 Schwarzschild radii for a $2.6 \cdot 10^6 M_\odot$ black hole. While the exact size of Sgr A* cannot yet be stated with absolute certainty, the latest observations fuel hopes that somewhere in the millimeter wave regime the intrinsic source size will finally dominate over interstellar broadening.

3.2 The Spectrum of Sgr A*

There also is some confusion in the current literature about the actual spectrum of Sgr A*. Duschl & Lesch (1994) compiled an average spectrum from the literature and claimed a $\nu^{1/3}$ spectrum indicative of optically thin emission from mono-energetic electrons. However, in early simultaneous multi-frequency VLA observations (Wright & Backer 1993) the actual spectrum was bumpy and the spectral index varied between $\alpha = 0.19 - 0.34$ ($S_\nu \propto \nu^\alpha$). Morris & Serabyn (1996) published a more recent spectrum that was a smooth power law with $\alpha = 0.25$ below 100 GHz. Moreover, in 24 simultaneous observations at 2.7 and 8 GHz between 1976 and 1978 the spectral index varied between $\alpha_{2.7/8} = 0.08$ and $\alpha_{2.7/8} = 0.55$ with a mean value of $\alpha_{2.7/8} = 0.23 \pm 0.01$ (Brown & Lo 1982). This data is apparently affected (inverted) by a possible low-frequency turnover of the spectrum around 1 GHz (Davies, Walsh, & Booth 1976) which seems to be variable in frequency with a time scale of several years: in 1976 the average 2.7 to 8 GHz spectral index was $\alpha_{2.7/8} = 0.34$ wile in the consecutive two years it was significantly lower at $\alpha_{2.7/8} = 0.23$. The simultaneous VLA observations of Sgr A* in 1990/91 by Zhao et al. (1992) indicate an average spectral index of $\alpha_{8.4/15} \simeq 0.22$ between 8.4 and 15 GHz and $\alpha_{15/22} \simeq 0.15$ between 15 and 22.5 GHz. The spectrum changes once more if one looks at higher frequencies: the average flux at 22.5 GHz is 1 Jy (Zhao et al. 1992) while it was 2.9±0.3 Jy at 230 GHz in the years 1987-1994 (Zylka et al. 1995) yielding $\alpha_{22/230} = 0.45 \pm 0.5$.

So why do we have to mention all these numbers? Mainly because there were heated debates in recent years about this spectrum. As Sgr A* may be an archetype for compact radio cores in other galaxies, extreme care has to go into the interpretation of its spectrum – most likely any other radio core will have much less information available, and any error we make here will propagate into endless space.

Of greatest interest for the future debate is the suggestion of a sub-millimeter (submm) bump in the spectrum (Zylka, Mezger, & Lesch 1992; Zylka et al. 1995), since in all models the highest frequencies correspond to the smallest spatial scales. In the case of Sgr A* one expects the sub-millimeter emission to come directly from the vicinity of the black hole (Falcke 1996b).

The existence of this bump was, however, uncertain due to the variability of Sgr A*. In order to determine the reality of this crucial feature in the spectrum, we have conducted an experiment to measure the spectrum of Sgr A* simultaneously from λ20cm to λ1mm. The Galactic Center (GC) was observed on three consecutive days on 25-27 October 1996 with four different telescopes (VLA, BIMA, Nobeyama 45 m, & IRAM 30 m) on three continents. The campaign was set up with redundancies in wavelengths and time coverage. The observations were prepared, performed, and reduced independently by four different groups and a description of observations and data reduction is given in Falcke et al. (1998).

Despite several lost datasets we were able to obtain a spectrum of Sgr A* which covers the range from 1.36 to 232 GHz (Fig. 3.1)

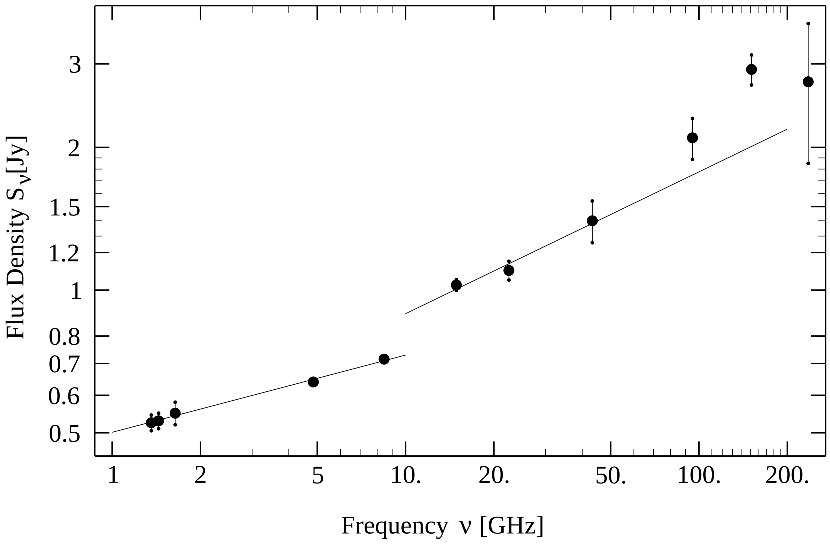

Figure 3.1: Quasi-simultaneous spectrum of Sgr A* plotted as the logarithm of the flux density vs. the logarithm of the frequency. Shown are the data averaged over the campaign period; flux densities at neighboring frequencies were also combined from the different mm-telescopes. Solid lines represent power law fits to the low- and high-frequency VLA data.

3.2.1 cm-Spectrum

The spectrum at lower frequencies between 1.36 and 43 GHz was successfully measured on two days by the VLA and is described by two power laws with spectral indices $\alpha = 0.17$ ($S_\nu \propto \nu^\alpha$) below and $\alpha = 0.30$ above 10 GHz, while there is a marked break between 8.5 and 15 GHz with $\alpha = 0.77$ (Fig. 3.1). We did not find any variability at and below 8.5 GHz between the two days (at the 1% level for 8.5 GHz). We find an increase by $\sim$15% in flux at 15 GHz between 26 & 27 Oct. 1996, however, in addition to the statistical errors, we may have a systematic error of up to $\sim$10% at frequencies 15 GHz and higher in the observations on 26 Oct 1996 due to possible improper correction of different air masses. Thus we cannot claim any significant intra-day variability of Sgr A* from our data at cm wavelengths.

3.2.2 mm-Spectrum

The errors of the mm-telescopes are much larger than those of the VLA and comparison of various data-sets indicate that the variability at λ3 & 2mm is not larger than 20% over a period of three days during the campaign at all frequencies below 150 GHz (see also Gwinn et al. 1991). We therefore first combined all available data for each telescope to obtain an average flux density measurement of Sgr A* over the campaign period.
Since the individual flux densities from the three mm-telescopes agree within the errors with each other we then combined the flux density measurements from the

different telescopes at $\lambda 3$ & 2mm and compared it with the time-averaged VLA flux densities.
First of all, we notice that the λ3mm flux density is only slightly above the extrapolation from the VLA observations which is reassuring concerning the possible systematic uncertainties in the thermal background subtraction. Hence, the fact that the λ2mm flux density – measured by the same telescopes – lies substantially (0.8Jy, $\sim 4\sigma$) above the extrapolation from the VLA cm data becomes even more significant. If we only consider $\lambda 7$, 3, & 2mm we find that the spectral index of Sgr A* increases to $\alpha = 0.52$ in the mm-range, while the λ3-to-2mm spectral index even becomes $\alpha = 0.76$, hence we conclude that there is a *significant mm-excess in the spectrum of Sgr A **. The λ1.3mm measurement is consistent with such an excess but, because of the large errors, has no significance for this discussion.

3.3 Implications of the Sgr A* Spectrum

A major problem in discussing the spectrum of Sgr A* and the reality of the mm-excess has been the non-simultaneity of the measurements and the comparison of array (low frequencies) and single dish (high frequencies) flux densities. Our simultaneous observations now show a smooth transition from the VLA to the mm-telescopes and an upturn in the spectrum of Sgr A* between λ3mm and λ2mm in the single dish observations alone. The results of all telescopes were consistent with each other and we conclude that the observed mm-excess is not due to variability or technical artifacts.
A concern that needs to be addressed in more detailed when studying the spectrum of Sgr A * is, however, confusion by other sources. The diffuse free-free emission in the GC obviously is a major source of confusion for single dish observations of Sgr A* and subtraction of this component was taken care of. Optically thick thermal emission, e.g., from cold dust, on a scale of a few arcseconds and beyond seems to be negligible in the mm-regime (Zylka et al. 1995) and comparison of single-dish and high-resolution interferometer flux density measurements (with OVRO) do not indicate the presence of such components at smaller scales as discussed by Serabyn, Carlstrom, & Scoville (1992) and Serabyn et al. (1997).
Finally, a major contribution of a yet unknown non-variable point source in the very vicinity of Sgr A* can also be ruled out. Based on high resolution VLA images with a resolution of $0\farcs1$ at $\lambda 13$ and $\lambda 7$ mm, the peak flux density for such a hypothetical source is below 5 mJy at λ7mm. The brightest regions near Sgr A* are IRS 13 ($3''$ SW to Sgr A*) which contributes 100 mJy (integrated within a $3''\times3''$ area) and IRS 2 (1-$2''$ south to IRS 13) which contributes 85 mJy (within a $2''\times2''$area) – the spectra of these sources are consistent with optically thin free-free emission. From the upper limits at lower frequencies it follows that any source which might be confused with Sgr A* would contribute negligibly to the total flux density of Sgr A* at mm-wavelengths. For a source with optically thick, thermal emission, for example, the contribution has to be less than 50 mJy at λ2mm in

order to be below the upper limits at λ7mm. We therefore conclude that the mm-excess is indeed an intrinsic feature of Sgr A*.
The submm-bump causing this excess is, in fact, very well explained by assuming the presence of a compact, self-absorbed synchrotron component in Sgr A*. As outlined in Falcke (1996b; see also Beckert & Duschl 1997) this submm component can be described in its most simple minded form by four parameters: magnetic field B, electron density n, electron Lorentz factor $\gamma_{\rm e}$, and volume $V = \pi R^2 Z$, using for simplicity a one-temperature (i.e. quasi mono-energetic) electron distribution and the distance being set to 8.5 kpc. On the other side we have three measurable input parameters: the peak frequency $\nu_{\rm max} \sim \nu_{\rm c}/3.5$ of a mono-energetic synchrotron spectrum (characteristic frequency $\nu_{\rm c}$), the peak flux $S_{\nu_{\rm max}}$, and the VLBI source size (see above). A fourth parameter can be gained if one assumes that magnetic field and relativistic electrons are in equipartition, i.e. $B^2/8\pi = k^{-1} n_{\rm e} \gamma_{\rm e} m_{\rm e} c^2$ with $k \sim 1$. With this condition we obtain (averaged over pitch angle) that

$$\gamma_{\rm e} = 326\, k^{1/7} \left(\frac{F_{\nu_{\rm max}}}{3.5{\rm Jy}}\right)^{-1/7} \left(\frac{\nu_{\rm max}}{10^{12}{\rm Hz}}\right)^{3/7} \left(\frac{R}{10^{13}{\rm cm}}\right)^{2/7} \left(\frac{Z}{4\cdot 10^{13}{\rm cm}}\right)^{1/7} \tag{3.1}$$

$$B = 10\,{\rm G}\, k^{-2/7} \left(\frac{F_{\nu_{\rm max}}}{3.5{\rm Jy}}\right)^{2/7} \left(\frac{\nu_{\rm max}}{10^{12}{\rm Hz}}\right)^{1/7} \left(\frac{R}{10^{13}{\rm cm}}\right)^{-4/7} \left(\frac{Z}{4\cdot 10^{13}{\rm cm}}\right)^{-2/7} \tag{3.2}$$

$$n_{\rm e} = \frac{1.4\cdot 10^4}{{\rm cm}^3} k^{2/7} \left(\frac{F_{\nu_{\rm max}}}{3.5{\rm Jy}}\right)^{5/7} \left(\frac{\nu_{\rm max}}{10^{12}{\rm Hz}}\right)^{-1/7} \left(\frac{R}{10^{13}{\rm cm}}\right)^{-10/7} \left(\frac{Z}{4\cdot 10^{13}{\rm cm}}\right)^{-5/7}. \tag{3.3}$$

Apparently the 'non'-equipartition parameter k enters only weakly and as long as one is not very far from equipartition the parameters are basically fixed: $\nu_{\rm max}$ is known within a factor three, $S_{\nu_{\rm max}}$ within 50%, and the source size within a factor of ten.
Because of the high compactness of Sgr A* synchrotron self-absorption becomes another important point to be considered. Using an absorption coefficient of $\kappa_{\rm sync} = 1.4 \cdot 10^{-9}{\rm cm}^{-1}(n_{\rm e}/{\rm cm}^{-3})(B/{\rm G})\gamma_{\rm e}^{-5} \left(\nu/\nu_{\rm c}\right)^{-5/3}$ one finds the synchrotron self-absorption frequency to be

$$\nu_{\rm ssa} = \frac{2.5\,{\rm GHz}}{k^{0.09}} \left(\frac{F_{\nu_{\rm max}}}{3.5{\rm Jy}}\right)^{0.69} \left(\frac{\nu_{\rm max}}{10^{12}{\rm Hz}}\right)^{-.46} \left(\frac{R}{10^{13}{\rm cm}}\right)^{-.77} \left(\frac{Z}{4\cdot 10^{13}{\rm cm}}\right)^{-.69}. \tag{3.4}$$

We can now make very solid arguments about the possible source size of Sgr A* at submm wavelengths. As VLBI measurements are only available at longer wavelengths one could still postulate arbitrarily large submm source sizes. However, if Sgr A*(submm) were optically thin and larger than $4 \cdot 10^{13}$ cm we should have seen the low frequency $\nu^{1/3}$ part of its spectrum with 3mm VLBI already. This

could only be avoided if the submm component becomes optically thick below $\sim$ 100 GHz. As shown above this is possible only for a very compact source where the dimensions of Sgr A* at submm wavelengths are substantially *smaller* than at λ3mm. Consequently Sgr A* has to be of the same size or smaller at submm wavelengths than at λ3mm.
If we now turn the argument around and assume a spherical source structure, we can calculate the actual size of the submm component to be

$$R \sim 1.5 \cdot 10^{12}\mathrm{cm} \quad k^{-1/17} \left(\frac{S_{\nu_{\max}}}{3.5\mathrm{Jy}}\right)^{8/17} \left(\frac{\nu_{\max}}{10^{12}\mathrm{Hz}}\right)^{-16/51} \left(\frac{\nu_{\mathrm{ssa}}}{100\mathrm{GHz}}\right)^{-35/51}. \quad (3.5)$$

This size is consistent with the upper limits ($\sim$1 AU) from VLBI (Rogers et al. 1994; Krichbaum et al. 1998) and lower limits ($\sim 10^{12}$cm) from scintillation experiments (Gwinn et al. 1991), as discussed above. In comparison we also note that the Schwarzschild radius (R_{S}) of the putative $2.6 \cdot 10^6 M_{\odot}$ black hole in the GC is already $R_{\mathrm{S}} = 0.77 \cdot 10^{12}$ cm and thus the compact submm component should correspond to a region in the very vicinity of the black hole. Most interesting is the possibility that this region is directly affected by general relativistic effects, and could for example be gravitationally amplified if the radiation is intrinsically anisotropic (e.g., similar to Cunningham 1975).
Finally, a compact component with the parameters as in Eq. 3.5 would be very interesting for mm-VLBI, since the black hole horizon could be imaged against the background of this submm emission. This will be discussed in greater detail below (Sec. 3.14).

3.4 Radio Variability

An important parameter for constraining the spectrum and nature of Sgr A* should be its variability. A major observational problem, however, is the relatively low elevation of Sgr A*, the large confusing structure of the Sgr A complex, and the scatter-broadening at low frequencies. The confusion is a major problem especially for single-baseline interferometers with short baselines like the Green Bank Interferometer (GBI) that is often used for variability studies. For this reason the exact nature of the variability of Sgr A* has remained inconclusive. Flux density variations are clearly seen between different epochs, but the time scale of the variability at various frequencies is not well determined and it is not clear whether some of the more extreme claims of variability are real or instrumental artifacts. So far, Zhao et al. (1989) and Zhao et al. (1992) probably have presented the largest database of Sgr A* flux-density measurements with the VLA. They found a number of outbursts at higher frequencies and tentatively concluded that the small-amplitude variability at longer wavelengths is caused by scattering effects in the ISM while the variability at higher frequencies is intrinsic.

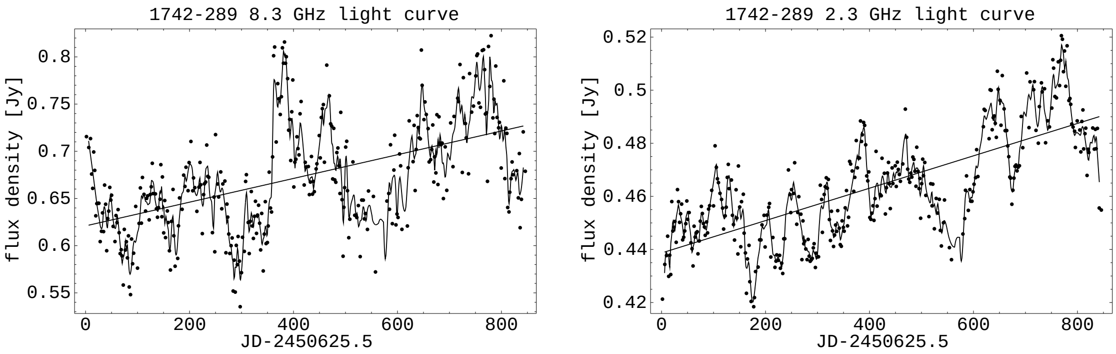

Figure 3.2: Radio light curves of Sgr A* at 8.3 GHz (left panel) and 2.3 GHz (right panel) measured with the GBI (dots). The solid line is the interpolated light curve for three-day averages. The straight line is a linear fit to the data to take out a long-term secular increase in the flux density

An alternative way to look at flux density variations is to use the GBI interferometer, which performs daily observations at two different frequencies. First results of this interferometer have been published in Falcke (1999). This paper also gives a short description of observation and data reduction techniques. It is important to note that all the observations were made at the same hourangle thus avoiding the problems mentioned before with spurious variability due to confusing flux. The database used consisted of about 540 days of continuous monitoring. Here we can now present the results of an expanded database, including 845 daily observations. The light curves have been smoothed with a moving average of three days and a secular increase in flux density of about 50 mJy and 100 mJy during the entire observing campaign at 2.3 GHz and 8.3 GHz respectively has been subtracted.

The light curves, before subtraction of the secular increase, are shown in Figure 3.2. One can see a peak-to-peak variability of 250 mJy and 60 mJy with an RMS (i.e. modulation index) of 6% and 2.5% at 8.3 & 2.3 GHz, respectively. The median spectral index between the two frequencies for the whole period is $\alpha = 0.28$ ($S_\nu \propto \nu^\alpha$), varying between 0.2 and 0.4. These number are basically unchanged with respect to our earlier results. Interestingly, there is still a clear trend for the spectral index to become larger when the flux density in both bands increases. This is shown in Figure 3.3. The spectral index vs. flux correlation and the different modulation indices at the two frequencies simply imply that outbursts in Sgr A* are more pronounced at higher and more damped at lower frequencies. The secular increase in flux density over the entire monitoring period shows a similar behavior.

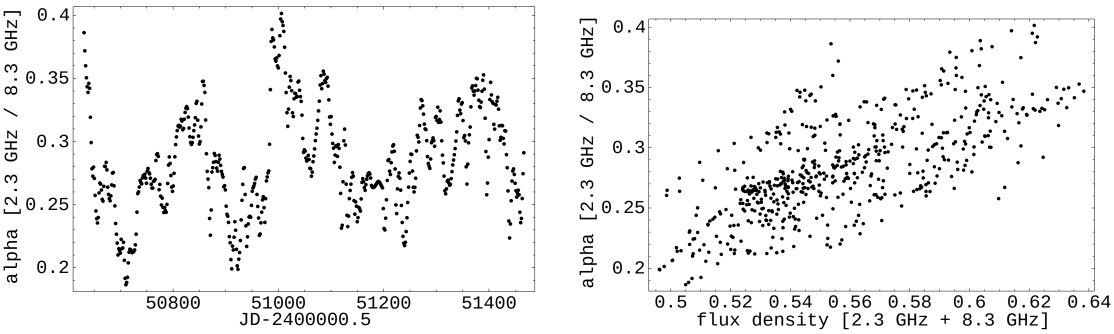

Figure 3.3: Left: Spectral index variation of Sgr A* between 2.3 and 8.3 GHz as a function of time. Right: Spectral index evolution as a function of combined flux density at 2.3 and 8.3 GHz – the higher the flux the more inverted the spectrum.

3.4.1 Autocorrelation, Structure Function, and Power Spectrum

To characterize the variability pattern better, Fig. 3.4 shows the structure function $D(\tau)$ of the two light curves as a function of the time delay τ, where

$$D(\tau) = \sqrt{\left\langle \left(S_\nu(t) - S_\nu(t \pm \tau)\right)^2 \right\rangle} \quad . \tag{3.6}$$

A maximum in the structure function indicates a characteristic time scale, a minimum indicates a characteristic period. A characteristic period in radio light curves usually does not persist for a long time, and hence, similar to X-ray astronomy, is commonly called a quasi-periodicity, even though the underlying physical processes are probably very different from those seen in X-ray binaries.
At both frequencies the characteristic time scale is somewhere between 50 and 250 days. The steepest increase and hence the time scale where the variability amplitude rises most rapidly is around a few ten days. During the period discussed in Falcke (1999) one could see a strong signal of a quasi-periodic variability with a period of 60 days over one year. As expected this periodicity has subsided, even though the structure function is still rather 'bumpy' at 2.3 GHz compared to 8.3 GHz. In contrast to this behavior we now find a minimum of the structure function at 8.3 GHz around 250 days that is also visible at 2.3 GHz – again a quasi-periodic behavior during a certain time range but now with a much longer period.
This quasi-periodicity is also visible in the power spectra – the Fourier transform of the light curves multiplied by their complex conjugates (Fig. 3.5). At 8.3 GHz we find a peak again at 250 days, indicating a periodicity. At 2.3 GHz we also see a flattening of the power spectrum but a clear location of the peak is difficult. At short delays of one to three days we see the effect of smoothing the data. If one subtracts a polynomial from the two power spectra one can also identify a peak around some ten days, corresponding to the onset of variability seen already in the structure function.

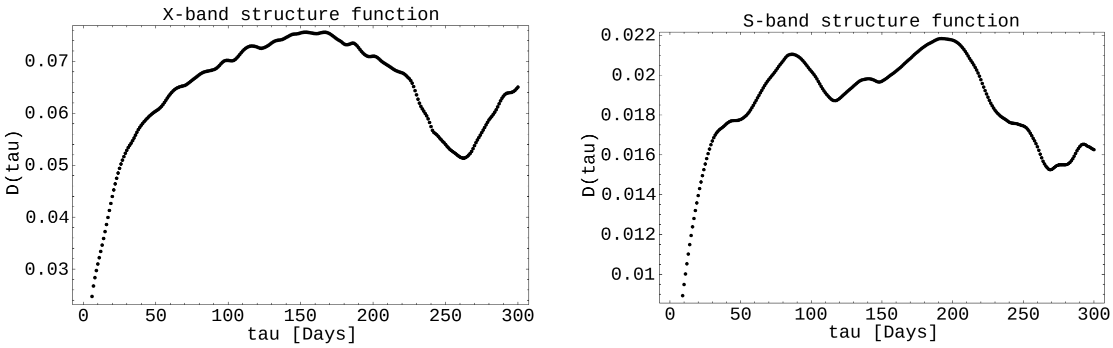

Figure 3.4: Structure function of the radio light curves of Sgr A* at 8.3 GHz (left panel) and 2.3 GHz (right panel). Maxima indicate a characteristic times scale, minima indicate a characteristic period

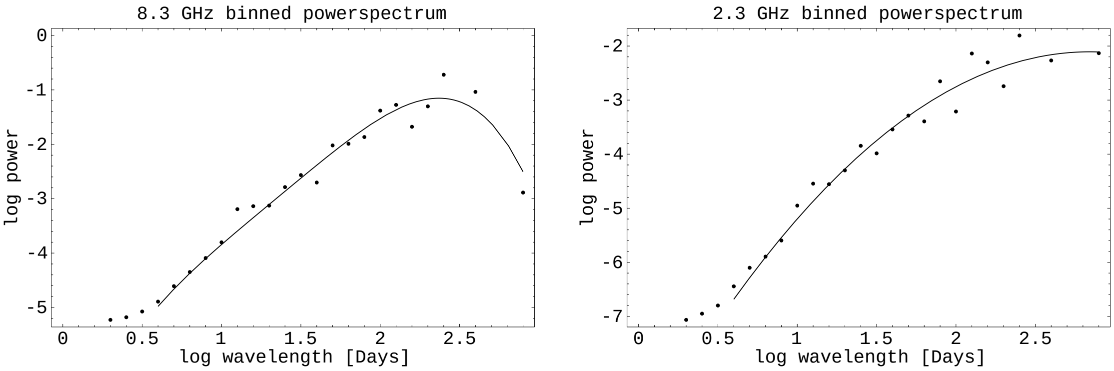

Figure 3.5: Power spectrum of the radio light curves of Sgr A* at 8.3 GHz (left panel) and 2.3 GHz (right panel). The spectra were bined in logarithmic intervals to reduce the scatter. The solid lines are 4th and 2nd order polynomial fits to the data.

Finally, we can look at the cross correlation between the two frequencies to see whether the variations are correlated or not. The resulting cross correlation in Fig. 3.6 has a marked peak at zero-lag indicating that indeed the variability is strongly correlated: both frequencies rise and fall together but with different amplitudes as already discussed in the context of the spectral index variations. In addition we see a second strong peak at the 250 day period indicating that the quasi-periodicity is recovered in both light curves.

3.4.2 Implications

To summarize the results one can say that there is clear evidence for variability of a few percent at cm wavelengths in Sgr A*. The variability does not seem to be consistent with a simple model of refractive interstellar scintillation (RISS) as suggested by Zhao et al. (1992). The time scales at 2.3 GHz and 8.3 GHz both seem to be comparable to the one found at 5 GHz by Zhao et al. (1992) and does not follow a $t \propto \lambda^2$ law. Moreover, the modulation index apparently decreases towards lower frequencies.

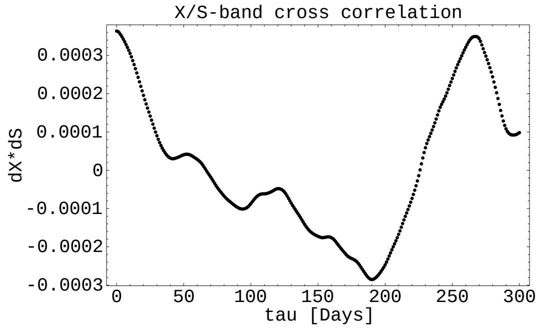

Figure 3.6: Cross correlation of 8.3 GHz and 2.3 GHz radio light curves of Sgr A*. Positive and negative time lags have been co-added.

The quasi-periodicity is reminiscent to those in some quasar cores. For example the QSO 0917+624 is know to show episodes of quasi-periodicity (Kraus et al. 1999). Unfortunately the frequency of these quasi-periodicities in quasar cores, and perhaps also in Sgr A*, may not be related to a well defined and constant (e.g., precession) frequency like the QPOs in X-ray binaries, but could simply be due to intermittent periodic phenomena in the accretion disk (e.g., waves) or the jet (e.g., helical motion). In the case of Sgr A* all characteristic time scales associated with a black hole or a relativistic outflow at these frequencies are less than a day and hence one might consider global accretion flow instabilities for such a behavior. On the other hand, the possibility that the quasi-periodicity could be produced by interstellar scattering needs to be explored as well. It remains to be seen whether any of the periods found so far will persist over longer periods of time. This can be done, e.g., by utilizing the treasures of the VLA archive (Bower et al., in prep.).
The most direct conclusion we can draw from the variability data is the high degree of correlation between 2.3 and 8.3 GHz. The lag is apparently less than three days which corresponds to a light travel distance of $\lesssim 10^{16}$ days ($\sim$ 60 milli-arcsecond at the Galactic Center and less than the scattering size). For models which a have frequency-dependent structure (e.g., the jet model) this will be an upper limit to the size scale at these frequencies. In models where the radio emission is produced in the accretion flow and where the travel time is given by the accretion velocity those scales would be much smaller.

3.5 Linear Polarization

The final parameter to be discussed in the context of the Sgr A* radio emission is its polarization. Early papers that looked into the radio emission of Sgr A did not find any significant polarization. Ekers, Goss, & Schwarz (1975) gave an upper limit of 1% linear polarization for the peak of Sgr A which was not well resolved in their 5 GHz Westerbork observations. Similarly, Yusef-Zadeh & Morris (1987) did not find any significant polarization in Sgr A with the VLA. In contrast to this, polarization measurements of AGN, where the linear polarization is typically a few percent, have been an important tool in understanding radiation mechanisms and basic processes governing the radio emitting plasmas, such as shock acceleration (Hughes, Aller, & Aller 1985; Marscher & Gear 1985). So, while polarization promises interesting insight, the early negative results on Sgr A* made this a non-issue for over a decade. Only recently, in a series of papers has polarization been revisited with some surprising answers (Bower, Falcke, & Backer 1999b; Bower et al. 1999a; Bower et al. 1999b).

Of course, one important question is, if indeed linear polarization in Sgr A* is low, why is this so? Two possibilities that come immediately to mind are that perhaps the scattering screen between the Galactic Center and the observer de-polarizes any radiation. One can imagine two possibilities: a) the Faraday rotation of the homogeneous medium is so high that within the bandwidth of the observation the polarization vector is rotated by more than 180 degrees and therefore is largely canceling itself. Or b) there is considerable variation of the Faraday rotation in the scattering screen so that every ray that reaches the observer gets rotated differently and hence the overall polarization is reduced significantly. Finally, one could wonder whether any such effect could lead to a conversion of linear polarization to circular polarization, after all we have an anisotropic scattering screen permeated by a large scale magnetic field (Yusef-Zadeh et al. 1994). This question will be discussed in the subsequent section.

To investigate the linear polarization – or its lack thereof – two different approaches have been followed. First, one needs to measure the linear polarization with high accuracy and then check whether a large Faraday rotation is present. This was done by Bower et al. (1999a) where continuum polarimetry at 4.8 GHz and spectro-polarimetric observations with the VLA of Sgr A* at 4.8 and 8.4 GHz were presented. The spectro-polarimetric observations were made to exclude strong Faraday rotation in the Galactic Center that could lead to a de-polarization of the radiation when observed in continuum mode integrating over a large bandwidth.

Faraday rotation is produced when radio waves pass trough an ionized and magnetized medium. Since left and right circularly polarized waves have different refractive indices for a given magnetic field orientation, a wavelength-dependent delay is induced which rotates the position angle $\phi_{\rm LP}$ of the linear polarization vector, yielding

$$\phi_{\rm LP} = {\rm RM}\lambda^2. \tag{3.7}$$

The parameter RM is called the rotation measure and can be determined by measuring the position angle of the linear polarization vector $\phi_{\rm LP}$ at different wavelengths λ. For a given frequency bandwidth $\Delta\nu$ significant de-polarization is obtained if $\phi_{\rm LP}$ changes by more than one radian, i.e. if

$${\rm RM} > 0.5\frac{\nu}{\lambda^2\Delta\nu}. \tag{3.8}$$

This means that for a typical VLA bandwidth of 50 MHz at 4.8 GHz the critical

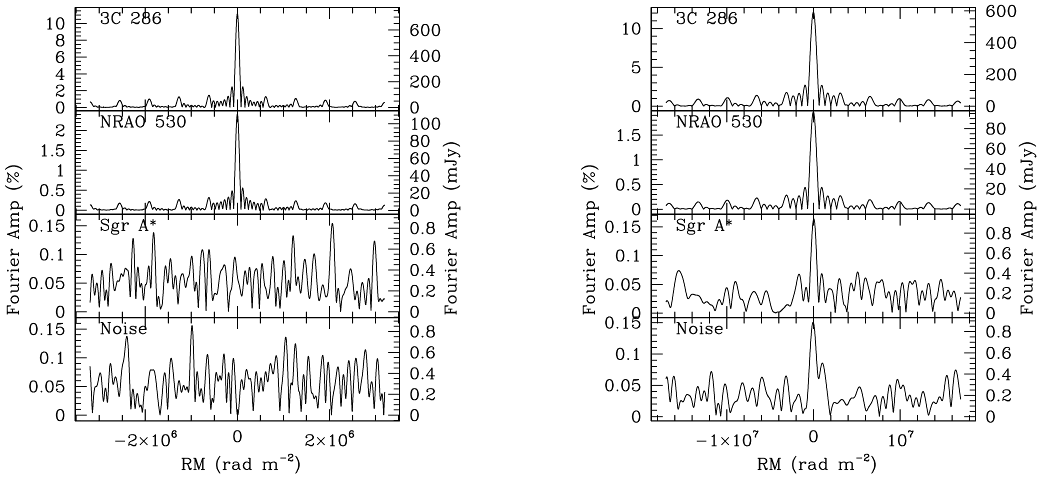

Figure 3.7: Fourier amplitude for 3C286, NRAO 530, Sgr A*, and a noise data set at 4.8 GHz (left) and 8.4 GHz (right). The Fourier amplitude is given in mJy and as a fraction of the total flux for each source. The scaling of the Gaussian noise data is set to match that of Sgr A*. There is no significant peak in Sgr A* for RMs within $\pm 3.5 \cdot 10^6$ rad m^{-2} at 4.8 GHz and within $\pm 1.5 \cdot 10^7$ rad m^{-2} at 8.4 GHz. The figures are taken from Bower, Zhao, Goss, & Falcke (1999).

rotation measure is $\sim 10^4$ rad m^{-2}. This value is not deemed to be so excessively high that it could not be present in the Galactic Center.

The results of the broad-band continuum polarimetry indeed confirmed the absence of linear polarization with a rather low upper limit of $< 0.1\%$ fractional polarization. In order to detect whether RM in excess of $\sim 10^4$ rad m^{-2} could cause this non-detection the spectro-polarimetric data, where $\Delta\nu$ is much smaller, was Fourier transformed to detect multiple rotations of the polarization vector across the entire band. While the resulting Fourier amplitude spectra (Fig. 3.7) do show significant peaks for the two calibrator sources at zero RM, the spectrum for Sgr A* is almost indistinguishable from a noise data set. Hence one can exclude that Faraday rotation by a plasma with rotation measures up to 10^7 rad m^{-2} is responsible for a de-polarization of Sgr A* for an upper limit of 0.2% percent linear polarization.

In order to clarify whether RM fluctuations in the scattering medium could depolarize the radiation of Sgr A* one could simply try to measure the linear polarization at progressively higher frequencies. Since the scattering size decreases with ν^{-2} the differential changes in the angles to the line of sight for light rays from Sgr A* will rapidly become smaller and smaller with increasing wavelength. In addition the Faraday rotation itself will also decrease with ν^{-2}. Bower et al. (1999b) have therefore investigated high-frequency polarization of Sgr A* with the VLA and found only upper limits. Figure 3.8 shows the upper limits for the fractional linear polarization of Sgr A* as a function of frequency. Since the sen-

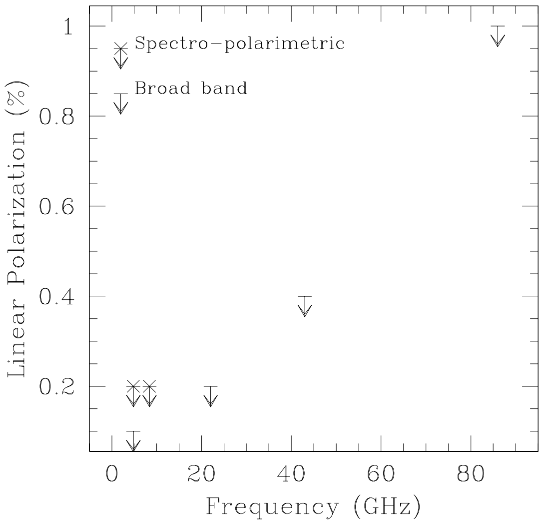

Figure 3.8: Upper limits to the linear polarization of Sgr A* measured with the VLA and BIMA (86 GHz). The figure is taken from Bower, Wright, Backer & Falcke (1999).

sitivity for observations at higher frequencies decreases the upper limits at 43 and 86 GHz are not as strict as at 4.8 GHz. However, in most AGN the linear polarization seems to rise towards higher frequencies (Aller, Aller, & Hughes 1992) and given the strong frequency dependence of Faraday rotation, de-polarization by the scattering medium becomes rather unlikely at present.
The very latest information now comes from linear polarization observations made with the SCUBA camera at the James Clerk Maxwell Telescope (JCMT) at 0.75, 0.85, 1.35, and 2 mm wavelengths (Aitken et al. 2000). The authors claim to have found fractional linear polarization at these wavelengths as high as 10% and above. One problem in these low-resolution observations is the strong confusion of the Sgr A* flux with dust emission from the surrounding circum-nuclear disk (CND). It is also difficult to reconcile the strong upper limits at λ3.5mm reported above and this new detection. On the other hand, for an ultra-compact region with a strong low-frequency cut-off at these wavelengths due to self-absorption (see Eq. 3.5) this may be possible. In any case this result will need further confirmation but is potentially very interesting.

3.6 Circular Polarization

3.6.1 First Detection of Circular Polarization

Another less well studied aspect of synchrotron radiation is circular polarization. Typically, the degree of circular polarization is $m_c < 0.1\%$ with only a few cases where m_c approaches 0.5% (Weiler & de Pater 1983). The degree of circular polarization usually peaks near 1.4 GHz and decreases strongly with increasing frequency.

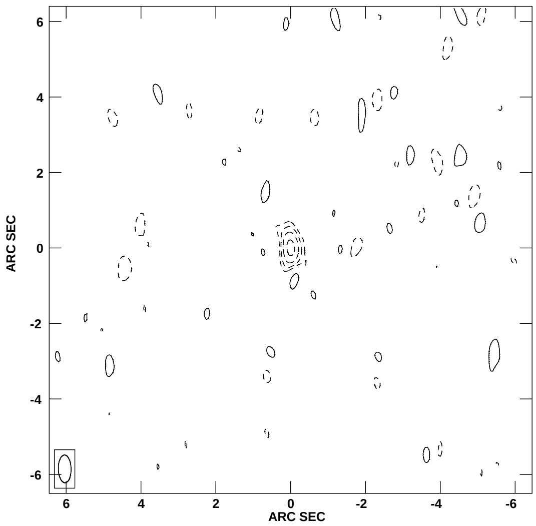

Figure 3.9: The Stokes V map for Sgr A* on 10 April 1998 at 4.8 GHz. The peak intensity is -1798 μJy beam^{-1} . The rms noise is 68 μJy beam^{-1}. Contour levels are -16, -8, -4, -2, -1, 1, 2, 4, 8 and 16 times 175 μJy beam^{-1}. Negative contours are shown with dashed lines.

Recently, VLBI imaging of 3C 279 has found $m_c \simeq 1\%$ in an individual radio component with a fractional linear polarization of 10% (Wardle et al. 1998). The integrated circular polarization, however, is less than 0.5%. The circular polarization is probably produced through the conversion of linear to circular polarization by low-energy electrons in the synchrotron source. This process is also known as re-polarization (Pacholczyk 1977).
Given the stringent limits on linear polarization of Sgr A* at cm-waves discussed in the previous section, the presence of circular polarization was not expected. Yet Bower, Falcke, & Backer (1999b) have detected circular polarization in this source at a surprisingly high level.
Figure 3.9 shows the Stokes V image of Sgr A* at 4.8 GHz from 10 April 1998. The peak at -1.8 mJy is more than 20 times the noise level of 68 μJy beam^{-1}. For the same epoch, the calibrator B1748-253 had a peak flux of 262 μJy in a map with a noise level of 58 μJy beam^{-1}.
The circular polarization was found to be $m_c = -0.36 \pm 0.05\%$ and $m_c = -0.26 \pm 0.06\%$ at 4.8 and 8.4 GHz, respectively. The errors are estimated from the variance of the three separate measurements for each frequency. These errors set an upper limit to the variability, as well. The average spectral index of the fractional circular polarization is $\alpha = -0.6 \pm 0.3$ for $m_c \propto \nu^\alpha$. The error in α is less than that expected from the errors in m_c. This is due to the fact that variations in m_c between epochs appear to be due to systematic errors that are common to both frequencies.
In the mean time the initial detection was confirmed by an Australian group (Sault & Macquart 1999) with a different telescope (Australia Telescope Compact Array) at 4.8 GHz.
Most recently the circular polarization observations of Sgr A* have been extended

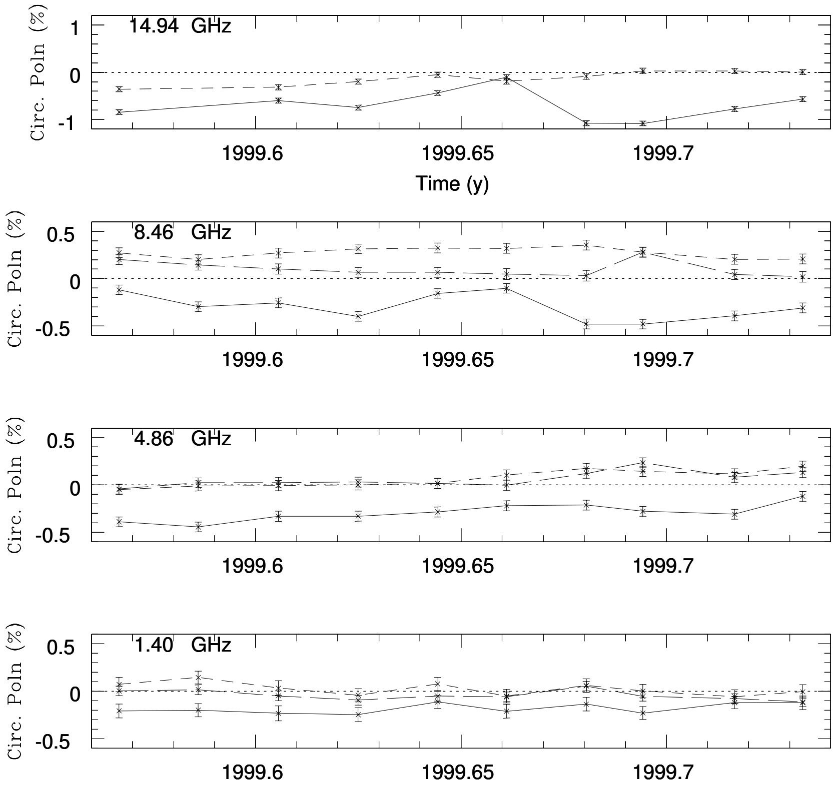

Figure 3.10: Light curves of fractional circular polarization in Sgr A* (solid lines), the calibrator J1744-312 (short-dashed), and the calibrator J1751-258 (long-dashed line) from VLA measurements at 1.4, 4.8, 8.4, and 14.9 GHz (Bower, Falcke, & Backer 1999c).

up to frequencies of 15 GHz and monitoring of the variability of the polarized flux has been performed with the VLA (Bower, Falcke, & Backer 1999a). The first results indicate that circular polarization is detected even at 15 GHz and that during certain periods the polarized flux is rising towards the highest frequencies. While the polarized flux density at 1.4 GHz and 4.86 GHz is relatively stable over two months, the variability amplitude seems to rise at 8.4 and 15 GHz. Figure 3.10 shows the light curves of the relative circular polarization in Sgr A* as measured with the VLA. For the monitoring period the mean spectrum is in fact highly inverted with a spectral index $\alpha \sim 0.6$ ($m_{\rm c} \propto \nu^{\alpha}$). It has to be noted, however, that this data is still being worked on and that supplementing higher frequency data is expected in the near future.

3.6.2 Mechanisms for the Production of Circular Polarization

While the detection of circular polarization for Sgr A* is in itself an unexpected result, two additional properties set this source apart from any other radio core and make the result very puzzling: the fact that circular polarization exceeds linear by more than a factor of two at cm-waves and the flatness (or inversion) of the circularly polarized spectrum.

One can consider now whether the circular polarization is produced not in the source, but in the intervening scattering screen. A birefringent scattering medium may produce scintillating circular polarization from an unpolarized background source. This effect is presently being studied in detail (Macquart & Melrose, in prep.). It requires a scattering region with a fluctuating rotation measure gradient. Such a mechanism is appealing due to the strong scattering medium and the strong observed gradients in RM in the GC region (Yusef-Zadeh, Wardle, & Parastaran 1997). The fact that the scattered image of Sgr A* itself is anisotropic might also indicate an anisotropic scattering medium. However, the diffractive effect has $\alpha = -4$ or steeper, which is not at all consistent with the measured spectral index. Further calculations of this relatively unexplored issue should show whether such a scattering model could nevertheless be made consistent with the observations.

Alternatively, one can ask whether the conversion mechanism or intrinsic synchrotron circular polarization could be at work in Sgr A* (Pacholczyk 1977; Jones & O'Dell 1977). Here, the main problem is the low level of linear polarization. Magnetic field reversals would reduce linear polarization, but most likely would affect circular polarization in the same way (Wilson & Weiler 1997). However, one important factor in the relative level of linear to circular polarization is the electron energy distribution, since low-energy electrons (with Lorentz factors less than 100) can lead to Faraday de-polarization of linear and/or conversion of linear to circular polarization.

As model calculations show (Jones & O'Dell 1977, their Fig. 1) circular polarization of a radio component peaks near the self-absorption frequency $\nu_{\rm ssa}$, where linear polarization drops to a minimum. In typical radio core components the strongest contribution to linear polarization therefore comes from the optically-thin power-law part of its spectrum. However, in Sgr A* such a power law is most likely absent or already ends at a frequency $\nu_{\rm max} \sim \nu_{\rm ssa}$, as indicated by the steep high-frequency cut-off in its spectrum towards the infrared (Serabyn et al. 1997; Falcke et al. 1998).

Such a situation has not yet been considered in synchrotron propagation calculations involving conversion. However, it may result in a high $m_{\rm c}$-to-$m_{\rm l}$ ratio if $\nu_{\rm max} \sim \nu_{\rm ssa}$ is true for the electrons that produce the low frequency spectrum. For example, Jones & O'Dell show that for a power law of electron energies with characteristic frequencies $\nu_{\rm min}$ extending at least a factor thirty below $\nu_{\rm ssa}$, circular polarization around $\nu_{\rm ssa}$ can exceed $m_{\rm l}$. With the absence of any higher frequency emission, linear polarization could be quenched. On the other hand, a narrow distribution with $\nu_{\rm min} \sim \nu_{\rm ssa} \sim \nu_{\rm max}$ would again lead to significant linear polarization even at the self-absorption frequency (Jones & Hardee 1979).

We consider here a simple synchrotron model of Sgr A*, where the flux density at 5 GHz is produced in a spherical component by a flat electron distribution with a power law index of $p = 1$ ranging over electron energies that correspond to the characteristic frequencies $\nu_{\rm max} = \nu_{\rm ssa} = 5$ GHz and $\nu_{\rm min} = \nu_{\rm max}/30$. This model corresponds to a single zone of a complete inhomogeneous model (e.g., Blandford & Königl 1979, also Chap. 2). The low and high energy electrons are fully mixed. Assuming equipartition, we find a magnetic field of 0.4 Gauss and a maximum electron Lorentz factor of 60. The electron distribution chosen here has an equal number of low- and high-energy electrons per logarithmic interval. According to Pacholczyk (1977, Eq. 3.152), such a power law will contain enough low-energy electrons near $\gamma_{\rm min}$ to produce the observed circular polarization through re-polarization. Intrinsic circular polarization could be as important as conversion in this model. The intrinsic synchrotron circular polarization is given by $m_{\rm c} = 3\%\,(B/{\rm Gauss})^{1/2}(\nu/{\rm GHz})^{-1/2} = 0.9\%$, assuming an angle of 60° between the magnetic field and the line of sight (Legg & Westfold 1968). However, field reversals and optical depth effects will decrease that number.

The polarization properties of models (e.g., ADAF and Bondi-Hoyle) that produce gyro-synchrotron emission with low temperature electrons are largely unexplored. However, Ramaty (1969) did show that circular polarization may dominate linear polarization in some simple gyro-synchrotron sources.

Obviously, a more self-consistent treatment of these problems is required. The circular and linear polarization spectrum will depend on the electron distribution and the temperature and magnetic field stratification in the source. Nevertheless, it seems as if a highly self-absorbed source with a low high-energy cut-off and a modest amount of low-energy electrons might explain the observed properties of Sgr A*.

The rise of the fractional circular polarization and its variability towards higher frequencies is another important clue. It is not clear whether this indicates that the circular polarization is mainly associated with the submm-bump since this is expected to cut-off rather sharply towards low frequencies. It could well be that this is another indication of hidden intrinsic structure within Sgr A*. In a model, where the Sgr A* spectrum is produced by a combination of self-absorbed components, such as in the jet model discussed below, a rather flat or even inverted spectrum is expected since the time-averaged fractional polarization at the self-absorption frequency should not change drastically when going from one spatial scale (and one peak frequency) to the next. In any case, this discovery opens a significant new parameter space for the study of the nearest supermassive black hole candidate and its environment.

3.7 Accretion Models – An Overview

If we now want to go beyond a mere description of Sgr A*, we have to ask how this source is powered and what the underlying engine producing the radio and X-ray emission actually is? One idea is that, if Sgr A* is a black hole, it should swallow some fraction of the strong stellar winds seen in the GC through spherical (Bondi-Hoyle) accretion.

The rate of infall depends only on the mass of the black hole and the wind parameters. Once we know the latter we can determine the black hole mass from the estimated accretion rate, which in turn could be derived from the spectrum of Sgr A*. The general validity of the Bondi-Hoyle accretion (without angular momentum) under these assumptions was demonstrated by 3D numerical calculations (Ruffert & Melia 1994) and the main uncertainties are related to the plasmaphysical effects associated with the infall. It is usually assumed that the magnetic field in the accreted plasma is amplified by compression up to a point where it reaches the equipartition value. Beyond this point the excess magnetic field is assumed to be dissipated and used to heat the plasma. The electron temperature is determined by the equilibrium between heating and cooling via cyclo-synchrotron radiation where one has to consider two domains for the solution of this problem: (1) hot electrons, where the typical electron Lorentz factors are of the order 100-1000 and (2) warm electrons, where the electron Lorentz factor is still close to unity.

The first domain is in a regime where synchrotron emission is important and also very effective. This requires only low accretion rates ($\dot{M} \sim 10^{-10} M_{\odot}/\mathrm{yr}$) and hence permits only moderately high black hole masses of the order $M_{\bullet} \simeq 10^{3-5} M_{\odot}$ (Ozernoy 1992; Mastichiadis & Ozernoy 1992). The radio spectrum in such a configuration is mainly due to the optically thin part of a quasi mono-energetic (or Maxwellian) electron distribution and was calculated also by Duschl & Lesch (1994), Beckert & Duschl (1997), and used with in the jet model (Falcke 1996b).

The second domain is in the transition regime between cyclotron and synchrotron radiation, which is less effective than pure synchrotron radiation and hence requires higher accretion rates ($\dot{M} \sim 10^{-4} M_{\odot}/\mathrm{yr}$) and a higher black hole mass of the order $M_{\bullet} \simeq 10^{6} M_{\odot}$ (Melia, Jokipii, & Narayanan 1992; Melia 1992a; Melia 1994).

The big advantage of the wind-accretion approach is that it, firstly, appears unavoidable and, secondly, self-consistently ties observable parameters and accretion rate to the mass of the central object.

On the other hand there are several problems to be considered: firstly, it is not at all clear that the wind-producing stars, as an ensemble, have zero angular momentum, thus producing a non-zero angular momentum of the winds to be accreted. This would diminish the accretion rate as pointed out by Falcke (1996b). Hydrodynamical simulations show that the exact distribution and velocity of stellar wind sources within the observationally allowed range indeed can change the expected accretion rate (Coker & Melia 1997). Another question is whether the stellar winds are indeed isotropic. The only resolved stellar wind seen in the Galactic Center so far, the wind of IRS 7 (Yusef-Zadeh & Morris 1991), looks like a cometary tail pointing *away* from Sgr A*. This raises the question whether there is a wind (Chevalier 1992) or expanding bubble pushing gas out of the Galactic Center.

There also could be residual angular momentum in Sgr A* itself, e.g., because of a fossil accretion disk which could catch the inflow further out, filling a reservoir of rather dense matter instead of directly feeding the black hole. The viscous time scales of such a disk can be very long – up to 10^7 years (Falcke & Heinrich 1994).

However, detailed calculations of such a process (Falcke & Melia 1997; Coker, Melia, & Falcke 1999) indicate that the impact of the wind onto the fossil disk should produce a non-negligible IR emission that is not seen.
An alternative to the models mentioned above was proposed by Narayan, Yi, & Mahadevan (1995) and Narayan et al. (1998), who explain the discrepancy between high accretion rate and low luminosity by the effects of an advection dominated accretion flow (ADAF) or disk. In this model more than 99.9% of the energy is not radiated but transported through the disk by advection and finally swallowed by the black hole. And, in fact, it appears as if advection is non-negligible in many accretion disks, but whether indeed such a high fraction of the energy is transported by advection alone is not at all clear. One also has to make sure that not a substantial fraction of the energy is released in the inner parts of the disk and that the energy is swallowed quietly by the black hole. Even if an advection dominated accretion flow is not the whole story, it may be an interesting part of it.
A major problem of the ADAF model is that it under-predicts the cm-wave emission in the spectrum of Sgr A* by more than an order of magnitude. In Narayan et al. (1998) this is fixed by artificially assuming a constant electron temperature in the accretion flow over a particular range in radius r. The range was hand-picked such that the cm-wave spectrum is fitted by a $\nu^{1/3}$ spectrum, reminiscent of the spectra produced by Ozernoy (1992) and Beckert & Duschl (1997). Another fix was proposed by Mahadevan (1998) who added a power-law distribution of protons producing high-energy pairs in hadronic interactions. The proton power law would require shock acceleration in the accretion flow which requires turbulent plasma waves (e.g., Schlickeiser, Campeanu, & Lerche 1993; Schneider 1993). It has to be ensured that these waves do not couple to electrons as well, otherwise this would lead to heating and shock acceleration of electrons. In this case the basic assumption of a two-temperature plasma, a fundamental assumption of ADAFs, would break down. In astrophysical plasmas we generally do see that electrons are accelerated at shocks – after all, this is the basic explanation for the power-law radio spectra one sees in AGN. Therefore, the predictions of the ADAF model in terms of the spectral characteristics of Sgr A* are less than satisfying at present. In the following section we will discuss as an alternative the application of the jet model to the observed characteristics of Sgr A*.

3.8 The Jet Model

The latest information for Sgr A* comes from the possible detection of Sgr A* at X-ray wavelengths with the satellite Chandra (Baganoff et al. 1999). The first epoch data show a point source at the location of Sgr A* with a rather low X-ray luminosity around $0.5 - 1 \cdot 10^{34}$ erg s^{-1} in the 0.5-10 keV band (Baganoff et al., priv. comm.) – even lower than the earlier ROSAT limit of $\sim 2 \cdot 10^{34}$ erg s^{-1} (Predehl & Trümper 1994). This new measurement provides a crucial constraint

for any model of radiative emission from Sgr A*.
Given these new observations and the possible recent mm-VLBI detection of a small-scale jet (Lo et al. 1998), it is perhaps timely to revisit the jet model for Sgr A* (Falcke, Mannheim, & Biermann 1993) with the additional constraints provided by the Chandra observations. Here, we will therefore look at refined numerical calculations developed by Falcke & Markoff (2000) for the jet model using more realistic electron distributions also including the contribution of synchrotron self-Compton (SSC) emission. Thus, we will be able to show that the jet model can account in detail for the observed properties of Sgr A*, specifically the spectrum from cm- to mm-waves, the low X-ray emission, the apparent lack of extended emission in VLBI observations, and the possibly frequency-dependent size of the radio core.
The basic model is already outlined in Chapter 2, for a magnetized, relativistic proton and electron plasma leaving a nozzle close to the black hole. The velocity field is described by Eq. 2.10. As before, the gravitational potential is ignored since its influence is rather small in the supersonic regime considered here. The size of the nozzle z_0, i.e. the location of the sonic point, remains a free parameter, since an undisputed model for the launching mechanism of astrophysical jets has not been found yet even though we know that they launch.
Given an initial magnetic field B_0, a relativistic electron total number density n_0 with a characteristic electron energy $\gamma_{\rm e,0}m_{\rm e}c^2$, radius r_0 of the nozzle, and taking only adiabatic cooling due to the longitudinal pressure gradient (i.e. $\propto \mathcal{M}^{\Gamma-1}$, where $\mathcal{M}$ is the Mach number) and dilution by the lateral expansion into account, one can determine the magnetic field $B(z_*)$, particle density $n(z_*)$, electron Lorentz factor $\gamma_{\rm e,0}(z_*)$, and jet radius as a function of the dimensionless distance from the nozzle $z_* = (z - z_0)/r_0$:

$$
\begin{aligned}
\mathcal{M}(z_*) &= \frac{\gamma_{\rm j}\beta_{\rm j}}{\gamma_{\rm s,0}\beta_{\rm s,0}}, && (3.9)\\
n(z_*) &= n_0 \cdot \left(r(z_*)/r_0\right)^{-2} \mathcal{M}^{-1}(z_*), && (3.10)\\
r(z_*) &= r_0 + z_*/\mathcal{M}(z_*), && (3.11)\\
\gamma_{\rm e}(z_*) &= \gamma_{\rm e,0} \cdot \mathcal{M}^{-1/3}(z_*), && (3.12)\\
B(z_*) &= B_0 \cdot \left(r(z_*)/r_0\right)^{-1} \mathcal{M}^{-2/3}(z_*). && (3.13)
\end{aligned}
$$

This fixes the basic parameters for synchrotron and SSC emission along the entire jet.
We assume that magnetic field and relativistic electrons are in approximate equipartition, with $k(B^2/8\pi) = \int E_e n_e(E_e) dE_e$, where $n_e(E_e)$ is the energy-dependent electron number density, and $k \approx 1$. The form of the electron distribution will be discussed below.
By approximating the jet as a series of cylindrical sections, we can calculate the total emission by integrating over the contributions from each component. For each segment the optical depth to synchrotron absorption is $\tau_\nu = \frac{\pi}{2}\alpha_\nu r(z_*)/D \sin\theta_i$,

where θ_i is the angle between the jet axis and the line of sight, α_ν is the absorption coefficient, $D = [\gamma(1-\beta\cos\theta_i)]^{-1}$ is the Doppler factor accounting for the angle aberration (e.g., Lind & Blandford 1985) due to the relativistic bulk velocity, $\beta(z_*)c$, in the jet. Using the transfer equation for source-only emission, assumed constant within the segment, we get $I_\nu(\tau_\nu) = (1-\mathrm{e}^{-\tau_\nu})S_\nu$ where $S_\nu = j_\nu/\alpha_\nu$ is the source function. Assuming isotropic emission in the rest frame of the cylindrical shell, the net flux out of the component is $F_\nu = 4\pi I_\nu$. The observed flux density is then $F'_{\nu'} = D^2 2r(D\sin\theta_i)\Delta z F_\nu/4\pi d_{gc}^2$, where the distance to the Galactic Center is assumed to be $d_{gc} = 8.5$ kpc and the $2r(D\sin\theta_i)\Delta z$ factor is the approximate projected surface area of the radiating cylinder. The $D\sin\theta_i$ term cancels in the optically thin regime and in the limits of $\tau\to 0$ and $\tau\to\infty$, we recover the correct optically thin and optically thick solutions.

To calculate the inverse-Compton up-scattered emission for the same segment, we can ignore projection effects since the optical depth for Compton scattering is small and use the self-absorbed synchrotron emission in the component frame calculated above. Then, using the general expression for Compton scattering (Blumenthal & Gould 1970) by a distribution of electrons (including the Klein-Nishina limit), we find the SSC emission in the frame of the component which then is transformed into the observers frame as before.

3.8.1 Radio Spectrum

The basic parameters for the jet – B_0, $\gamma_{\mathrm{e},0}$, and r_0 – are fixed within a factor of a few by the location of the submm-bump in the spectrum and which, in this model, is mainly produced by emission from the nozzle (Falcke 1996b). The steep spectral cut-off towards the IR further constrains the electron distribution. It indicates the lack of a power-law tail of high-energy electrons, which usually produces the optically thin high-frequency emission seen, for example, in Blazars. Here, we explore two seemingly prevalent possibilities for the electron distribution. First, we consider a narrow power law with a sharp cut-off at roughly $5\gamma_{\mathrm{e},0}$. Alternatively we consider a relativistic thermal Maxwellian distribution with $\gamma_{\mathrm{e},0} \approx 3.5\frac{kT}{m_\mathrm{e}c^2}$. Since the allowed width of the electron distribution is very narrow in all cases, the different distributions do not produce a significantly different cm- to mm-wave radio spectrum, but slightly affect the high-energy cut-off and the SSC spectrum. Figure 3.11 shows a fit to the submm and cm radio spectrum for the two electron distributions with the nozzle parameters given in the plot. We are plotting F_ν rather than νF_ν thus allowing one to better judge the quality of the spectral fit at cm-waves. The nozzle component accounts for most of the submm-bump, as well as the main Compton component, and the low-frequency spectrum stems from the emission of the more distant parts along the jet. Within the model, the slope of the cm-wave spectrum and the ratio between cm and submm emission is mainly determined by the inclination angle. The parameters we obtain for jet and nozzle are very close to those used by Falcke (1996b), Beckert & Duschl (1997), and Falcke & Biermann (1999). The jet-specific parameters appear reasonable: the

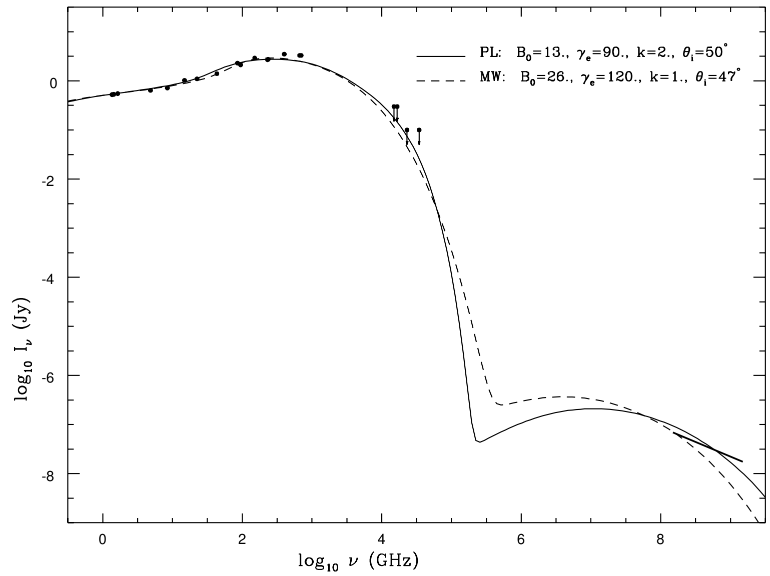

Figure 3.11: Broad-band spectrum of Sgr A* for a power-law distribution of electrons (PL) and a relativistic Maxwellian distribution (MW). The width of the nozzle is $r_0 = 4R_\mathrm{s}$ and $r_0 = 3R_\mathrm{s}$ respectively, while its height is $z_0 = 3r_0$. The dots are the simultaneous spectrum measured by Falcke et al. (1998) with additional high-frequency data discussed by Serabyn et al. (1997). In the hard X-rays we show the possible detection of Sgr A* with Chandra as a short straight line (Baganoff, Morris, priv. comm.). At this point the spectral index is not yet well determined and could possibly become steeper. For the MW, we can also obtain a similar fit as the PL, but we show one with no hard X-rays in order to indicate the flexibility in the X-ray fluxes.

inclination angle is rather average, size of the nozzle is a few times R_s, and the system is very close to equipartition.

3.8.2 X-ray Flux

Once the radio spectrum due to synchrotron emission is fixed, so is the Compton up-scattered spectrum. The peak frequency of the latter is $\sim 4\gamma_\mathrm{e}^2$ times the peak frequency of the synchrotron emission being up-scattered. Hence, in order to produce soft X-ray emission from 1 THz synchrotron emission one needs electron Lorentz factors in the range of a few hundred. This is just the range required to produce the correct radio emission from the nozzle.

In Figure 3.11, we compare the SSC spectrum with the currently available data for Sgr A* from the X-ray satellite Chandra (Baganoff, Morris, priv. comm.). Since it is not clear at present whether this flux is entirely from a point source or contains extended emission as well this again should be taken as a tentative number or possibly an upper limit. For a narrow power-law distribution we get roughly the correct X-ray luminosity and a slightly steeper slope than the reported value. However, at the time of writing the spectral shape of the observed X-ray emission was still subject to scrutiny. For a Maxwellian distribution the predicted slope in the model is slightly steeper. By changing the nozzle parameters within the range allowed by the radio data, the X-ray spectrum can be shifted around the measured value, as demonstrated in the figure.

The predictions from this model are clear: we would expect significant SSC emission in the EUV and the softer X-ray band. Given the variability of the radio emission we also expect to see correlated submm and X-ray variability. The spectral shape in the X-rays is not expected to be a perfect power law. It remains to be seen, how much of the observed X-ray emission is from extended hot gas in and outside the accretion region and how much is SSC emission from Sgr A* itself. A mixture of both components is certainly possible; in that case the nozzle should most likely reveal itself through variability in the soft X-ray bands. Complete absence of X-ray variability would argue against SSC emission giving a major contribution. This is possible if the width of the electron distribution is even narrower thus cutting off the SSC X-ray spectrum at even lower energies.

3.8.3 VLBI Size and Extended Emission

Possibly the most important constraints for any model are the VLBI measurements of the size of Sgr A*. Since most models have a stratified structure, the size of Sgr A* is expected to be a function of frequency. We note that for a given observing frequency the emission in the jet model is highly concentrated to one spatial scale. The emission from the jet at a particular frequency is self-absorbed at small distances from the origin and cuts off at large distances where the decreased magnetic field shifts the synchrotron cut-off frequency below the observing frequency. This is illustrated in Fig. 3.12, where we show a longitudinal cut through the jet based on our model. Each line corresponds to a different observing frequency and one can see that the flux towards larger distances from the core falls off rather steeply, i.e. exponentially rather than with a power law.

Thus, extended emission from the jet is highly (almost exponentially) suppressed and the size of the detectable core will be a power law $z \propto \nu^{-\aleph}$ with $\aleph$ in the range 0.9 to 1. This also implies a shift of the location of the core with frequency. Figure 3.13 compares the predicted full width at half maximum (FWHM) of major and minor axis of the emission predicted by the jet model with the constraints imposed by high-frequency VLBI observations. Throughout the cm-wave range the emission basically resembles one elliptical component decreasing in size with wavelength and only at mm-waves (i.e. above 30 GHz) an even more compact core-component, the nozzle, appears. Hence, as long as the FWHM predicted in the model is compatible with the observed values it will be difficult to distinguish the Sgr A* source structure at one frequency from a Gaussian VLBI component.

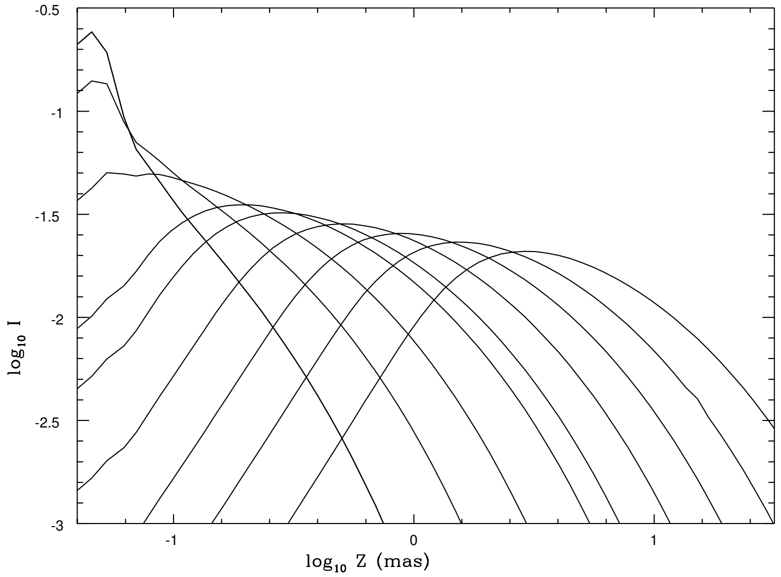

Figure 3.12: Longitudinal cuts along the jet axis for our model (Maxwellian electron distribution) at various frequencies. Plotted are the observed flux per segment in arbitrary units versus the observed separation in milli-arcseconds (mas) from the black hole. Curves to the left represent higher frequencies and the spikes in the left-most flux distributions are due to the nozzle.

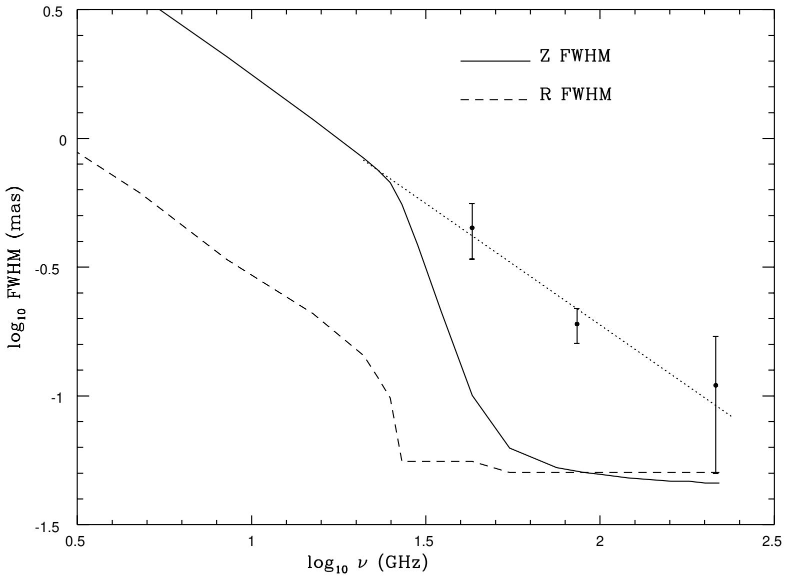

Figure 3.13: FWHM of the major and minor axis of the jet model as a function of frequency. The filled dots mark the FWHM as measured by Lo et al. (1998; 43 GHz) and Krichbaum et al. (1998; 86 & 215 GHz). At frequencies above 30 GHz one obtains a two component structure with an increasingly stronger core (nozzle, solid dashed line) and a fainter jet component (dotted line).

3.8.4 Conclusions from Applying the Jet Model

The spectrum of Sgr A*, including the new X-ray observations from Chandra, can be modeled entirely by emission from this jet alone. We can also show that the radio emission satisfies all constraints imposed by VLBI observations. This shows that the basic model introduced by Falcke, Mannheim, & Biermann (1993) can provide a detailed explanation of the Sgr A* radio and X-ray spectrum. It also fits Sgr A* within the frame work of compact radio cores discussed in Chapters 2 and 4.

One counter argument often heard in the context of modeling Sgr A* as a jet is that one does not **see** a jet. However, in typical AGN core-jet sources the extended jet structure is due to an optically thin power law. Here this extended emission is greatly suppressed due to the steep cut-off in the electron spectrum, required by the IR limits. This naturally can explain the compact jet structure as seen by Lo et al. (1998). Sgr A*, basically is a naked core without much jet emission. The lack of optically thin emission could also help to reduce the level of linear polarization in Sgr A* compared to more powerful AGN (see Sec. 3.5), since the degree of polarization decreases to zero near the self-absorption frequency due to radiation transfer effects.

The main assumption of the model is the presence of a nozzle close to the central black hole collimating a relativistic plasma with approximate equipartition between the magnetic field and relativistic particles. The evolution of magnetic field and particle density is calculated self-consistently and does not require additional parameters beyond those fixed for the nozzle. The spectra we obtain are therefore generic for collimated outflows from any accretion flow – whether a magneto-hydrodynamical jet from a standard accretion disk or an outflow from an ADAF – provided the accretion flow can produce the required magnetic field, electron temperature, and density near its inner edge. For an ADAF or Bondi-Hoyle type accretion the presence of a jet near the black hole could thus aid those models in accounting for the cm-wave radio emission, which is especially difficult. The energy requirements to produce such a jet (see Falcke & Biermann 1999) are rather small compared to the power available through accretion of nearby winds (Coker & Melia 1997).

It remains to be seen whether one can construct a self-consistent model which couples an outflow as described here together with, for example, an ADAF model. Particularly interesting in this context is whether one could reproduce the unusual electron distribution found in Sgr A*. As pointed out in Falcke (1996b) the typical electron Lorentz factors required in the nozzle are close to those expected from pair production in proton-proton (pp) collisions. Mahadevan (1998) showed that an ADAF could in principle provide the environment where pp-collisions could play an important role even though in this paper a power-law distribution of protons had to be artificially added. More detailed calculations in this direction should therefore be undertaken in the future.

3.9 Future Prospects - Imaging of the Event Horizon

As one can easily see from the previous sections the ever growing interest in Sgr A* has already yielded a number of tantalizing results, the most important being that Sgr A* is the best supermassive black hole candidate we know. VLBI observations are already approaching scales which are not far from the actual scale of the black hole and the presence of the submm-bump indicates that even more compact emission is present at yet smaller scales – possibly as close in as the event horizon of the black hole. It is therefore worth exploring whether we have in principal a chance to actually approach this scale with imaging techniques and to ask what we would expect to see. This naturally will have to be done at the highest radio frequencies where the resolution is highest and the scatter-broadening of Sgr A* is the lowest.

At submm wavelengths, the various models indeed predict that the synchrotron emission of Sgr A* is not self-absorbed, allowing a view into the region near the event horizon. The size of this event horizon is $(1+\sqrt{1-a_*^2})R_g$, where $R_g \equiv GM/c^2$, M is the mass of the black hole, G is Newton's constant, c the speed of light, $a_* \equiv Jc/(GM^2)$ is the dimensionless spin of the black hole in the range 0 to 1, and J is the angular momentum of the black hole.

Bardeen (1973) described the idealized appearance of a black hole in front of a planar emitting source, showing that it literally would appear as a 'black hole'. At that time such a calculation was of mere theoretical interest and limited to just calculating the envelope of the apparent black hole. Falcke et al. (1998) suggested to apply this basic idea also to Sgr A* where it could possibly be tested with submm-VLBI. To further check whether there is indeed a realistic chance of seeing this 'black hole' in Sgr A* (Falcke, Melia, & Agol 2000) reported calculations obtained with a general relativistic (GR) ray-tracing code that allows one to simulate observed images of Sgr A* for various combinations of black hole spin, inclination angle, and morphology of the emission region directly surrounding the black hole and not just for a background source.

3.9.1 The Appearance of a Black Hole

The appearance of the emitting region around a black hole was determined by Falcke, Melia, & Agol (2000) under the condition that it is optically thin. For Sgr A* this might be the case for the submm-bump (Falcke et al. 1998) indicated by the turnover in the spectrum, and can always be achieved by going to a suitably high frequency. For the qualitative discussion the emissivity was assumed to be frequency independent and to be either spatially uniform or to scale as r^{-2}. These two cases cover a large range of conditions expected under several reasonable scenarios, be it a quasi-spherical infall, a rotating thick disk, or the base of an outflow.

The calculations took into account all the well-known relativistic effects, e.g., frame dragging, gravitational redshift, light bending, and Doppler boosting. The code is valid for all possible spins of the black hole and for any arbitrary velocity field of the emission region.

For a planar emitting source behind a black hole, a closed curve on the sky plane divides a region where geodesics intersect the horizon from a region whose geodesics miss the horizon (Bardeen 1973). This curve, which is referred to as the "apparent boundary" of the black hole, is a circle of radius $\sqrt{27}R_g$ in the Schwarzschild case ($a_* = 0$), but has a more flattened shape of similar size for a Kerr black hole, slightly dependent on inclination. The size of the apparent boundary is much larger than the event horizon due to strong bending of light by the black hole. When the emission occurs in an optically thin region *surrounding* the black hole, the case of interest here, the apparent boundary has the same exact shape since the properties of the geodesics are independent of where the sources are located. However, photons on geodesics located within the apparent boundary that can still escape to the observer experience strong gravitational redshift and a shorter total path length, leading to a smaller integrated emissivity, while photons just outside the apparent boundary can orbit the black hole near the circular photon radius several times, adding to the observed intensity (Jaroszynski & Kurpiewski 1997). This produces a marked deficit of the observed intensity inside the apparent boundary – the "shadow" of the black hole.

We here consider a compact, optically-thin emitting region surrounding a black hole with spin parameter $a_* = 0$ (i.e., a Schwarzschild black hole) and a maximally spinning Kerr hole with $a_* = 0.998$. In the set of simulations shown in Fig. 3.14, the viewing angle i was taken to be 45° with respect to the spin axis (when it is present) with two distributions of the gas velocity v. The first has the plasma in free-fall, i.e., $v^r = -\sqrt{2r(a^2 + r^2)}\Delta/A$ and $\Omega = 2ar/A$, where v^r is the Boyer-Lindquist radial velocity, Ω is the orbital frequency, $\Delta \equiv r^2 - 2r + a^2$, and $A \equiv (r^2+a^2)^2 - a^2\Delta\sin^2\theta$. (We have set $G = M = c = 1$ in this paragraph.) The second has the plasma orbiting in rigidly rotating shells with the equatorial Keplerian frequency $\Omega = 1/(r^{3/2} + a)$ for $r > r_{ms}$ with $v^r = 0$, and infalling with constant angular momentum inside $r < r_{ms}$ (Cunningham 1975), with $v^\theta = 0$ for all r.

In order to display concrete examples of how realistic the proposed measurements of these effects with VLBI will be, the expected images were simulated for the massive black hole candidate Sgr A* at the Galactic Center. For its measured mass (Eckart & Genzel 1996; Ghez et al. 1998) $M = 2.6 \times 10^6\ M_\odot$, the scale size for this object is the gravitational radius $R_g = 3.9 \times 10^{11}$ cm, which is half of the Schwarzschild radius $R_s \equiv 2GM/c^2$.

To simulate an observed image one has to take two additional effects into account: interstellar scattering and the finite telescope resolution achievable from the ground. Scatter-broadening at the Galactic Center is incorporated by smoothing the image with an elliptical Gaussian with a FWHM of 24.2 μarcsecond$\times(\lambda/1.3\,\mathrm{mm})^2$ along the major axis and 12.8 μarcsecond$\times(\lambda/1.3\,\mathrm{mm})^2$

along the minor axis (Lo et al. 1998). The position angle of this ellipse is arbitrary since one does not know yet the spin axis of the black hole on the sky and PA=90° was assumed for the major axis. The telescope resolution – in an idealized form – is then added by convolving the smoothed image with a spherical Gaussian point-spread function of FWHM 33.5 μarcsecond$\times(\lambda/1.3\,\mathrm{mm})^{-1}(l/8000\mathrm{km})^{-1}$ – the possible resolution of a global interferometer with 8000 km baselines (Krichbaum 1996). In reality the exact point-spread-function will of course depend on the number and placement of the participating telescopes.

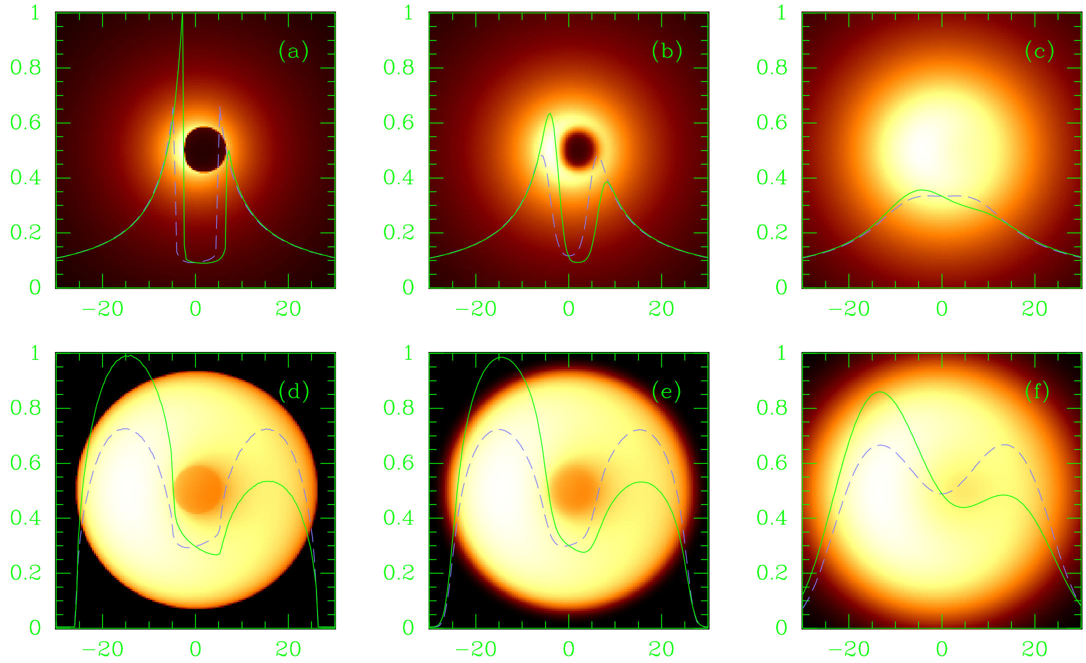

Figure 3.14: An image of an optically thin emission region surrounding a black hole with the characteristics of Sgr A* at the Galactic Center. The black hole is here either maximally rotating ($a_* = 0.998$, panels a-c) or non-rotating ($a_* = 0$, panels d-f). The emitting gas is assumed to be in free fall with an emissivity $\propto r^{-2}$ (top) or on Keplerian shells (bottom) with a uniform emissivity (viewing angle $i = 45°$). Panels a&d show the GR ray-tracing calculations, panels b&e are the images seen by an idealized VLBI array at 0.6 mm wavelength taking interstellar scattering into account, and panels c&f are those for a wavelength of 1.3 mm. The intensity variations along the x-axis (solid green curve) and the y-axis (dashed purple/blue curve) are overlayed. The vertical axes show the intensity of the curves in arbitrary units and the horizontal axes show the distance from the black hole in units of R_g which for Sgr A* is 3.9×10^{11} cm ~ 3 μarcseconds.

The results of the two different models with and without scattering at two different observing wavelengths are shown in Fig. 3.14. The two distinct features that are evident in the top panel for a rotating black hole are (1) the clear depression in I_ν – the shadow – produced near the black hole, which in this particular example represents a modulation of up to 90% in intensity from peak to trough, and (2) the size of the shadow, which here is $9.2R_\mathrm{g}$ in diameter. This represents a projected size of 27 μarcseconds, which is already within a factor of two of the current VLBI resolution (Krichbaum et al. 1995). The shadow is a generic feature of various other models one can look at, including those with outflows, cylindrical emissivity, and various inclinations or spins.

This black hole shadow is also visible in the second illustrated case for a non-rotating black hole with a modulation in I_ν in the range of 50-75% from peak to trough, and with a diameter of roughly $10.4\,R_g$. In this case, the emission is asymmetric due to the strong Doppler shifts associated with the emission by a rapidly moving plasma along the line-of-sight (with velocity v_ϕ).

The important conclusion is that the diameter of the shadow – in marked contrast to the event horizon – is fairly independent of the black hole spin and is always of order $10R_{\rm g}$. Indeed, this is consistent with the observed 0.8 mm size limit $> 4R_g$ of Sgr A* from a lack of scintillation (Gwinn et al. 1991). The presence of a rotating hole viewed edge-on will lead to a shifting of the apparent boundary (by as much as 2.5 R_g, or 8 μarcseconds) with respect to the center of mass, or the centroid of the outer emission region.

Interestingly, the scattering size of Sgr A* and the resolution of global VLBI arrays become comparable to the size of the shadow at a wavelength of about 1.3 mm. As one can see from Figures 3.14c&f the shadow is still almost completely washed out for VLBI observations at 1.3 mm, while it is very apparent at a factor two shorter wavelength (Figures 3.14b&e). In fact, already at 0.8 mm (not shown here) the shadow can be easily seen. Under certain conditions, i.e., a very homogeneous emission region, the shadow would be visible even at 1.3 mm (Fig. 3.14f).

3.9.2 How Realistic is Such an Experiment?

The arguments for the feasibility of such an experiment are rather compelling. First of all, the mass of Sgr A* is known within 20%, the main uncertainty being the exact distance to the Galactic Center and the exact choice of the mass estimator to interpret the stellar proper motions. Since, as shown, the unknown spin of the suspected black hole contributes only another 10% uncertainty, one can conservatively predict the angular diameter of the shadow in Sgr A* from the GR calculations alone to be $\sim 30 \pm 7\,\mu$arcseconds independent of wavelength. As seen in Fig. 3.14, the finite telescope resolution and the scatter broadening will make the detectability of the shadow a function of wavelength and emissivity; however, the size of the shadow will remain of similar order of magnitude and cannot become smaller under any circumstance.

The technical methods to achieve such a resolution at wavelengths shortwards of 1.3 mm are currently being developed and a first detection of Sgr A* at 1.4 mm with VLBI has already been reported. The challenge will be to push this technology even further towards 0.8 or even 0.6 mm VLBI. Over the next decade many more telescopes are expected to operate at these wavelengths. Depending on how short a wavelength is required, the projected time scale for developing the necessary VLBI techniques may be about ten years. A fundamental problem preventing such an experiment is not now apparent, but in light of our results, planning of the new submm-telescopes should include sufficient provisions for VLBI experiments. A potential problem with the model could be the unknown morphology of the emission region. Strong velocity fields and density inhomogeneities would make an identification of the shadow in an observed image more difficult. However, inhomogeneities are unlikely to be a major issue, since the time scale for rotation around the black hole in the Galactic Center is only a few hundred seconds and hence much less than the typical duration of a VLBI observation. The strong shear near the black hole would tend to smooth out any inhomogeneities very quickly. Indeed, submm variability studies on such short time scales (Gwinn et al. 1991) have yielded negative results. The same argument applies to emission models which are offset from the black hole, e.g., are one-sided. Since the shadow of the black hole has a very well defined shape it would under any conditions appear as a distinct feature, given that the dynamic range of the map is large enough (i.e., $\gtrsim$100:1, considering a range of emission models, Agol et al., in prep.).

Finally, synchrotron self-absorption could pose a problem. So far the available submm spectra show a flattening of the spectrum around 1.3-0.6 mm indicating a turnover towards an optically thin spectrum.

The importance of the proposed imaging of Sgr A* at submm wavelengths with VLBI cannot be overemphasized. The bump in the spectrum of Sgr A* (Sec. 3.2 strongly suggests the presence of a compact component whose proximity to the event horizon is predicted to result in a shadow of measurable dimensions in the intensity map. Such a feature seems unique and Sgr A* seems to have all the right parameters to make it observable. The observation of this shadow would confirm the widely held belief that most of the dark mass concentration in the nuclei of galaxies such as ours is contained within a black hole, and it would be the first direct evidence for the existence of an event horizon largely independent of any modelling. A non-detection with sufficiently developed techniques, on the other hand, might pose a major problem for the standard black hole paradigm. Because of this fundamental importance, the experiment proposed here should be a major motivation for intensifying the current development of submm astronomy in general and mm- and submm-VLBI in particular.

This result also shows the outstanding position Sgr A* has among known radio cores. For other supermassive black holes, with the exception perhaps of the very massive black hole in M87, the shadow will be much smaller than in Sgr A* because of the much larger distances.

Chapter 4

Low-Luminosity AGN

In Chapter 2 we have discussed the general theory of compact radio cores and the jet-disk symbiosis. The conclusion was that compact radio cores are rather scale invariant and only subject to changes in the accretion rate onto the central black hole. As a consequence, the paper by Falcke & Biermann (1996) basically predicted the presence of a large number of galaxies with faint radio cores at low levels of activity. With the finding of black holes in many nearby galaxies and the identification of a huge crowd of low-luminosity AGN, many of them compiled in the spectroscopic atlas by Ho, Filippenko, & Sargent (1995), it was clear that from this theory one would expect a large number of galaxies with compact radio cores (see also Perez-Fournon & Biermann 1984). These radio cores should bridge the gap between Sgr A* and quasars. The imperative then was to find them in a significant number and compare their properties with more luminous counter parts.

This comparison is also important since the question of how central engines in high and low-luminosity AGN are related to each other and why they appear so different despite being powered by the same type of object is of major interest. For many nearby galaxies with low-luminosity nuclear emission-lines, it is not even clear whether they are indeed powered by an AGN or by star formation – despite many of them being dubbed LLAGN.

Earlier surveys have shown that E and S0 galaxies often have compact, flat-spectrum radio sources in their nuclei (Wrobel & Heeschen 1984; Slee et al. 1994). Some of the most prominent flat-spectrum nuclear radio sources in nearby galaxies are found in galaxies with LINER nuclear spectra (O'Connell & Dressel 1978), but so far there has been no comprehensive study of radio nuclei in a significant sample of LINER galaxies, which make up the majority of galaxies with low-level nuclear activity. We have, therefore, recently conducted a survey of LINER galaxies with the Very Large Array (VLA; Thompson et al. 1980) in its A configuration at 15 GHz (resolution $\sim 0\farcs15$) and the VLBA (Napier et al. 1994) at 5 GHz (resolution $\sim 0\farcs002$) to search for compact radio emission (Nagar et al. 2000; Falcke et al. 2000b). In the following sections the results of this search for "siblings of Sgr A*" and their interpretation are presented.

4.1 Detection of Flat-Spectrum Radio Cores with the VLA

Observations were made of two samples (Nagar et al. 2000; Falcke et al. 2000b). All sources were drawn from the extensive and sensitive spectroscopic study of the complete, magnitude-limited sample of 486 nearby galaxies mentioned above (Ho, Filippenko, & Sargent 1995), one third of which showed LINER-like activity (Ho, Filippenko, & Sargent 1997). From these active galaxies with a LINER spectrum a subsample (dubbed "48 LINERs" sample) of 48 bright sources was drawn with no well-defined selection criterion other than that they had been observed with other telescopes as well, e.g., ROSAT, the HST (UV imaging, Maoz et al. 1996; Barth et al. 1998), and the VLA at 1.4 and 8.4 GHz in A and B configuration (van Dyk & Ho 1998). The sample also included so-called transition objects which have spectra intermediate between LINER and H II region galaxies. While the project was being conducted a few sources in the original LINER sample were re-classified as low-luminosity Seyfert galaxies. Transition objects were included because for these objects it was not clear whether their emission-line spectrum is produced by intense star formation or whether they are simply LINERs with a very faint AGN.

In a second step we compiled a distance limited sample (dubbed "96 LLAGN" sample) from the (Ho, Filippenko, & Sargent 1995) atlas, selecting all galaxies with LINER, Seyfert, and transition spectra within 19 Mpc. This will reduce the effects of any bias that might have come from the rather ill-defined selection criterion of the first sample. By including LINERs, Seyferts, and Transition objects we will also be able to see possible differences in the detection rates between the different types. By choosing a distance limited sample, constrained to the very local universe, we also make sure to study the faintest AGN we can find today.

Both samples were observed with the VLA at 15 GHz in its largest configuration (A) providing maximal resolution, i.e. up to $0\farcs15$ corresponding to a linear scale of 14 pc at a distance of 19 Mpc. The 5σ detection limit was around 1 mJy.

The rationale behind going to this setup is that the extended emission from AGN is optically thin and steep-spectrum. Radio cores, on the other hand – if they are produced on scales very close to the AGN – are optically thick, and compact at milli-arcsecond scales. This means that by going to the configuration with the highest resolution one will resolve out most of the extended emission and get a clearer view on the compact structure. At higher frequencies this effect is even stronger since the beam size is inversely proportional to the frequency, reducing the extended flux per beam. The steep spectrum will diminish the flux density of the extended emission even further. The reason that one does not go to even higher frequencies is simply a technical one, since the achievable sensitivity with the current instrumentation of the VLA becomes increasingly worse at 22 and 43 GHz.

The results of the first survey for the 48 LINERs is summarized in Table 4.1.

The first striking result is that we detected relatively many, namely 18 out of 48 galaxies (37%). Split into the different groups we detected only 1 out of 18 transition objects, but 6 out of 8 Seyferts and 11 out of 22 LINERs, yielding a combined detection rate for Seyferts and LINERs of 57% compared to only 6% for transition objects.
Using literature data (the VLA data at lower frequencies is still being processed by another group) it was possible to determine whether the detected cores should be considered as flat- or steep-spectrum cores. Out of the 18 detected cores only two apparently had a steep radio spectrum. Hence, the 15 GHz VLA observations were indeed properly designed to discriminate against steep-spectrum emission and to pick out the flat-spectrum cores.
The high detection rate is confirmed by observations of the second sample summarized in Table 4.2. Since this is a distance limited sample selection effects should be minimized. The detection rate is 40 out of 96 galaxies, i.e. 42%. In the sample we detected only 5 out of 28 transition galaxies (18%), while we detected 35 out of 68 Seyferts and LINERs (51%). At least 28 out of 68 Seyferts and LINERs have flat-spectrum cores (41%), while only 3 out of 28 transition objects do (11%), two of which are in doubt.
We can therefore conclude that galaxies with Seyfert and LINER spectra are much more likely to contain flat-spectrum radio cores than transition objects. The latter are therefore probably significantly weaker AGN or are largely dominated by starbursts. On the other hand, if one considers flat-spectrum cores as evidence for a black hole powered AGN, we can conclude that at least about half of LINERs and Seyferts are indeed genuine AGN. If we can combine both samples we find no significant difference in the detection rates between Seyferts and LINERs. Given the difficulty of finding clear AGN evidence in these weakly active galaxies by looking for broad emission-lines (Ho et al. 1997) the VLA survey at 15 GHz seems to be a relatively efficient way of identifying AGN.
However, these conclusions all rest on the assumption of flat-spectrum cores being AGN related. In principle the flat spectrum could also be produced by a giant free-free emission region in a star forming region. To exclude this possibility one needs to go to even higher resolution and observe the respective galaxies with VLBI. This will allow one to probe brightness temperatures around 10^8 K for the cores of interest here and distinguish between the two cases. The attempt to do this is described in the next chapter.

4.2 Detection of Flat-Spectrum Radio Cores with the VLBA

Our 15 GHz VLA survey found a surprisingly large number of galaxies with compact radio cores and flat spectral indices. The prediction from this VLA study and from our theoretical modeling was that this radio emission comes from high

Table 4.1. NEW 2 CM VLA OBSERVATIONS OF LOW-LUMINOSITY AGNs

Name (1)	Activity Type (2)	T (3)	R.A. (B1950) (4)	Dec. (B1950) (5)	Δ ('') (6)	Peak A (mJy) (7)	Total A (mJy) (8)	Dist. (Mpc) (9)	Log P_{2cm}^{core} (W Hz^{-1}) (10)	α (11)
NGC 185	S2	-5.0	00 36 09.993	48 03 50.20	14.5	0.8	0.8	0.7	16.67	?
NGC 266	L1.9	2.0	00 47 05.247	32 00 20.04	1.9	4.1	4.1	62.4	21.28	F
NGC 404	L2	-3.0	···	···	···	< 1.3	< 1.3	2.4	< 17.95	···
NGC 2655	S2	0.0	08 49 08.450	78 24 48.31	2.4	6.0	6.0	24.4	20.63	S
NGC 2681	L1.9	0.0	···	···	···	< 1.4	< 1.4	13.3	< 19.48	···
NGC 2787	L1.9	-1.0	09 14 49.468	69 24 50.81	1.6	7.0	7.0	13.0	20.15	F
NGC 3147	S2	4.0	10 12 39.818	73 39 00.79	1.6	8.0	8.1	40.9	21.21	F
NGC 3169	L2	1.0	10 11 39.413	03 42 52.60	3.5	6.8	6.8	19.7	20.50	F
NGC 3226	L1.9	-5.0	10 20 43.173	20 09 06.52	0.9	5.0	5.4	23.4	20.55	F
NGC 3642	L1.9	4.0	···	···	···	< 1.3	< 1.3	27.5	< 20.06	···
NGC 3692	T2	3.0	···	···	···	< 1.2	< 1.2	29.8	< 20.09	···
NGC 3705	T2	2.0	···	···	···	< 1.2	< 1.2	17.0	< 19.61	···
NGC 3917	T2 :	6.0	···	···	···	< 1.2	< 1.2	17.0	< 19.63	···
NGC 3953	T2	4.0	···	···	···	< 1.3	< 1.3	17.0	< 19.64	···
NGC 3992	T2 :	4.0	···	···	···	< 1.3	< 1.3	17.0	< 19.64	···
NGC 4036	L1.9	-3.0	11 58 52.765	62 10 27.73	2.4	< 1.5	< 1.5	24.6	< 20.04	···
NGC 4111	L2	-1.0	···	···	···	< 1.3	< 1.3	17.0	< 19.64	···
NGC 4143	L1.9	-2.0	12 07 04.547	42 48 44.27	1.5	3.3	3.3	17.0	20.06	F
NGC 4145	T2 :	7.0	···	···	···	< 1.3	< 1.3	20.7	< 19.81	···
NGC 4192	T2	2.0	12 11 15.488	15 10 39.62	1.5	< 1.3	< 1.3	16.8	< 19.64	···
NGC 4203	L1.9	-3.0	12 12 33.943	33 28 30.35	1.0	9.5	9.5	9.7	20.03	F
NGC 4216	T2	3.0	12 13 21.559	13 25 38.16	0.5	< 2.0	< 2.0	16.8	< 19.83	···
NGC 4220	T2	-1.0	···	···	···	< 1.4	< 1.4	17.0	< 19.70	···
NGC 4278	L1.9	-5.0	12 17 36.307	29 33 29.56	0.5	88.3	89.7	9.7	21.00	F
NGC 4419	T2	1.0	12 24 24.661	15 19 25.84	3.2	< 2.8	< 2.8	16.8	< 19.98	···
NGC 4429	T2	-1.0	···	···	···	< 1.1	< 1.1	16.8	< 19.57	···
NGC 4435	T2/H:	-2.0	···	···	···	< 1.1	< 1.1	16.8	< 19.57	···
NGC 4527	T2	4.0	···	···	···	< 1.1	< 1.1	13.5	< 19.38	···
NGC 4548	L2	3.0	12 32 55.276	14 46 17.60	1.8	1.2	1.2	16.8	19.61	F
NGC 4550	L2	-1.5	12 32 58.493	12 29 49.50	9.3	0.7	0.7	16.8	19.37	F
NGC 4565	S1.9	3.0	12 33 52.014	26 15 45.87	3.9	3.7	3.7	9.7	19.62	F
NGC 4569	T2	2.0	···	···	···	< 1.1	< 1.1	16.8	< 19.57	···
NGC 4579	S1.9/L1.9	3.0	12 35 12.000	12 05 34.85	0.7	27.6	28.3	16.8	20.98	F
NGC 4636	L1.9	-5.0	12 40 16.660	02 57 41.64	2.5	1.6	1.9	17.0	19.82	S
NGC 4639	S1.0	4.0	···	···	···	< 1.1	< 1.1	16.8	< 19.57	···
NGC 4651	L2	5.0	···	···	···	< 1.1	< 1.1	16.8	< 19.57	···
NGC 4866	L2	-1.0	···	···	···	< 1.1	< 1.1	16.0	< 19.53	···
NGC 5005	L1.9	4.0	···	···	···	< 1.1	< 1.1	21.3	< 19.78	···
NGC 5033	S1.5	5.0	13 11 09.169	36 51 30.37	1.3	1.4	1.4	18.7	19.77	F
NGC 5055	T2	4.0	···	···	···	< 1.1	< 1.1	7.2	< 18.83	···
NGC 5273	S1.5	-2.0	···	···	···	< 1.1	< 1.1	21.3	< 19.78	···
NGC 5566	L2	2.0	···	···	···	< 1.1	< 1.1	26.4	< 19.96	···
NGC 5701	T2 :	0.0	···	···	···	< 1.1	< 1.1	26.1	< 19.95	···
NGC 5866	T2	-1.0	15 05 07.121	55 57 17.77	0.3	7.1	7.5	15.3	20.32	F
NGC 6500	L2	1.7	17 53 48.137	18 20 39.90	1.5	83.5	85.0	39.7	22.21	F
NGC 7217	L2	2.0	22 05 37.830	31 06 51.50	2.7	< 0.6	< 0.6	16.0	< 19.23	···
NGC 7742	T2/L2	3.0	···	···	···	< 1.1	< 1.1	22.2	< 19.81	···
NGC 7814	L2 ::	2.0	···	···	···	< 1.1	< 1.1	15.1	< 19.48	···

Columns are: (1) galaxy name; (2) nuclear activity type as given by H97a. 'L' represents LINER, 'S' represents Seyfert, 'H' represents an H II region type spectrum, and 'T' represents objects with transitional 'L' + 'H' spectra. The ':' and '::' symbols represent uncertain, and highly uncertain, classifications, respectively; (3) Hubble morphological parameter T as listed in H97a; (4) and (5) 2 cm radio position, from our maps; (6) offset, in arcsec, between the 2 cm radio position and the position of the galaxy optical nucleus listed in Cotton et al. 2000; (7) and (8) peak and total flux density, obtained by fitting a single Gaussian, using task JMFIT, to the radio peak in the A-array image; (9) distance in Mpc to galaxy, as listed in H97a; (10) the logarithm of the core radio power (derived from the *peak* radio flux in the A-array image); (11) indication of whether the radio spectrum of the A-array 2 cm detected core is **S**teep or **F**lat; (H97a=Ho, Filippenko, Sargent 1997a)

Table 4.2. NEW 2 CM VLA OBSERVATIONS OF A DISTANCE-LIMITED LLAGN SAMPLE

Source	Typ	T	D [Mpc]	log Hα [erg/sec/cm^2]	$S_{15\mathrm{GHz,p}}$ [mJy]	$S_{15\mathrm{GHz,t}}$ [mJy]	$S_{1.4\mathrm{GHz}}$ [mJy]	α		RA (B1950)	DEC (B1950)
(1)	(2)	(3)	(4)	(5)	(6)	(7)	(8)	(9)	(10)	(11)	(12)
NGC2541	T2/H:	6	10.6	-14.9		< 1.0				–	–
NGC2683	L2/S2	3	5.7	-14.4		< 0.9				–	–
NGC2685	S2/T2:	-1	16.2	-13.8		< 0.9				–	–
NGC2787	L1.9	-1	13.0	-13.8	11.1	11.4	11.3	-0.01	F	09:14:49.47	69:24:50.82
NGC2841	L2	3	12.0	-13.7	1.1	2.1	35.9	-1.34	F	09:18:35.84	51:11:24.11
NGC3031	S1.5	2	3.3	-12.7	164.1	164.8	88.9	0.25	F	09:51:27.31	69:18:08.15
NGC3368	L2	2	8.1	-13.6		< 1.0				–	–
NGC3379	L2/T2::	-5	8.1	-13.9		< 1.0				–	–
NGC3486	S2	5	7.4	-14.0		< 0.9				–	–
NGC3489	T2/S2	-1	6.4	-13.5		< 0.9				–	–
NGC3623	L2:	1	7.3	-14.0		< 0.9				–	–
NGC3627	T2/S2	3	6.6	-13.2	1.1	2.9	< 324.9	>-2.27		11:17:38.48	13:15:55.74
NGC3628	T2	3	7.7	-15.0	1.5	28.0	291.7	-1.96	∗	11:17:40.34	13:51:46.10
NGC3675	T2	3	12.8	-14.1		< 1.0				–	–
NGC3718	L1.9	1	17.0	-14.1	10.5	10.8	16.5	-0.19	F	11:29:49.91	53:20:38.47
NGC3982	S1.9	3	17.0	-13.3		< 1.0				–	–
NGC4013	T2	3	17.0	-14.7		< 1.0				–	–
NGC4051	S1.2	4	17.0	-12.5		< 1.0				–	–
NGC4138	S1.9	-1	17.0	-14.0	1.5	1.3	20.5	-1.15	F	12:06:58.34	43:57:48.12
NGC4143	L1.9	-2	17.0	-13.8	9.8	10.0	10.8	-0.03	F	12:07:04.55	42:48:44.26
NGC4150	T2	-2	9.7	-13.9		< 1.0				–	–
NGC4168	S1.9:	-5	16.8	-14.9	3.0	3.1	6.0	-0.29	F	12:09:44.27	13:28:59.62
NGC4203	L1.9	-3	9.7	-13.7	8.8	9.0	6.6	0.13	F	12:12:33.94	33:28:30.48
NGC4216	T2	3	16.8	-14.0	1.2	1.3	6.9	-0.73	F?	12:13:21.62	13:25:38.11
NGC4258	S1.9	4	6.8	-13.4	2.6	3.0	< 2.5	> 0.04	F	12:16:29.37	47:34:53.19
NGC4278	L1.9	-5	9.7	-12.9	83.8	87.7	385.5	-0.63	F	12:17:36.16	29:33:29.27
NGC4293	L2	0	17.0	-13.8	0.7	1.4	19.3	-1.26		12:18:41.00	18:39:35.31
NGC4314	L2	1	9.7	-13.6		< 1.0				–	–
NGC4321	T2	4	16.8	-13.5		< 0.9				–	–
NGC4346	L2::	-2	17.0	-15.0		< 1.0				–	–
NGC4350	T2::	-2	16.8	-14.3		< 0.9				–	–
NGC4374	L2	-5	16.8	-13.6	180.7	183.7	<3179.4	>-1.21	F	12:22:31.58	13:09:49.82
NGC4388	S1.9	3	16.8	-12.5	2.2	3.7	120.4	-1.59		12:23:14.64	12:56:20.10
NGC4394	L2	3	16.8	-14.2		< 0.9				–	–
NGC4395	S1.8	9	3.6	-13.3		< 0.9				–	–
NGC4414	T2:	5	9.7	-14.0		< 0.9				–	–
NGC4419	T2	1	16.8	-13.3	2.7	3.6	55.4	-1.24		12:24:24.72	15:19:26.54
NGC4438	L1.9	0	16.8	-13.2		< 0.9				–	–
NGC4450	L1.9	2	16.8	-13.7	2.0	2.7	10.3	-0.64	F?	12:25:58.28	17:21:40.94
NGC4457	L2	0	17.4	-13.0		< 1.0				–	–
NGC4459	T2:	-1	16.8	-13.8		< 1.0				–	–
NGC4472	S2::	-5	16.8	-14.9	3.7	4.1	221.3	-1.74		12:27:14.18	08:16:36.00
NGC4477	S2	-2	16.8	-13.7		< 1.0				–	–
NGC4486	L2	-4	16.8	-13.1	2725.7	2835.7	138488.0	-1.67	F	12:28:17.57	12:40:01.74
NGC4494	L2::	-5	9.7	-14.5		< 0.8				–	–
NGC4501	S2	3	16.8	-13.6		< 1.1				–	–
NGC4548	L2	3	16.8	-14.1	1.4	1.6	< 2.5	>-0.24	F	12:32:55.28	14:46:17.65
NGC4552	T2:	-5	16.8	-14.0	58.1	58.6	103.1	-0.25	F	12:33:08.29	12:49:53.58
NGC4565	S1.9	3	9.7	-14.1	3.1	3.1	58.3	-1.23		12:33:52.02	26:15:45.89
NGC4579	S/L1.9	3	16.8	-13.1	20.8	20.6	98.2	-0.66	F	12:35:12.00	12:05:34.85
NGC4596	L2::	-1	16.8	-14.6		< 1.1				–	–
NGC4636	L1.9	-5	17.0	-14.3	1.6	1.8	78.7	-1.63	F	12:40:16.66	02:57:41.58
NGC4698	S2	2	16.8	-13.8		< 1.0				–	–
NGC4713	T2	7	17.9	-14.4		1.1				–	–
NGC4725	S2:	2	12.4	-14.1		< 0.9				–	–
NGC4736	L2	2	4.3	-13.6	1.9	1.7	269.9	-2.13	F	12:48:31.92	41:23:31.36
NGC4762	L2:	-2	16.8	-15.0	0.9	1.3	< 2.5	>-0.38	F	12:50:25.14	11:30:03.27
NGC4772	L1.9	1	16.3	-14.0	3.3	3.4	< 2.5	> 0.13	F	12:50:56.00	02:26:22.36
NGC4826	T2	2	4.1	-13.1		< 0.9				–	–
NGC5194	S2	4	7.7	-13.0		< 1.1				–	–
NGC5195	L2:	10	9.3	-14.1		< 1.1				–	–
NGC5879	T2/L2	4	16.8	-14.2		< 1.1				–	–
NGC6503	T2/S2:	6	6.1	-14.1		< 1.0				–	–

Here we only list the galaxies not yet listed in Table 4.1. The distance-limited sample consists of all galaxies with D<19 Mpc in Table 4.1 and Table 4.2. Columns are: (1) galaxy name; (2) nuclear activity type as given by H97a. 'L' represents LINER, 'S' represents Seyfert, 'H' represents an H II region type spectrum, and 'T' represents objects with transitional 'L' + 'H' spectra. '2' implies that no broad Hα is detected, '1.9' implies that broad Hα is present, but not broad Hβ, and '1.0' or '1.5' implies that both broad Hα and broad Hβ are detected, with the specific type depending on the ratio of the flux in [O III] λ5007 to the flux in broad + narrow Hβ (e.g., Osterbrock 1981). The ':' and '::' symbols represent uncertain, and highly uncertain, classifications, respectively; (3) Hubble morphological parameter T as listed in H97a; (4) distance in Mpc to galaxy, as listed in H97a; (5) Hα-luminosity as listed in H97a; (6) and (7) peak and total flux density, obtained by fitting a single Gaussian, using task JMFIT, to the radio peak in the A-array image; (8) flux density at 1.4 GHz obtained from the NVSS survey – the beam is more than a hundred times larger than at 15 GHz and can include a lot of extended emission; (9) spectral index between 1.4 GHz (NVSS) and 15 GHz – is meaningless for sources with a large extended emission but useful for finding flat spectrum cores; (10) spectral index flat: "F" marks sources where comparison with data from the literature at other frequencies indicates a flat-spectrum core in conjunction with our 15 GHz data, ∗NGC3628 has very extended 15 GHz emission belonging to a known star forming region; (11) and (12) 15 GHz radio position, from our maps; (H97a=Ho, Filippenko, Sargent 1997a)

Table 4.3. Properties of VLBA LINER sample

(1) Name	(2) D [Mpc]	(3) T	(4) spec.	(5) R.A. (J2000)	(6) Dec. (J2000)	(7) $\Delta_{\rm pos}$ [mas]	(8) $S_{\rm 5GHz}^{\rm total}$ [mJy]	(9) $S_{\rm 5GHz}^{\rm peak}$ [mJy]	(10) $T_{\rm b}$ [10^8K]	(11) P.A. [°]	(12) $S_{\rm 15GHz}^{\rm VLA}$ [mJy]	(13) α
NGC 266	62.4	2	L1.9	00 49 47.8174	+32 16 39.749	55	3.8	3.2	0.25		4.1	0.07
NGC 2787	13.0	-1	L1.9	09 19 18.6095	+69 12 11.690	10	11.5	11.2	0.87		7.0	-0.45
NGC 3169	19.7	1	L2.0	10 14 15.0500	+03 27 57.844	14	6.6	6.2	0.48		6.8	0.03
NGC 3226	23.4	-5	L1.9	10 23 27.0113	+19 53 54.496	150	4.8	3.5	0.27	(64)	5.0	0.04
NGC 4203	9.7	-3	L1.9	12 15 05.0519	+33 11 50.359	55	8.9	8.9	0.69		9.5	0.06
NGC 4278	9.7	-5	L1.9	12 20 06.8254	+29 16 50.715	1	87.3	37.2	2.9	163	88.3	0.01
NGC 4565	9.7	3	S1.9	12 36 20.7820	+25 59 15.632	55	3.1	3.2	0.25		3.7	0.16
NGC 4579	16.8	3	L1.9	12 37 43.5222	+11 49 05.488	1	21.3	21.3	1.7		27.6	0.23
NGC 5866	15.3	-1	T2.0	15 06 29.4989	+55 45 47.568	1	8.4	7.0	0.55	(11)	7.1	-0.15
NGC 6500	39.7	2	L2.0	17 55 59.7827	+18 20 17.661	14	83.6	35.8	2.8	39	83.5	0.00

Note. — The columns are: (1) galaxy name; (2) distance in Mpc; (3) host galaxy morphological type from RC3; (4) spectroscopical AGN classification: L=LINER, S=Seyfert, T=H II Transition galaxy; (5 & 6) VLBI J2000 coordinates; (7) position uncertainty of phase referencing calibrator in milli-arcsecond (mas); (8) total flux density at 5 GHz (VLBA); (9) peak flux density at 5 GHz (VLBA); (10) brightness temperature in 10^8 K; (11) position angle, measured N through E, of 5 GHz radio core if extended; values in brackets are very uncertain; (12) peak VLA flux density at 15 GHz (Nagar et al. 2000); (13) spectral index between peak 15 GHz (VLA) and total 5 GHz (VLBA) flux densities. Columns 2-4 are from Ho et al. (1997).

brightness temperature radio cores produced by genuine AGN. In this section we present Very Long Baseline Array (VLBA) observations of these galaxies to test this notion and to investigate the central region of LINER galaxies at the sub-parsec scale. Such investigations were made for both samples described above. Data reduction and evaluation for the distance limited sample is still going on and here we will concentrate on observations of the 48 LINERs.

From our 48 LINERs sample (previous chapter), we selected all eleven galaxies with both nuclear flux densities above 3.5 mJy at 15 GHz and a flat spectrum ($\alpha > -0.5,\ S_\nu \propto \nu^\alpha$). Only one source, NGC 2655, was above the flux density limit and was excluded because of its steep spectrum. The flux density limit was chosen so that we could detect all sources with the VLBA in snapshot mode in a single 12 hr observation if most of the 15 GHz emission were indeed compact on milli-arcsecond (mas) scales. Because of the low flux densities the phase-referencing technique had to be used. The observations of NGC 3147 failed since the phase-calibrator was not detected, thus reducing our sample to ten sources. The data reduction is more extensively described in Falcke et al. (2000b).

In the observations all ten remaining sources were detected with the VLBA. The results are shown in Table 4.3, where we list the galaxy names, distances (from Ho et al. 1997), Hubble galaxy type from RC3 (de Vaucouleurs et al. 1991) and spectroscopic classification from Ho et al. (1997) in columns 1 - 4. The detected sources are equally distributed between early- and late-type galaxies. We also give the positions of the radio sources (columns 5 and 6). The internal

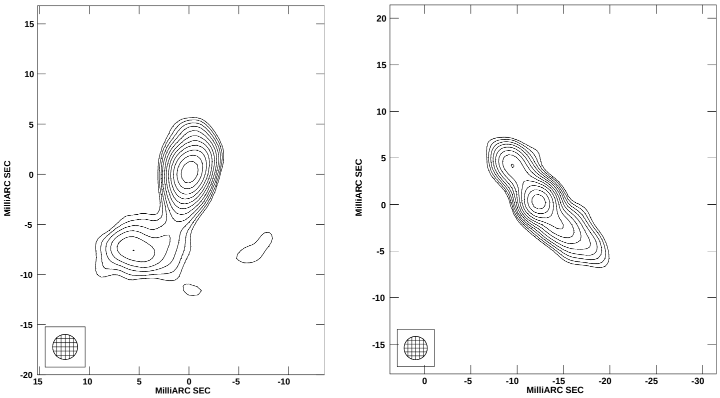

Figure 4.1: VLBA maps of NGC 4278 (left) and NGC 6500 (right). The beam is 2.5 milli-arcsecond and contours are integer powers of $\sqrt{2}$, multiplied by the $\sim 5\,\sigma$ noise level of 0.9 mJy. The peak flux densities are 37.3 mJy and 35.8 mJy respectively.

errors of the positions should be about the beam size (2.5 milli-arcsecond) or better for the stronger ones, but the absolute astrometric accuracy is limited by the uncertainty in the positions of the phase calibrators, (listed in column 7). In addition, we list the total and peak flux densities in the VLBA maps and the brightness temperature (column 10, defined below). Our 1σ rms noise is typically 0.2 mJy and hence for the weakest source we obtain a dynamic range of 15:1. For extended sources we give the position angle (column 11) of an elliptical Gaussian component fitted to the core. For comparison we also list the peak VLA flux density at 15 GHz (column 12) from our previous survey and the (non-simultaneous) spectral index α between the peak VLA 15 GHz and total VLBA 5 GHz flux densities (column 13).
The two brightest sources in our sample, NGC 4278 & NGC 6500, for which we have the largest dynamic range, show core plus jet structures (Fig. 4.1). NGC 6500 has a core and a symmetric two-sided jet, while NGC 4278 has an extended core and an elongated lobe towards the SE. The other sources are point-like with the possible exceptions of NGC 3226 and NGC 5866, although phase errors may be responsible for the extension in these faint sources. The spectral indices range from $\alpha = -0.5$ to $\alpha = 0.2$, with an average $\langle\alpha\rangle = 0.0 \pm 0.2$. We note that the VLBA does not provide spacings as short as the VLA. The VLBA measurements at 5 GHz may then underestimate the true flux density if the sources are extended below the 150 milli-arcsecond scale, so the actual spectrum might be less inverted (i.e. the spectral index smaller) than we measure here.
From the flux densities and the sizes we have measured, we can calculate the brightness temperatures for a Gaussian flux density distribution with the following equation

$$T_{\rm b} = 7.8 \times 10^6\ {\rm K} \left(\frac{S_\nu}{\rm mJy}\right) \left(\frac{\theta}{2.5\,{\rm mas}}\right)^{-2} \left(\frac{\nu}{5\,{\rm GHz}}\right)^{-2} \tag{4.1}$$

where θ is the FWHM of the Gaussian beam (e.g., Condon et al. 1982). Using our beam size of 2.5 milli-arcsecond and the peak 5 GHz flux densities in Table 4.3, we find brightness temperatures in the range $T = 0.25 - 2.9 \times 10^8$ K for our sample, with an average brightness temperature for all sources of $\langle T_\mathrm{b} \rangle = 1.0 \times 10^8$ K. Since most of our sources are unresolved, these values are usually lower limits.

Our result has a number of interesting implications. The presence of high brightness temperature radio cores in our LINER sample confirms the presence of AGN-like activity in these galaxies. It is unlikely that the radio sources represent free-free emission, as has been claimed for example in NGC 1068 (Gallimore, Baum, & O'Dea 1997), since a much higher soft X-ray luminosity than is typically observed in low-luminosity AGN would result. The emission coefficient for thermal bremsstrahlung from a gas at temperature T is (e.g., Longair 1992, eq. 3.43)

$$\epsilon_\nu \; = 6.8 \times 10^{-51} Z^2 T^{-\,^1\!/_2} N_p N_e g(\nu, T) exp(-h\nu/kT)\, \mathrm{Wm}^{-3}\mathrm{Hz}^{-1} \tag{4.2}$$

where $g(\nu, T)$ is the Gaunt factor. If we consider a plasma at temperature $T \simeq 10^8$ K, then at 5 GHz, the exponential factor in Eq. (4.2) is 1, while the Gaunt factor is ~12. In the soft X-ray regime, taken as 0.4 keV to 2 keV, the Gaunt factor varies between 1.7 and 0.8, respectively, while the exponential factor in Eq. 4.2 varies between 0.95 and 0.8, respectively. Therefore, the luminosity, per Hertz, at 0.4 keV and 2 keV is ~0.25 times and ~0.05 times that at 5 GHz, respectively. The geometric mean monochromatic luminosities of the nuclei observed by us is $10^{27.5\pm0.6}$ erg sec^{-1} Hz^{-1} at 5 GHz. If this emission traces thermal bremsstrahlung we would expect the total 0.4–2 keV luminosity of these nuclei to be $10^{43.9}$ erg s^{-1}. However, the observed 0.4-2 keV luminosities for low-luminosity AGN tend to be of the order of 10^{39-40} erg s^{-1} (e.g., Ptak et al. 1999) – many orders of magnitude lower and thus rendering a thermal origin of the radio emission very unlikely. Of course photo-electric absorption could attenuate some of the soft X-ray emission, however, since seven of our galaxies show broad Hα emission (spectral type 1.9) the absorption should only be moderate. To make this argument more watertight one will need to investigate multiwavelength data for our galaxies on a case-by-case basis.

On the other hand, the compact, flat-spectrum cores we have found are similar to those typically produced in many AGN. Hence we can take the presence of compact, non-thermal radio emission as good evidence for the presence of an AGN in our galaxies. The 100% detection rate with the VLBA, based on our selection of flat-spectrum cores found in a 15 GHz VLA survey, shows that for statistical purposes we could have relied on the VLA alone for identification of these compact, high brightness radio sources. Hence, with 15 GHz VLA surveys of nearby galaxies one has an efficient tool for identifying low-luminosity AGN. This complements other methods for identifying AGN, such as searching for broad emission-lines or hard X-rays, and has the advantage of not being affected by obscuration.

If we only consider galaxies with a LINER spectrum, we found at least eleven flat-spectrum radio cores at 15 GHz in a sub-sample of 24 LINERs observed in the "48 LINERs" sample. Eight of these eleven LINERs are included in our sample here, yielding a lower limit to the AGN fraction for LINERs of at least $33 \pm 12\%$ (8/24). Based on our 100% detection rate of these flat-spectrum cores with the VLBA, we can, however, argue that all eleven flat spectrum sources found in the VLA study are likely to be AGN, raising the AGN fraction of LINERs to at least $46 \pm 14\%$ (11/24). These ratios do not change significantly if we include the galaxies classified as Seyferts. Since the selection of our parent sample is not very well defined, we could still be subject to an unquantifiable bias. However, the VLA observations of the distance-limited sample reported above seem to indicate that the bias is not large.

The two brightest radio sources in our sample show extended structure suggestive of jet-like outflows, and the other seven sources are unresolved or slightly resolved. Our very limited dynamic range is not good enough to prove or exclude the presence of jets for the latter. VLBA observations of M81 (Bietenholz, Bartel, & Rupen 1999) have shown that jets in low-luminosity AGN can be very compact and difficult to detect. The only clue we therefore have is the spectrum which is flat or slightly inverted. Such a behavior is predicted by simple jet models (Falcke 1996a; Falcke & Biermann 1999), where the spectral index ranges from $\alpha = 0.0$ to 0.23 as a function of inclination angle to the line-of-sight. In no case do we find a spectral index as high as $\alpha = 0.4$ as predicted in the ADAF model (Yi & Boughn 1998). This does not necessarily exclude the ADAF model, but argues for the parsec scale radio emission at centimeter radio waves being dominated by another component, such as a radio jet or a wind. A combination of an underluminous disk or an ADAF and a radio jet is one possibility (e.g., Donea, Falcke, & Biermann 1999).

Finally, it is worth pointing out that Nagar et al. (2000, in prep.) have started to extend the VLBI sample to all galaxies in our two samples with detected compact cores above 3 mJy. Preliminary data reduction indicates that all galaxies, with the exception of NGC2655 which has a steep-spectrum core, were detected at the level expected from our 15 GHz VLA observations by assuming a flat spectrum. Among these, two galaxies show again jet-like structures and since M87 and M81 are well-known jet sources belonging to our sample, the six brightest radio cores in our combined samples all have core-jet structures.

4.3 Radio Cores in LLAGN – the Grand Perspective

Assuming the cores detected in the VLA & VLBA survey are produced by randomly oriented, maximally efficient jets from supermassive black holes (of order $10^8 M_\odot$) we can use Eq. 2.36 to calculate that for an average monochromatic luminosity of $10^{27.5}$ erg sec^{-1} Hz^{-1} at 5 GHz the jets would require a minimum *total* jet power of order $Q_{\rm jet} \gtrsim 10^{42.5}$ erg sec^{-1}. The way the model was constructed one has to consider this a minimum energy estimate. Compared to quasars this is a rather low value and supports the conclusion, based on their low UV and emission-line luminosities, that the cores are powered by under-fed black holes. On the other hand this jet power is well within the range of the bolometric luminosity of typical low-luminosity AGN (10^{41-43} erg sec^{-1}; Ho 1999) and, compared to radiation, jets should be a significant energy loss channel for the accretion flow.

This similarity between jet power and (accretion) luminosity, of course, appeals again to the jet-disk symbiosis picture discussed at the beginning of this work. We can now take the radio cores detected in our survey and put them on the correlation predicted in Falcke & Biermann (1996). A problem one encounters is how to estimate the accretion disk luminosity. To make the different AGN comparable we will use the narrow Hα line that is measurable in all AGN, and apply the same conversion factor between Hα and $L_{\rm disk}$ as used for quasars. For narrow Hα Eq. 2.6 then reads

$$\lg(L_{\rm disk}/{\rm erg\ s}^{-1}) = 4.85 + \lg(L_{{\rm H}\alpha,{\rm n}}/{\rm erg\ s}^{-1}). \tag{4.3}$$

Figure 4.2 shows the predicted Radio/$L_{\rm disk}$ correlation together with LLAGN found in our survey. The galaxies almost fill the gap between quasars and X-ray binaries on this absolute scale and fall in the predicted range. This illustrates that we have a continuation from high-luminosity to low-luminosity AGN, *the latter being the silent majority within the AGN family.*

We can investigate the optical/radio correlation in greater detail. For the VLBI-sample, i.e. the well-detected cores above 3 mJy in both samples, for which we have basically established that the radio emission is AGN-related, we can look at correlations between radio, emission-line, and bulge luminosities. Figure 4.3 (right panel) shows that there is a trend for galaxies with higher Hα emission to have more luminous radio cores. Interestingly, elliptical and spiral host galaxies are offset from each other. The same effect can be seen in Fig. 4.2 where one finds a string of sources connecting to FR I radio galaxies and falling somewhat above the top line predicted by the model. This are the large elliptical galaxies which are probably faint versions of radio galaxies. Does this reflect a radio-loud/radio-quiet dichotomy for LLAGN?

There is another important factor: the galaxy bulge luminosity. We do see a weak trend for the radio luminosity to be related to bulge luminosity; also the ratio between radio and Hα luminosity tends to increase with increasing bulge luminosity. Hence, galaxies apparently become more efficient in producing radio emission relative to Hα in bigger bulges. This also holds if we look at the entire VLA detected sample (Fig. 4.4). Whether this is due to increasing obscuration, effects intrinsic to the AGN, or a selection effect is unclear. In any case, we are comparing here pumpkins with apples. Since ellipticals and spirals in our sample are nicely separated between the top and bottom end of the bulge luminosity distribution, an apparent dichotomy in Fig. 4.3 is a natural consequence of this trend.

If the bulge luminosity is proportional to the central black hole mass (Kormendy

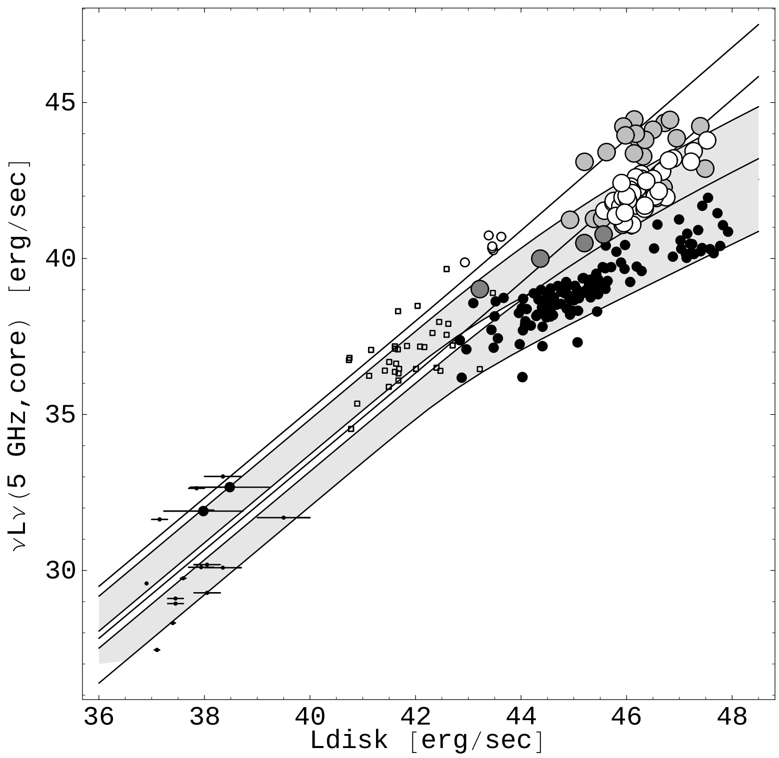

Figure 4.2: The same as Fig. 2.3, showing the correlation between thermal emission from the accretion disk (with the exception of X-rays this is basically normalized to their narrow Hα emission) and the monochromatic luminosity of AGN radio cores. Open circles: Radio-loud quasars; small open circles: FR I radio galaxies; open gray circles: Blazars and radio-intermediate quasars (dark grey); black dots: radio-quiet quasars and Seyferts; small dots: X-ray binaries; small boxes: detected sources from the from the "48 LINERs" sample. The latter apparently confirm the basic prediction of Falcke & Biermann (1996) and almost close the gap between very low (on an absolute scale) accretion rate objects and high accretion rate objects. The shaded bands represent the radio-loud and radio-quiet jet models as a function of accretion as shown in the aforementioned paper.

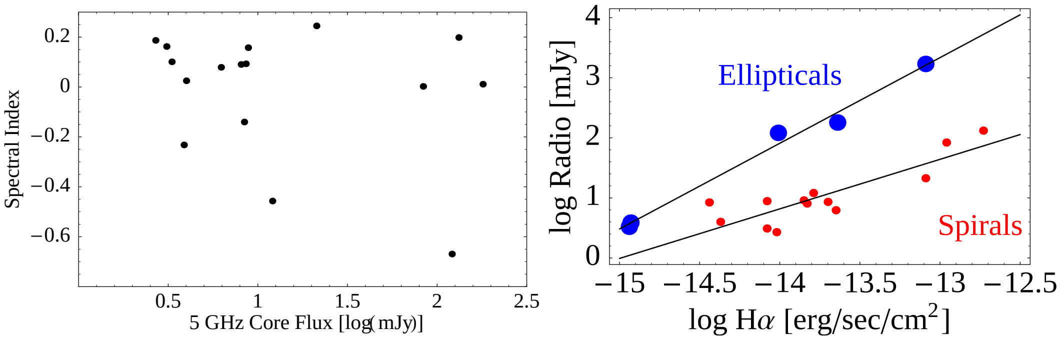

Figure 4.3: Left: Spectral indices of LLAGN in our two samples with $S_{15\mathrm{GHz}} > 3$ mJy between 5 GHz (VLBI) and 15 GHz (VLA) as a function of radio core flux at 5 GHz. Right: $S_{15\mathrm{GHz}}$ plotted versus narrow Hα flux for the same sample; ellipticals and spirals are distinguished by big and small dots respectively.

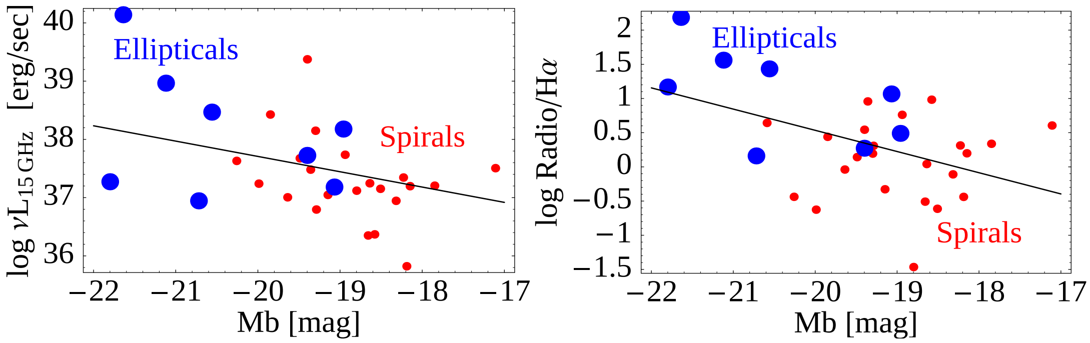

Figure 4.4: Left: Radio luminosity (νL_ν) at 15 GHz of LLAGN in our sample with $S_{15\text{GHz}} > 1.5$ mJy as a function of blue bulge magnitude. Right: Ratio between 15 GHz radio core and narrow Hα flux as a function of blue bulge magnitude in the same sample. Ellipticals and spirals are distinguished by big and small dots respectively.

& Richstone 1995), the ellipticals in our sample are more likely to have larger black hole masses. This means they have a larger 'headroom' with respect to their Eddington limit and are more likely to have larger accretion rates. Moreover, if an accretion disk becomes radiatively less efficient the further away it is from the Eddington limit, we could reproduce the scaling of the Radio/Hα-ratio. Another explanation for the latter could be that the larger bulges of these ellipticals contain more obscuring material towards our line of sight and hence optical emission is more strongly suppressed.

To summarize: we find that at least 40% of optically selected LLAGN with Seyfert and LINER spectra have compact radio cores. VLBI observations show that these cores are similar to radio jets in more luminous AGN with high brightness temperatures, jet-like structures, and flat radio spectra. The radio emission seems to be related to the luminosity of the emission-line gas and hence both are probably powered by genuine AGN operating at low powers. We found no evidence for high frequency components with highly inverted spectra as predicted in ADAF models. Hence, for these models one should probably not include radio fluxes in broad-band spectral fits.

We also find only a weak correlation between radio and bulge luminosity, which could imply a scaling of radio emission with black hole masses. Such an effect was claimed earlier and interpreted within the ADAF models as a possibility to measure black hole masses with the radio data (Franceschini, Vercellone, & Fabian 1998). However, this result was based on a much smaller, ill-selected sample and gave a much steeper dependence which we cannot confirm. Strangely, this sample even included galaxies like M87 – one of the most famous radio galaxies, where we know for many decades now that the radio emission is produced by a radio jet and not an ADAF. As we have seen here, the radio-Hα correlation is a much stronger effect. If the Hα is a tracer of the accretion disk luminosity, this most likely means that the radio power is much more dependent on the accretion rate than on the black hole mass. One will therefore have to continue to measure black hole masses in the traditional way, mainly through spectroscopy.

Chapter 5

Jets and Radio Cores in Radio-Quiet AGN

In the last two chapters we have moved from an almost inactive galaxy, like the Milky Way, to weakly active galaxies such as LINERs and dwarf-Seyferts. In both classes we find strong radio cores. If we move up to even higher luminosities we arrive at Seyfert galaxies and quasars. As outlined in the introduction already, at this luminosity level radio cores in radio-loud quasars are relatively well understood and studied in great detail. However, the majority of quasars are radio-quiet, i.e. they have very little radio emission. We have argued in passing (Chap. 2; esp. Fig. 2.1 & 2.2) that also in these radio-quiet quasars, which one should rather call radio-weak quasars, the radio emission is also produced by jets and consequently its flux was treated within the framework of the jet-disk symbiosis model. But, is it really true that all AGN have jets – even the radio-quiet ones? And, if it is true, what kind of jets are these?

In comparison to stellar winds it is often argued that the escape speed from the central object is an important factor that determines the terminal jet speed. If that is true and since we believe that most of the AGN are powered by a black hole one should assume that if an AGN produces a jet it should *always* be relativistic. Consequently the crucial question then becomes: Do all AGN have relativistic jets including those deemed radio-quiet? In Falcke (1994) and Falcke & Biermann (1995) we proposed that, since black holes do not have many free parameters, AGN should be similar in their basic properties ("the universal engine") and hence one should *ab initio* assume that all AGN, rather than only a few sub-classes, have relativistic jets. Using Occam's razor we also suggested that jets and accretion process (accretion disk) should form a symbiotic system in the sense that both are always required for an AGN. As it turned out, this hypothesis, in its simplicity, was surprisingly successful and has motivated most of the research presented here. In a review Livio (1997) comes to a similar conclusion, i.e. that a majority of accretion disk systems produce jet-like outflows.

5.1 Radio-Quiet Quasars

One class of sources where the jet-disk symbiosis principle was used first was the UV/radio-correlation of quasars (Fig. 2.1 & 2.2). If one looks at the distribution of the radio-to-optical flux ratios (R-parameter) of an optically selected quasar sample (here the PG quasar sample) one finds a clear dichotomy between radio-loud and radio-quiet sources. This is especially true if one selects only steep-spectrum quasars, which are supposedly unaffected by orientation effects (see Fig. 5.1). VLA observations of the steep-spectrum radio-loud PG quasars (Miller, Rawlings, & Saunders 1993; Kellermann et al. 1994) have clearly established, that they have FR II-type radio jets. The radio dichotomy was occasionally attributed to the fact that radio-quiet quasars do not show and do not have radio-jets at all. However, as we all know, 'absence of evidence is not evidence of absence' – especially not, if one has not even looked yet. Following the jet-disk symbiosis principle, one would rather think that radio-quiet quasars should have jets as well.

5.1.1 Predictions for Boosted Radio-Quiet Jets

We therefore have to ask: How can we obtain evidence for or against the presence of jets in radio-quiet quasars? One direction to go would be to look for relativistic boosting. In an optically selected sample, we would expect that, if radio-quiet quasars have relativistic jets, some of these quasars are accidentally pointing towards us, thus producing a population of 'weak Blazars' with the following properties:

a) similar to flat-spectrum, core-dominated, variable radio quasars but with relative low radio-to-optical flux ratio (R),

b) apparent brightness temperatures close to $\sim 10^{12}$K or above,

c) superluminal motion,

d) very faint (i.e. radio-quiet) extended radio emission,

e) number of sources in a well selected sample, and their Doppler-boosting relative to radio-quiet quasars both imply the same Lorentz factor,

f) luminosity- and redshift-distribution consistent with radio-quiet parent population,

g) host galaxies compatible with those of radio-quiet quasars.

This list is quite helpful, as it allows an either/or decision: if we do not find a population of weak Blazars, we can exclude that relativistic jets in radio-quiet quasars exist (or one would have to invent an argument why these jets never point towards us); if we find them, we can prove that radio-quiet quasars must have relativistic jets. Interestingly, in the PG quasar sample we indeed find a

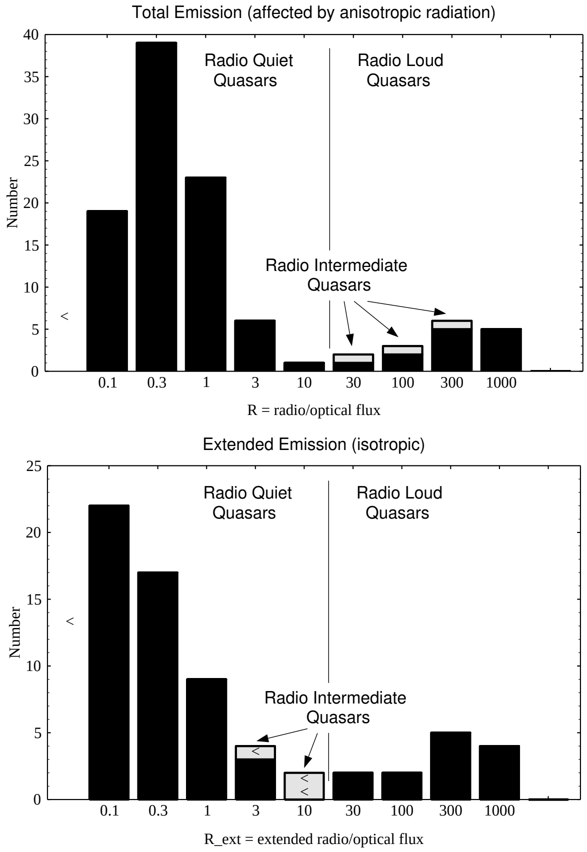

Figure 5.1: Distribution of the R-parameter (ratio between radio and optical flux) for an optically selected sample of quasars with steep radio spectra (from Falcke et al. 1996a). The RIQ are added with gray shades. While in total flux they rival some of the fainter radio-loud quasars with their bright, flat-spectrum radio core, their extended emission is comparable only to radio-quiet quasars.

population of quasars, which at least partially fulfill most of the criteria listed above and most likely are such weak Blazars.

5.1.2 Radio-Intermediate Quasars

Miller, Rawlings, & Saunders (1993), Falcke (1994), and Falcke, Sherwood, & Patnaik (1996) identified a small sample of radio-intermediate quasars (RIQ) which sparsely fill the space in R between radio-loud and radio-quiet quasars. They have optical+UV luminosities between 10^{45} and 10^{47} erg/sec, just like the bulk of the radio-quiet quasars and unlike radio-loud quasars which can be found only above 10^{46} erg/sec in the PG sample. They are typical flat-spectrum, core-dominated quasars, but their R parameter is too low for them to be boosted radio-loud quasars. If they were boosted radio-quiet quasars instead, their number and R-distribution would indicate a bulk Lorentz factor of $\gamma_{\rm j}$=2-4. For at least the three low-redshift RIQ, there is no extended emission above a level of a few mJy – far below what is expected for any radio-loud quasar – neither on the VLA A- & D-array (Kellermann et al. 1994) nor on the EVN & MERLIN scales (Falcke, Patnaik, & Sherwood 1996). At least one source, III Zw 2, has shown outbursts indicating a brightness temperature of 10^{12} K (Terasranta & Valtaoja 1994) which requires relativistic boosting, while VLBI observations of the three low-z sources indicate at least lower limits of several 10^{10} K. III Zw 2 is the most interesting source in this respect since it is the most variable source with a huge outburst every few years but which has for a long time resisted attempts to resolve any structure with VLBI (e.g., Kellermann et al. 1998). Here we will now focus on most recent results for this galaxy.

III Zw 2 was classified as a Seyfert I galaxy (e.g., Arp 1968; Osterbrock 1977), and was later also included in the PG quasar sample (Schmidt & Green 1983). The host galaxy was classified as a spiral (e.g., Hutchings & Campbell 1983) and a spiral arm was found (Hutchings 1983). A galaxy disk model was later confirmed by fitting of model isophotes to near-IR images (Taylor et al. 1996).

Because of its frequent outbursts the flux-density of III Zw 2 was monitored frequently, leading to the discovery of a new outburst in 1997. A first VLBA observations in the early phase of the outburst then revealed a high-brightness temperature around $3 \cdot 10^{11}$ K, a very compact double structure, and a highly inverted spectrum with a peak at 43 GHz (Falcke et al. 1999). Continued monitoring of the outburst with the VLBA then finally led to the detection of superluminal motion in this source (Brunthaler et al. 2000) – the first time superluminal motion was ever found in a spiral galaxy (later than S0) and which, judged from its extended radio emission, is clearly not a radio galaxy.

Figure 5.2 shows four epochs of VLBA observations. In the last two epochs the source clearly starts to expand. If one considers the expansion speed of the blob one finds basically no expansion in the early phase of the outburst, but a rapid expansion with apparent velocity 1.25 ± 0.09 c at the end. This apparent superluminal motion – an optical illusion – can only occur, if the underlying jet itself expands with a velocity close to the speed of light. Hence, one can conclude that at least III Zw 2 contains a relativistic jet.

Key to this success was the frequent monitoring of the source with the VLBA. In a parallel program (Ulvestad et al. 1998) we have been studying the expansion velocity of two other Seyfert galaxies, Mrk 348 and Mrk 231, and found only sub-relativistic expansion speeds. It could well be, that those sources could also show phases of faster expansion that we have missed so far.

It is known that radio-loud AGN almost never reside in spiral galaxies (e.g., Bahcall et al. 1997, Kirhakos et al. 1999) whereas radio-quiet quasars appear both in spiral and in elliptical host galaxies. Furthermore, all relativistically boosted jets with superluminal motion and typical Blazars have been detected in early type galaxies (e.g., Urry et al. 2000). Therefore, the detection of superluminal motion in III Zw 2 provides a significant breakthrough.

In addition, one of three low-redshift RIQs, PG 1309+355, was part of recent

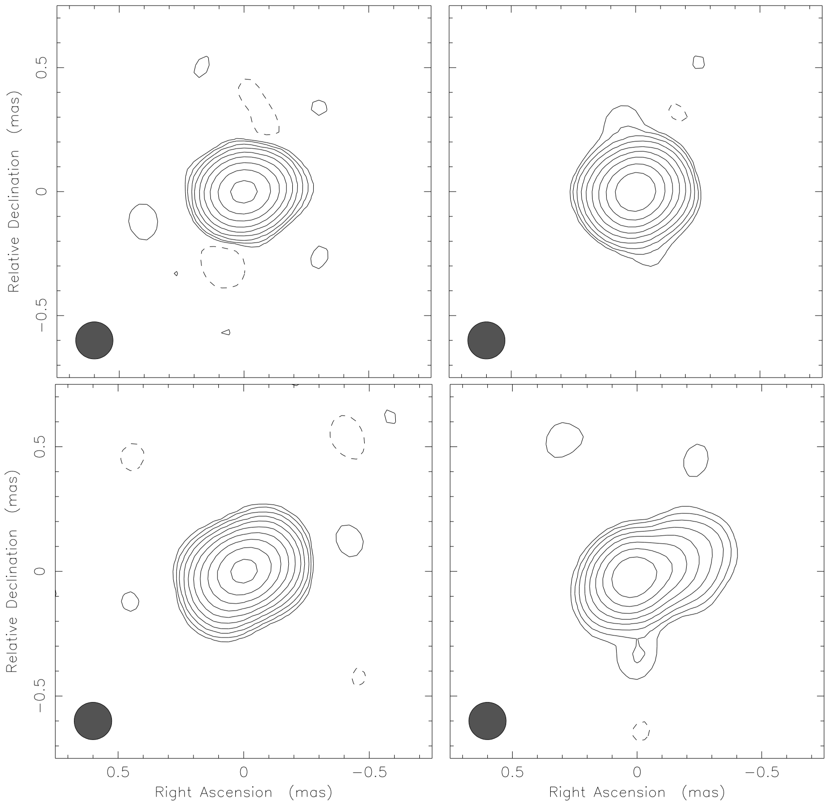

Figure 5.2: Four epochs of VLBA maps of III Zw 2 at 43 GHz convolved with a super-resolved beam of 150 μas. The original beam sizes were 0.29×0.12 milli-arcsecond at a position angle (P.A.) of -5° in June 1998, 0.31×0.16 at a P.A. of 11° in September 1998, 0.38×0.17 at a P.A. of -4° in December 1998 and 0.5×0.14 at a P.A. of -18° in June 1999.

HST host galaxy study (Bahcall et al. 1997) and found to be a spiral as well. Hence, together with III Zw 2 at least two of the three RIQs are in spiral galaxies, confirming the prediction that host galaxies of RIQs should resemble those of radio-quiet quasars rather than those of radio-loud quasars.

In summary, the so far identified and studied RIQ meet all the requirements for intrinsically radio-quiet quasars, whose relativistic jets accidentally point towards us. Moreover, since only a very small fraction of quasars will point towards us, one can infer also that a large number – if not all – of the remaining radio-quiet quasars must harbor relativistic jets. Further VLBI studies of radio-quiet quasars (Blundell & Beasley 1998) indeed conclude that also radio-quiet quasars with weaker radio emission have compact cores resembling those of radio-loud quasars, albeit at a much fainter level. Therefore, we have direct evidence that fainter, unboosted counterparts do exist and the idea of radio-quiet AGN having relativistic jets has made a big step towards becoming an established view. It also strengthens the notion that all black holes are equal.

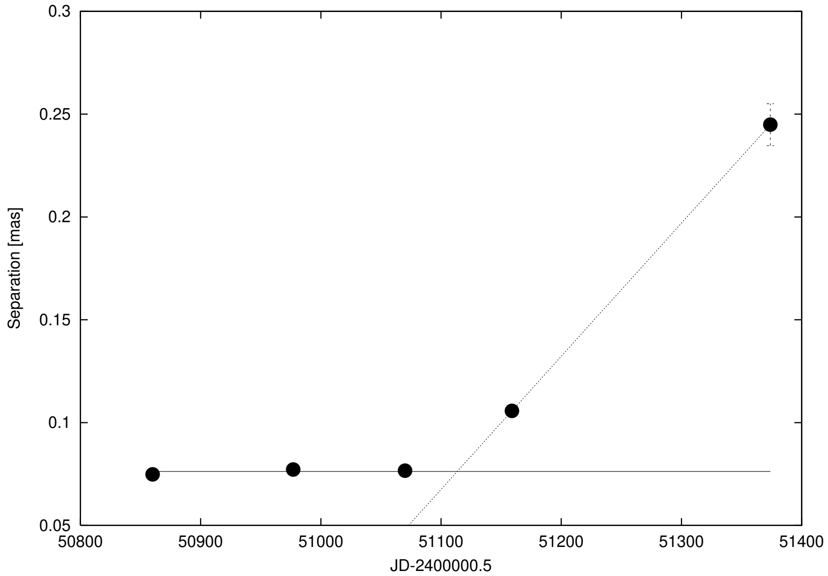

Figure 5.3: Component separation from model fitting of point-like components to the closure phases and amplitudes of III Zw 2 at 43 GHz. The separation of the first three epochs is consistent with an expansion speed $\leq 0.04\ c$ (solid line). The expansion speed between the fourth and fifth epoch is $1.25 \pm 0.09\ c$. Formal error bars are a few μarcseconds only for the first four epochs.

5.2 Imaging of Large-Scale Jets in Radio-Quiet AGN

A second route to establish that jets play a significant role in radio-quiet AGN is deep, high-resolution VLA imaging of the extended radio structures which were seen already in some snapshot maps. First results of such a project seem to indicate that radio-quiet quasars indeed harbor Seyfert-like jets (Kukula et al. 1998).

Fortunately, already now are results available which can, at least in part, answer whether direct evidence for jets in radio-quiet quasars exists at all. First of all VLA observations of Kellermann et al. (1994) have already revealed a number of radio-quiet quasars with weak, bi-polar radio-structure. Secondly, there is a large regime, where the Seyfert galaxies and quasar classifications blend into each other and it may be useful to study Seyferts rather than radio-quiet quasars and their jets in greater detail. Seyferts are closer and appear brighter on the sky. In this section we will discuss some results we have obtained using the HST and the VLA for Seyfert galaxies and which might be helpful for the interpretation of quasars as well.

5.2.1 Seyferts

Seyfert galaxies were first noted because of their strong emission-lines coming from their nucleus, which is emission of hot gas ionized by an AGN. After the advent of the VLA a number of radio surveys have shown that, besides their extended emission-line regions, Seyferts also possess – sometimes very faint – radio emission which is very often bi-polar (Ulvestad & Wilson 1984, and previous papers). Seen at higher resolution one finds a strong tendency for the circumnuclear emission-line and radio morphologies to be aligned in Seyfert galaxies (Unger et al. 1987; Pogge 1988; Haniff, Wilson, & Ward 1988). This strongly suggested that the ejection of the radio plasma and the excitation of the emission-line gas were related and that the ionizing radiation escapes preferentially from the active nucleus along the radio axis. Here the Hubble Space Telescope (HST) has made an enormous impact: seen with the superior resolution of this telescope the structure of the emission-lines gas was revealed and in some cases shown to be well-defined cones (e.g. NGC 1068, Evans et al. 1991; NGC 5728, Wilson et al. 1993; NGC 5643, Simpson et al. 1997), which seemed to confirm an anisotropic escape of ionizing photons from the nucleus. This is most popularly explained by the presence of an optically thick 'obscuring torus' (Antonucci 1993), which is able to collimate the intrinsically isotropic ionizing radiation (see, e.g., Storchi-Bergmann, Mulchaey, & Wilson 1992) from the AGN. In addition, a number of galaxies display the 'ionization cone' morphology when an excitation map is made, e.g. in [O III]/(Hα+[N II]).

The close connection between the radio ejecta of Seyfert nuclei and their narrow-line regions (NLRs) initially became apparent from their similar spatial extents and from strong correlations between radio luminosities and [O III]λ5007 luminosity and line width (de Bruyn & Wilson 1978; Wilson & Willis 1980; Whittle 1985; Whittle 1992b). Spectroscopic studies of the NLR (Baldwin, Wilson, & Whittle 1987; Whittle et al. 1988), have revealed that the kinematics of the gas are often clearly affected by the radio jets. Such interactions could play a role in determining the structure of the NLR within the region ionized by the nucleus. In a handful of cases, HST has shown a clear spatial correspondence between the radio and emission-line distributions (e.g., NGC 5929, Bower et al. 1994; Mrk 78, Capetti et al. 1994 & Capetti et al. 1996; Mrk 1066, Bower et al. 1995; Mrk 3, Capetti et al. 1996; ESO 428–G14, Falcke et al. 1996), indicating that the radio ejecta strongly perturb the ionized gas, at least in these objects. It has also been suggested that the hot gas associated with the shocks generated by the interaction between the radio ejecta and the ambient medium is a significant source of ionizing radiation (e.g., Dopita & Sutherland 1995 or Bicknell et al. 1998).

It is therefore of great importance to study more Seyfert galaxies at the high spatial resolution which only HST can provide, to determine whether the morphology of the NLR is determined by the nuclear ionizing radiation or by the interaction of radio jets with the interstellar medium, or by a combination of both.

In Falcke, Wilson, & Simpson (1998) we presented images taken with the Wide

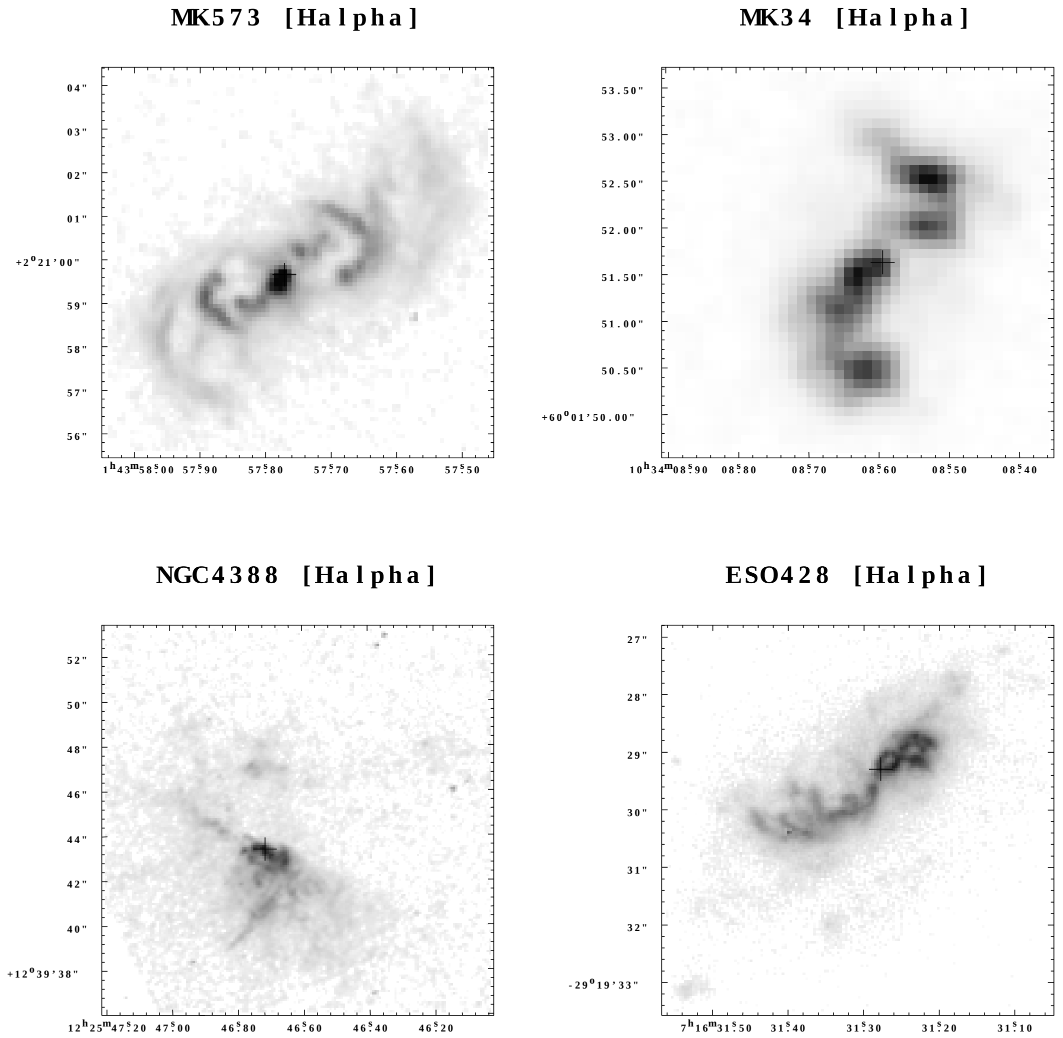

Figure 5.4: Narrow band HST images of Seyfert 2 galaxies in the Hα emission line from Falcke et al. (1998)

Field and Planetary Camera 2 (WFPC2) of seven Seyfert 2 galaxies (see Fig. 5.4), selected on the basis of possessing either extended emission-line regions (as seen in ground-based images) or broad emission-lines in polarized light. For each galaxy images in the light of the [O III] λ5007 line and the Hα+[N II] $\lambda\lambda$6548,6583 blend were taken. In addition we also obtained new radio maps taken with the Very Large Array (VLA), almost all in 'A-configuration', providing an angular resolution comparable with that of the HST images. Taken together, these allowed us to compare directly the structures of the line-emitting gas and the radio plasma on scales of tens of parsecs.

And indeed in four of the seven galaxies (Mrk 573, ESO 428−G14, Mrk 34, NGC 4388) we found bi-polar structures in the excitation maps (i.e. the maps obtained by dividing the [O III] by the Hα+[N II] map, Fig. 5.5) and a number of finer structures in the emission-line regions of all galaxies (with the exception

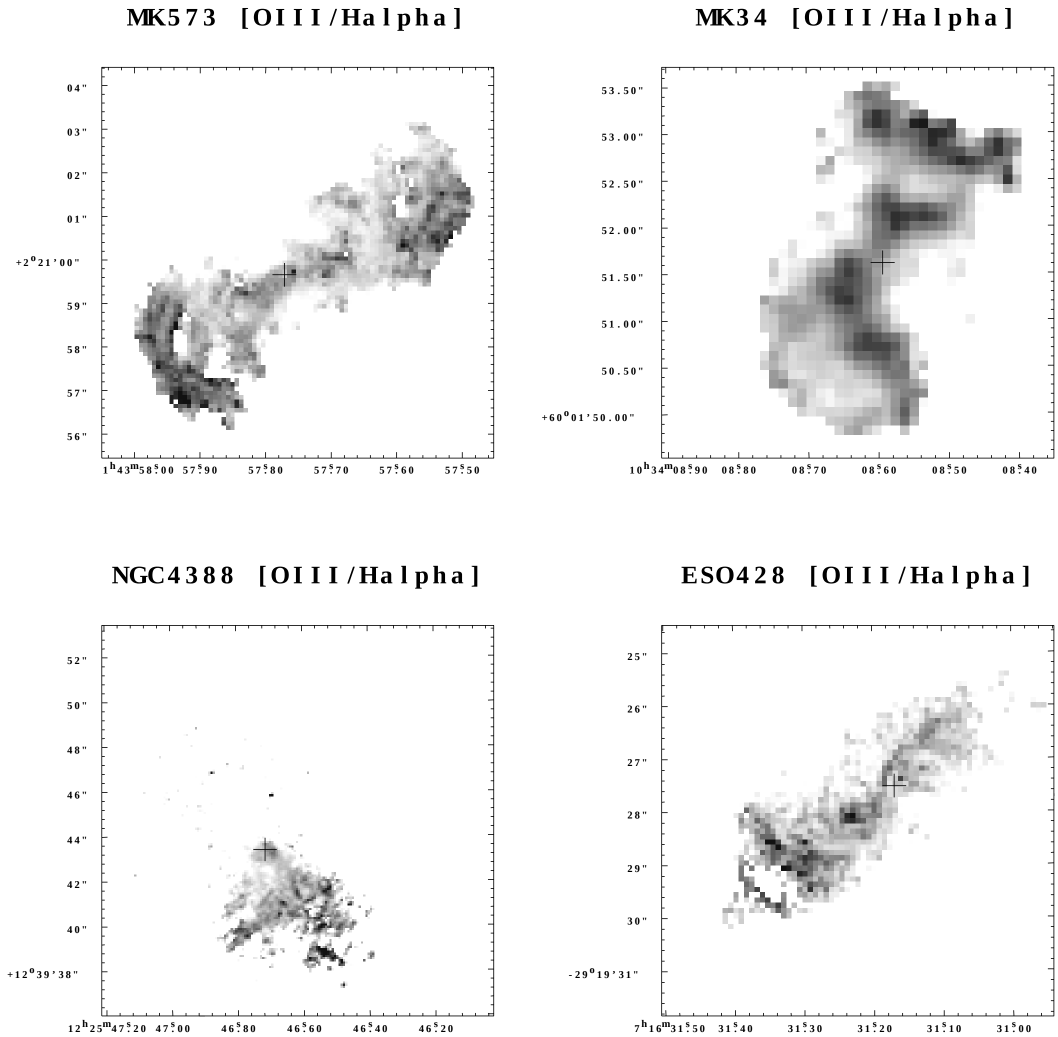

Figure 5.5: Excitation maps (O III/Hα) for the galaxies in Fig. 5.4. Dark shades indicate higher excitation. The overall structure of the highly excited gas resembles cones and bi-cones.

of one, Mrk 1210, which was basically unresolved). In addition, the high quality radio maps of the galaxies we obtained, show the considerable diversity one can find in the radio structure of Seyferts, all of which indicate the presence of a jet outflow: narrow, filamentary jets (ESO 428$-$G14), triple structures with a core and two hotspots (Mrk 573), jets plus two hotspots (Mrk 34), radio plumes and limb-brightened lobes (NGC 4388), etc. (Fig. 5.6).

Even though the dynamic range of Seyfert radio maps is naturally lower than what one can obtain for the much brighter radio galaxies, this diversity is much larger than what we find in the latter. This is of course readily understood, since Seyfert jets are much more subject to jet-ISM interaction than FR II radio galaxies, because of their orders of magnitude lower absolute jet powers and smaller extents. Morphologically, this interaction can be seen in many images of the HST:

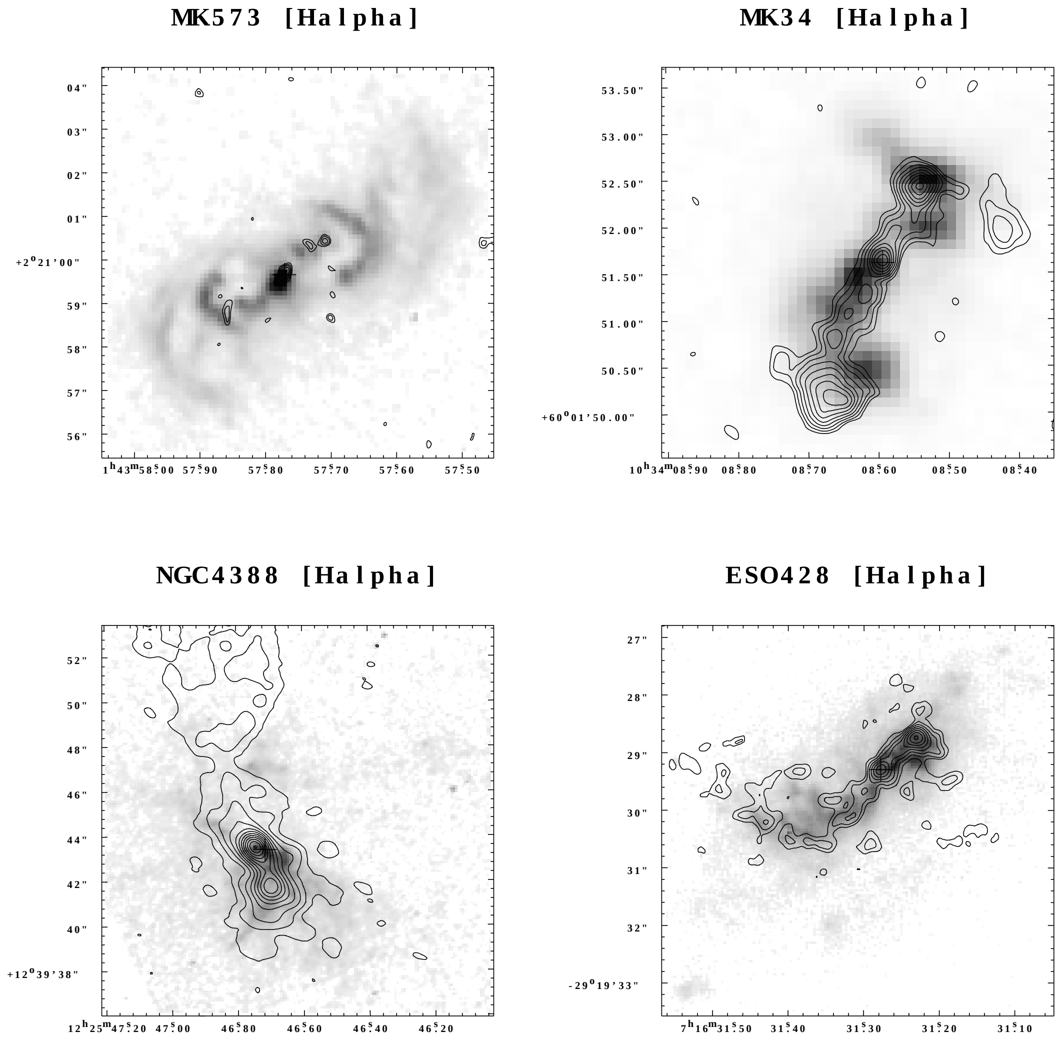

Figure 5.6: The same images as in Fig. 5.4 with the VLA radio contours overlaid. The observed wavelengths are 3.5cm for Mrk 34 and NGC 4388 and 2 cm for Mrk 573 and ESO428–G14. The direct relation between radio and optical emission is obvious.

e.g., in Mrk 573 and Mrk 34 the radio hotspots coincide with regions of reduced excitation, the bow-shock structure in the emission-line gas of Mrk 573 is most certainly caused by the action of an outflow as indicated by the presence of the radio hotspots, and the filamentary emission-line structure in ESO 428–G14 finds its detailed counterpart in the filamentary radio jet.

It is quite obvious from this data that there is not only a close correlation between the radio and the emission-line morphologies, but that *the radio jet-ISM interaction is an important effect which strongly influences the excitation and morphology of the NLR*.

Does this mean the unified scheme is wrong? Is the bi-polarity of the NLR and are the ionization cones just illusions of a weary astronomer's soul longing for a simple scheme to explain the Seyfert world? Are all the structures seen in the NLR produced by widening, self-excited matter outflows as Dopita and others suggest?

Fortunately, in at least two cases we can find good arguments, that the anisotropic photon escape scheme remains still valid: In Mrk 573 and NGC 4388 'ionization cones' (Pogge & de Robertis 1995; Capetti et al. 1996; Pogge 1988; Corbin, Baldwin, & Wilson 1988) were already known from ground-based observations on the arcsecond scale and we found an equivalent counterpart on the sub-arcsecond scale with identical opening angle. This continuation and the straightness of the cones clearly favor some kind of obscuring 'torus' with well defined inner edges around the nucleus that leads to a beamed ionizing continuum. Attributing these cones to the action of an outflow seems unreasonable, since the radio ejecta we do see have not only a very different appearance in both galaxies despite similar cone structures, the jets are also themselves subject to collimation by the galaxy, e.g., as seen in the constriction of the northern lobe of NGC 4388, and therefore are nothing like the proposed freely expanding, conical outflows. On the other hand, Mrk 573 has not only a straight 'excitation cone' but, with its bow-shaped emission-line strands, is also the clearest example of a jet-shaped NLR. Consequently, any successful model of the NLR of this galaxy will require a *composite model that includes photo-ionization from a central source* and *the impact of a radio jet* (see Ferruit et al. 1999).

Other examples for the shaping of the NLR by the jet are ESO 428−G14 and NGC 4388. The former exhibits well collimated, irregular emission-line strands on one side and a figure "eight" morphology on the other. The latter has been interpreted as two helical emission-line strands wrapping around a radio jet (Falcke et al. 1996). The overall structure of the NLR and of the radio jet in ESO 428–G14 is perhaps the most bizarre case one can find. In NGC 4388 a bright spike is seen in the ionized gas at the end of the southern jet, while the radio plasma to the north flows apparently unhampered out of the galaxy disk and forms a large (~ 1 kpc) radio plume. This structure is reminiscent of the radio lobe found, for example, in NGC 3079 (Seaquist, Davis, & Bignell 1978) and a few other galaxies (Ford et al. 1986). This kind of limb-brightened radio lobe stands in marked contrast to the well-collimated, stranded jets in ESO 428−G14 and NGC 4258 (e.g., Cecil, Wilson, & Tully 1992). An important difference is that NGC 3079 and NGC 4388 have jets which escape almost perpendicular to the galaxy plane, while in NGC 4258 and perhaps ESO 428–G14 the jet appears to be directed into the disk of the galaxy. The difference in radio morphology may then be ascribed to the much higher external gas density when the jet is in the disk rather than in the galaxy halo.

What remains unclear, however, is the exact nature of the jet-ISM interaction in our Seyferts. To what degree are jet-induced shocks responsible for the excitation of the gas? Are there regions, where shock excitation dominates the photo-ionization from the nucleus? What amount of energy is locally dissipated in the jets due to this interaction? To answer these questions the observation of only two emission-lines is not enough and long-slit spectroscopy will be needed. For

ESO 428–G14, the necessary HST time for such observations has been allocated, and other projects will address similar questions in the future. Moreover, some recent results obtained with the FOC on board the HST already now strongly support the jet-ISM interaction picture (Winge et al. 1997).

At least in a very simple way the jets must have an influence on the excitation of the gas: e.g., the reduced excitation (i.e. [O III]/(Hα+[N II]) ratio) of the inner emission-line arcs in Mrk 573 is consistent with a lower ionization parameter which can be understood if the arcs represent gas which has passed through a radiative bow shock, cooled and increased in density. A similar effect is seen in Mrk 34, in which the radio lobes coincide with a low-excitation region, while the jet itself is surrounded by high-excitation gas. The wiggles seen in the radio jet of this galaxy could possibly be interpreted as some kind of Kelvin-Helmholtz instabilities between the radio plasma and the surrounding, ionized gas. Looking at all the galaxies in our sample, there seems to be indeed a tendency for radio lobes to coincide with lower excitation regions, presumably a result of compression of the ambient gas.

Finally, we can now come back to our initial question about the presence and importance of jets in general. Especially with respect to the situation in radio-quiet quasars, we are now much more prepared to give a positive answer. Some of our galaxies (e.g., Mrk 34 and Mrk 573) have [O III] luminosities comparable to radio-quiet, low-redshift quasars. Hence, for such objects, we are discussing a regime in which the quasar and Seyfert classifications indeed overlap. From their radio flux it is clear that the Seyferts in our sample belong to the radio-quiet class of AGN, yet they not only show jets, but the jets are also kinematically important for the emission-line gas. The jets we find in Mrk 34 and Mrk 573 would in fact resemble some of the double structures seen by Kellermann et al. (1994) in radio-quiet quasars, if placed at a larger distance and observed with lower sensitivity.

5.2.2 Megamaser Galaxies

When looking at the large-scale jet structure in Seyferts there remains one important question to be solved: how are the large-scale jets and the central AGN with its alleged torus and compact radio core connected? Clearly, if, as seen in III Zw 2, jets start out relativistically, they have to slow down on their way out to explain the rather diffuse radio ejecta discussed in the previous section. The slow expansion in the early phase of the III Zw 2 outburst and the sub-relativistic expansion we found in Mrk 348 and Mrk 231 (Ulvestad et al. 1998) seems to indicate that a significant slow-down is happening already at the sub-parsec scale and may possibly be related to the obscuring torus itself. An excellent way to get information about molecular gas at this scale is through water megamasers.

In recent years a number of active galaxies have been found to have powerful H_2O maser emission in their nuclei (Braatz, Wilson, & Henkel 1994; Braatz, Wilson, & Henkel 1994). It is known that the H_2O megamaser phenomenon is associated with nuclear activity since all such megamaser sources are in either Seyfert 2 or LINER nuclei.

It appears reasonable to infer that the masers trace molecular material associated with the obscuring torus or an accretion disk that feeds the nucleus. This notion was confirmed in great detail by VLBI observations of the megamaser in NGC 4258 (Miyoshi et al. 1995 & Greenhill et al. 1995, see also Fig. 2.5). The positions and velocities of the H_2O maser lines show that the masing region is a thin disk in Keplerian rotation around a central mass of $3.9 \cdot 10^7 M_\odot$ at a distance of $\approx$0.16 pc from that mass (Herrnstein et al. 1999).

Although plausible scenarios for the megamaser phenomenon exist (e.g., Neufeld & Maloney 1995), it is by no means clear how the material which obscures the nucleus (the "obscuring torus") and the masing disk are related. The masing disk may be part of a geometrically thin, molecular accretion disk at smaller radii than the torus, or the thin, central plane of a thick torus in which the column density is high enough for strong amplification. Alternatively, the whole structure could be a warped thin disk, so the masing gas might be misaligned with the central accretion disk. The most straightforward picture consistent with current data would, however, have the masing disk, obscuring torus and any more extended molecular cloud distribution as one coherent accretion structure feeding the central engine, with the ionized thermal and non-thermal radio plasma roughly along the rotation axis.

We have therefore started a program to observe the narrow-line regions (NLR) of all known megamaser galaxies with the Hubble Space Telescope (HST) to establish this often suggested link between the molecular disk responsible for the maser emission and the obscuring torus responsible for the ionization cones. We are also obtaining continuum color images to search for the obscuring material directly.

The most luminous known H_2O maser source is found in the galaxy TXS2226-184 (IRAS F22265-1826; Koekemoer et al. 1995), at a redshift of z=0.025 (luminosity distance D=101 Mpc for $H_0 = 75$ km sec^{-1} Mpc^{-1} and $q_0 = 0.5$; in the images $0\farcs1$ correspond to 46 pc). Here we present Hα+[N II]$\lambda\lambda$6548,6583 and broad-band radio continuum observations of TXS2226-184 obtained with the HST and the VLA. Our results indeed show a linear Hα+[N II] structure along the radio axis and perpendicular to a dust lane. This supports the connection between megamaser emission, dusty disk, obscuring torus, and the narrow-line region discussed above. Observational details are given in Falcke et al. (2000c).

A slightly super-resolved map of TXS 2226-184 at 8.46 GHz using a circular restoring beam of $0.2''$ is shown in Figure 5.7 (right) where we have subtracted the central point source to show the extended emission more clearly. The source is resolved with a peak flux density of 15 mJy and a total flux density of 23 mJy. The emission is elongated in PA $-37°$ towards the NW and in PA 146° towards the SE. The position of the central radio component is $\alpha = 22^h26^m30\fs07$, $\delta = -18°26'09\farcs6$ (B1950).

Our HST images are shown in Figure 5.7. The continuum map, which is the

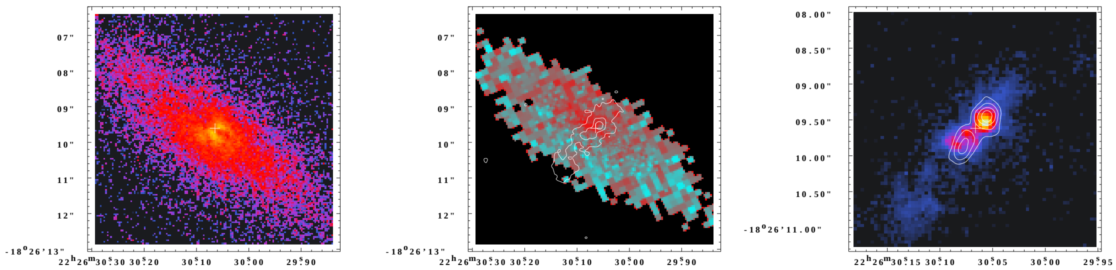

Figure 5.7: Left: continuum map obtained by averaging the red and green images taken with the Planetary Camera (0.″0455 pixel size). The centroid of the continuum in the inner part of the galaxy (see text) is marked here and in the following panels by a cross, and the B1950 coordinates are from the VLA astrometry (assuming the radio nucleus and the optical centroid are coincident). Middle: color map obtained by dividing the green by the red continuum image (same spatial scale as left). The flux density ratio ranges from 0.4 (red colors) to 1.5 (blue colors) which roughly corresponds to V–I colors ranging from 2.2 to 0.8. The gray areas are around V–I$\sim$1.3. Contours overlaid are of the Hα+[N II] image (right). Right: continuum subtracted Hα+[N II] image of TXS2226-184. The Hα+[N II] flux in a rectangular $1.7'' \times 3.2''$ aperture is 2.5×10^{-14} erg s^{-1} cm^{-2} and the intensity scale is proportional to the square root of the brightness. Contours overlaid are of the 8.46 GHz VLA radio continuum (contours starting at 0.3 mJy and increasing by factors of $\sqrt{2}$). We have subtracted the central point source from the radio map to show the extended structure more clearly.

combination of the red and green filters used also for off-band subtraction, reveals a highly elongated galaxy along PA 55°. The inner region ($1''$ diameter) is bisected by a dark band, presumably a nuclear dust lane. The presence of this dust lane is further strengthened by the color map, which shows a region of high reddening along PA 60° extending roughly $1''$ across the nucleus.

The Hα+[N II] map shows a highly elongated structure roughly along PA $-40° \pm 5°$, i.e. in the same direction as the radio emission, with a bright spot 0.″2 NW of the supposed nucleus. The emission extends further towards the SE, with a broad, "wiggly" structure near the nucleus and a "plume" 1.″5 from the nucleus. The adopted nucleus in the HST images is within 1.″5 – the typical error in absolute HST astrometry – of the radio nucleus.

We have fitted elliptical isophotes to the red continuum image of the galaxy ignoring the innermost few pixels which are heavily affected by the dust lane. For a disk + bulge model (a) we obtained a good fit (reduced $\chi^2 = 0.86$) with the parameters $\mu_0 = 18.0$ mag arcsec^{-2}, $R_0 = 2.''4$ (1.1 kpc), $\mu_{\rm e} = 19.7$ mag arcsec^{-2}, and $R_{\rm e} = 0.''6$ (0.29 kpc). For a bulge component only (b), i.e. an elliptical galaxy profile, the fit is much worse (reduced $\chi^2 = 4.9$). The ellipticity of TXS2226-184 ($e = 1 - b/a = 0.61$ at $2.''7 < R < 6.''0$) indicates an inclination of the galaxy to the line of sight of 70° (using $i = \arcsin\sqrt{(1-(b/a)^2)/0.96}$, e.g., Whittle 1992a).

Koekemoer et al. (1995) have classified this galaxy as an elliptical or S0 and speculated whether the unusually broad line-width of the megamaser emission seen in this galaxy and in NGC1052 might be typical of elliptical galaxies. Our HST images reveal that TXS2226-184 is almost certainly not an elliptical, so NGC1052 remains the only known megamaser in an elliptical galaxy (Braatz, Wilson, & Henkel 1994). On the other hand, the high inclination of TXS2226-184 strengthens the tentative conclusion of Braatz, Wilson, & Henkel (1997) that megamasers are preferentially found in highly inclined galaxies. This excess suggests that nuclear and large scale dust disks in many active spiral galaxies are indeed related.

The NLR in TXS2226-184 is very elongated and reminiscent of the jet-like NLR seen in many Seyfert galaxies, as imaged by HST (see previous section). These gaseous structures are believed to be produced in the interaction between outflowing radio ejecta and the ISM. The fact that our radio map is elongated along exactly the same direction as the NLR supports this view.

In addition to the NLR and radio jet, we find a dust lane in the nucleus which aligns with the galaxy major axis and presumably represents its normal interstellar medium. The elongation of the NLR and the radio source perpendicular to the NE-SW dust lane suggests that the nuclear accretion disk and the obscuring torus are more or less coplanar with the stellar disk in TXS2226-184. Preliminary results of VLBA observations of the masers in this galaxy indeed seem to roughly show a NE-SW orientation along PA 20° (Greenhill, priv. comm.).

However, if one interprets this megamaser structure in analogy to NGC 4258 as a molecular disk it would indicate a certain degree of warping between large-scale and small-scale disks and jets. The same is seen in the galaxy NGC 3079 (Fig. 5.8) – another galaxy in our HST program – where the masing "disk" and the nuclear radio jet are inclined by 45°. On even larger scales the axis of the outflow is determined by huge bubbles seen in radio and Hα (see Seaquist, Davis, & Bignell 1978, also Fig. 5.8) along the minor axis of the galaxy. If one looks at Seyfert galaxies as a whole, however, there is quite a distribution of misalignments between AGN axes and galaxy minor axes (e.g., Nagar & Wilson 1999 an refs. therein). These few examples already indicate that the radio jets in these radio-quiet objects apparently encounter many obstacles on their way out. Already on the parsec-scale the "torus" or just a molecular gas layer could have its rotation axes misaligned with the jet axis and deflect or slow down the jet. Further out, the interaction with the gas in the ISM, that we see as the NLR, further impacts the jet structure and can lead to a diverse morphological appearance at random angles. While this can produce spectacular structures it will make quantitative studies of jets in radio-quiet AGN difficult. Hence, only at the very smallest scales where radio cores are produced, and possibly at the highest frequencies, do we stand a chance to study the AGN practically in isolation. This, to some degree, justifies the special attention those cores have received in the previous chapters and sections.

Note added in Proof: As a postscriptum and late addition to this chapter, it should be mentioned that on 17 March 2000 we (i.e. together with C. Henkel, A. Peck, and Y. Hagiwara) discovered yet another megamaser galaxy with the Effelsberg 100 m dish. This in itself is exciting, since megamasers are rare and of great scientific interest. What makes this new discovery even more interesting is that the galaxy, Mrk 348, is one of the Seyferts with the brightest and most variable radio cores. Though not as extreme, it is comparable in spectrum and variability to III Zw 2 discussed in the previous section. The radio core flux in Mrk 348 now underwent a similarly strong outburst as III Zw 2 with a radio flux exceeding 1 Jy at high frequencies. At the same time the previously undetected megamaser emission appeared. It should warrant some curiosity that even though only 5% of Seyferts show megamaser emission, among those 19 discovered so far quite a few belong to the small class of Seyferts with relatively bright (several tens of mJy) radio cores. Mrk 348 is the most recent example of a growing list that also includes NGC 2639, NGC 1068, NGC 3079, and Mrk 1210. Clearly the radio cores are needed to provide seed photons for the megamaser, but is there another, deeper connection we do not understand yet? This question will be left to future research.

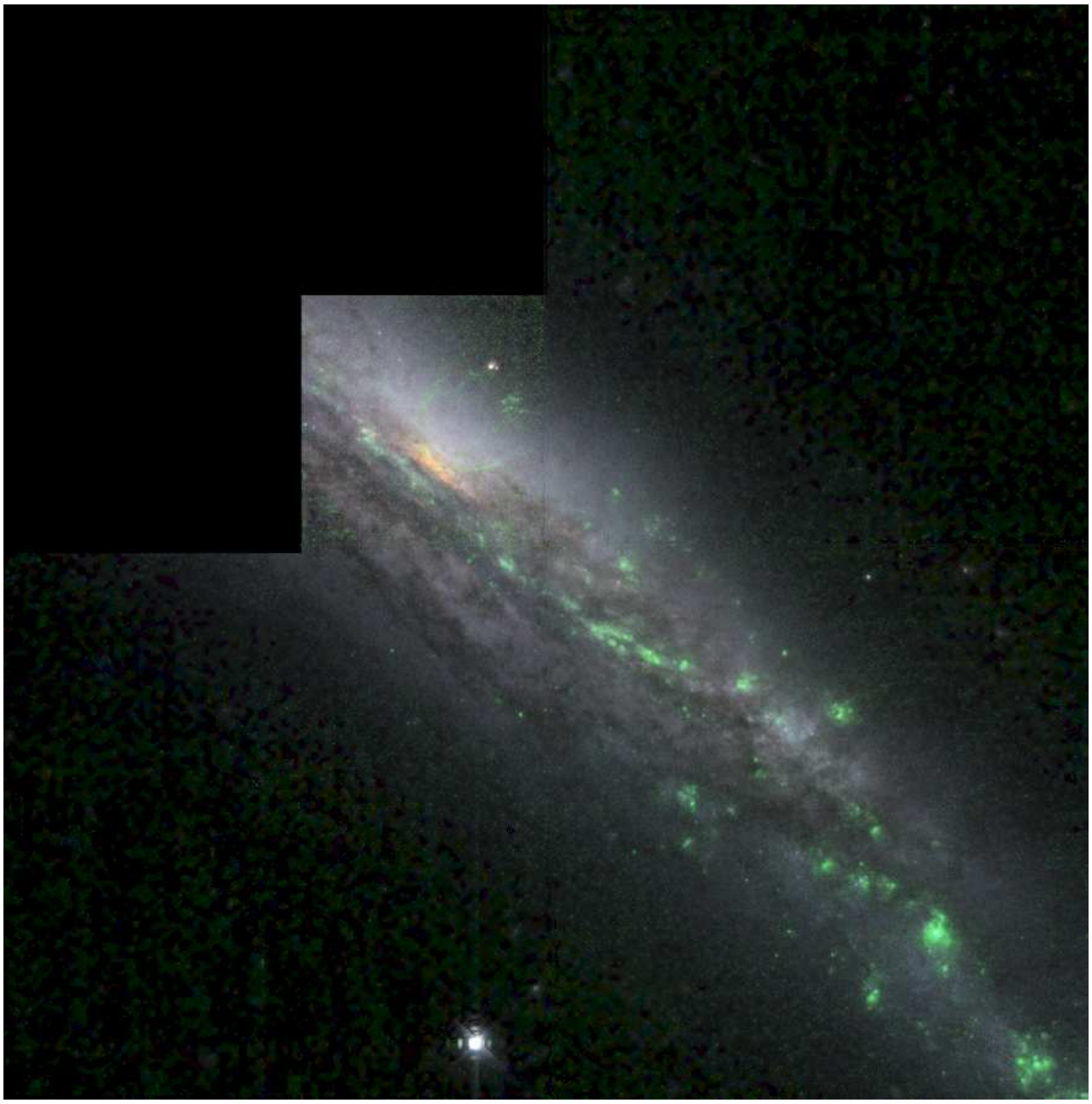

Figure 5.8: Composite (false-color) HST image of the megamaser galaxy NGC 3079. Green colors represent the Hα emission and red and blue colors represent the emission seen in the two continuum filters. Aside from many star forming regions one can see a faint "bubble" of ionized Hα-emitting gas emerging from the center. The center is obscured by a highly reddened dust lane. The nuclear maser "disk" seems to align with this dust disk, while the central radio jet is inclined by roughly 45° to this disk (Trotter et al. 1998), pointing towards one of the arms of the bubble.

Chapter 6

Conclusions and Outlook

After many pages of a detailed analysis of black holes, radio cores, and jets, summarizing many years of research, it is now time to reflect on the results. "The universe is simple, it just looks complicated" could be one of the messages. AGN can come in many different disguises, producing a large variety of classifications, yet the underlying astrophysical scheme remains the same. Whether we talk about quasars, Blazars, radio galaxies, CSOs, Seyferts, LINERs, or even some X-ray binaries, the common engine seems to be an accreting black hole.
Of course, we are still far from understanding how these black holes work and what physical processes play which role. There is certainly significant plasma physics involved which is a great challenge for a distant observer. One should just imagine how difficult it would be for an alien astronomer to predict something like lightning on a planet called Earth with a piece of paper and a telescope – without being able to be in the midst of a thunderstorm.
So, while some of the ripples we see in the emission from black holes may just be space weather, there are some fundamental constants as well. Radio cores and jets are one example. In part based on the findings presented here, we can say that in all types of active sources with a black hole, radio cores have been found. While this cannot yet be claimed for every single black hole, it is still true that there is no region of the explored parameter space where not at least one black hole produces such a radio core. We find them in high- or low-luminous, radio-loud or radio-quiet, supermassive or even stellar mass black holes. The intermediate radio cores we have found in LLAGN illustrates this huge range: it would be equally correct to call them "giant Sgr A*'s" or "dwarf quasars". The radio cores in the different objects all have very similar properties: high brightness temperatures, flat radio spectrum, variable emission, and in many cases a jet structure. This homogeneity makes it very likely that they are all produced by one basic process. The theoretical foundation to explain the emission from these cores has been described at the beginning of this work. The basic idea being a flow of relativistic plasma collimated near the black hole and ejected along the rotation axis of the disk. When calculated it turns out that this can reproduce the observed properties of radio cores in great detail. The emission is produced close to the black hole

where it dominates its environment. Moreover, a black hole has only two basic parameters: the mass and the angular momentum. In addition we only have the mass accretion rate as a major free parameter, thus explaining why radio cores are so similar over an amazingly large range of astrophysical situations. While it is not yet proven that all these jets are relativistic it is certainly implied by the model. The finding of the first superluminal jet in a Seyfert galaxy presented here could be the first step in establishing this idea.

In general, the existence of radio cores at all scales also shows that jet formation is apparently possible under all circumstances. Even though we do not exactly know why and how jets are formed, it seems that nature always finds a way to make them. This suggests that jets are an integral part of accretion physics and thus also of black hole physics. It should no longer be possible to just calculate how much matter is flowing into the black hole, one should always also have to consider how much is flowing out. The drain of mass and energy, presumably near the inner edge of the accretion flow, is an important boundary condition for all accretion models. The idea of a "jet-disk symbiosis" formulated in our earlier papers therefore seems an appropriate description of this relation.

What else can the radio cores offer for the future? First, it is important to have established the clear link between radio cores and black holes/AGN. Black holes may be black, but they are not dark – at least not in the radio regime. In the optical, searching for a black hole can often be a search for a needle in a haystack. In the Galactic Center it certainly is. With radio interferometers at high frequencies the haystack is gone and only the needle remains. Consequently, with more sensitive arrays we will be easily able to pinpoint black holes in the local and distant universe. Telescopes like the planned Square-Kilometer-Array with a hundred-fold increase in sensitivity over the VLA will therefore pick out literally thousands of new black hole candidates.

Among other things this will provide us with the most accurate measurement of the center of mass of galaxies, assuming that supermassive black holes are just this. The astrometric precision reached with VLBI is now approaching 100 μarcseconds and in some cases can already be pushed to tens of μarcseconds. With such precision and enough sensitivity, one could in principle detect the proper motion of the center of M31 rotating around the Milky Way within a few years. Even slightly more distant galaxies, like M81 with its bright radio nucleus, are not completely out of reach for such a project, given somewhat longer time scales. Like the stellar proper motions in the Galactic Center this would allow one to more reliably determine the large scale gravitational potential, e.g., of the Local Group, and confirm the presence of dark matter.

As outlined in Chap. 3.9, radio cores can also serve to illuminate the immediate surroundings of a black hole, thus probing the smallest scales of a gravitational potential – the event horizon. For the Galactic Center the shadow of the black hole is already within reach of current and planned radio-interferometers at mm- and submm-wavelengths. If not achieved earlier, this will be an important project for the upcoming ALMA (Atacama Large Millimeter Array) telescope. With its high sensitivity at the highest frequencies in a southern location it is an ideal backbone for a submm-VLBI array imaging the event horizon in Sgr A*. With the exception perhaps of M87, we may have to wait much longer to do a similar experiment in any other compact radio core. However, in principle it is just a question of technological progress until even this will be possible in other sources as well.

Finally, with a better understanding of the physics of radio cores and the detection of more faint ones, we will also pick out more cores at higher redshifts and perhaps be able to use them as cosmological probes. So far we are biased towards the brightest objects, i.e. those which are relativistically boosted and pointing towards us. Once we see the entire range of radio cores and can get a better estimate of their apparent sizes and luminosities we should be able to distinguish between different cosmologies.

These ideas just summarize what is possible in principle. Many other, perhaps more ordinary, applications may follow. Radioastronomy with its interferometric technique provides a unique tool, making black holes readily accessible. Perhaps, some day, black hole physics will almost become an ordinary experimental science. At least we know: their radio cores are out there, waiting to be explored.

Chapter 7

Summary

Radio jets are the “smoking guns” of active galactic nuclei (AGN). They are also the site of many high-energy processes, including X-ray and γ-ray emission as well as high-energy particle acceleration. Early on it was the radio emission from these jets which drew people’s attention to quasars and led to their discovery. Today we know that radio jets are relativistic, magnetized plasma flows ejected at velocities close to the speed of light most likely from the immediate vicinity of black holes. At the smallest scales, the radio emission from these jets appears as very compact radio cores with a flat and variable radio spectrum. With Very Long Baseline Interferometry this emission can often be resolved into a core-jet structure sometimes showing apparent superluminal motion caused by the relativistic ejection velocity. However, similar radio cores have also been found in quite a number of other sources, including the center of the Milky Way (Sgr A*), X-ray binaries (stellar mass black holes and neutron stars), and some nearby galaxies. Despite being interesting in their own right, none of these sources can compare in their power output and violence with quasars. On the other hand it is thought that in all these cases black holes (and in a few cases also neutron stars) are involved as well, possibly accreting at much lower levels – in absolute terms – than quasars.
In this review we investigate how these low-luminosity radio cores are related to their much more powerful siblings in quasars, radio galaxies, and Blazars. It is suggested that all radio cores can be described in a very similar fashion as jets coupled to an accretion disk, with jet and disk being symbiotic features in an accretion scenario of black holes. At some level every black hole will accrete material and only a minority of sources reach the enormous power levels of quasars. The “silent majority” of black holes therefore operates at much lower levels producing much fainter radio cores.
Based on this idea of a “jet-disk symbiosis” a general emission model for radio cores is presented which describes the radio emission of a collimated relativistic plasma flow after leaving its collimation region – the nozzle. This part of the jet is most likely dominated entirely by free expansion and is relatively independent of environmental influences. This leads to a relatively homogeneous appearance of compact radio cores in different sources with the jet power or the accretion rate

being the main parameter.

The model is used to describe some "famous" and relatively well-constrained radio cores, ranging from a Galactic X-ray binary to a megamaser galaxy. One can show that despite the vastly different scales in accretion rates and black hole masses the model describes radio cores properties, i.e. size and flux as a function of frequency, correctly.

An even more detailed investigation is presented of the radio core and supermassive black hole candidate Sgr A* in the Galactic Center. Its quasi-simultaneous radio spectrum was determined in an international observing campaign, confirming the existence of an inverted cm-wave spectrum and a "submm-bump". Daily flux density monitoring over more than two years reveal variations on characteristic time scales of ten to hundred days and phases of quasi-periodic oscillations which are possibly related to variations intrinsic to the accretion flow. The polarization of the Sgr A* radio spectrum is rather unusual with only upper limits for linear polarization but an unexpected new discovery of circular polarization. The entire spectrum can be described very well by the jet model mentioned before, including the most recent X-ray observations, and taking new high-frequency VLBI limits on the extended structure into account. Finally, it is pointed out that the submm-bump in the spectrum, which is most certainly produced on the smallest scales in the system, can be used as a background against which one could image the event horizon of the black hole. Using 3D general relativistic ray-tracing calculations one can show that the shadow cast by the event horizon onto the submm-emitting region has a size of 30 μarcseconds – a size within reach of the currently developed new generation of high-frequency VLBI arrays.

To extend the view further, results of a search for Sgr A*-like radio cores in a sample of nearby Low-Luminosity AGN (LLAGN) is presented. Almost half of the surveyed LINER and dwarf-Seyfert galaxies indeed show compact flat-spectrum radio emission. The AGN nature is confirmed by high-resolution VLBI observations. The brightest sources do show core-jet structures and the spectral index is within the range expected from a jet model, while being too flat for emission from an Advection Dominated Accretion Flow (ADAF). The measured radio fluxes as a function of optical luminosity fall just within the range predicted by the jet-disk symbiosis model and confirm that these radio cores are the faint counterparts to radio cores in quasars.

Finally, the radio emission from radio-quiet AGN – which make up the majority of quasars and Seyferts – are considered. Hubble Space Telescope and Very Large Array observations of Seyfert and megamaser galaxies reveal that even in radio-quiet AGN jets are powerful enough to significantly shape their environment. VLBI observations of one particular spiral galaxy with a bright Seyfert nucleus show for the first time superluminal motion in a galaxy type which usually is exclusively associated with radio-quiet AGN. This galaxy was considered to be a part of a small sample of radio-intermediate quasars which were proposed to be relativistically boosted radio-quiet quasars or Seyferts. The observations confirm

that even in radio-quiet AGN relativistic jets are present and validates the use of the radio core/jet model also for these sources.
To conclude, one can say that the production of a relativistic jets seems to be an inevitable consequence of accreting black holes and is possible even at very low accretion rates. Therefore, compact radio cores are an ideal tracer of black holes in the near and distant universe. With the increasingly higher resolution and sensitivity of radiointerferometers, they allow an intimate look at how black holes work at various scales and in different contexts. In the future, radio cores could also be used as cosmological probes and as reference points to precisely measure even the proper motions of entire galaxies in search for dark matter.

Chapter 8

Zusammenfassung

Radiojets sind, im wahrsten Sinne des Wortes, die herausragendsten Zeichen aktiver galaktischer Kerne (AGN). Sie sind auch verantwortlich für viele Hochenergieprozesse in der Astrophysik, von der Röntgenemission, über γ-Emission bis hin zur Teilchenbeschleunigung bei höchsten Energien. Schon ganz am Anfang zog die Radioemission der Jets die Aufmerksamkeit von Wissenschaftlern auf sich, was zur Entdeckung der Quasare führte. Heute wissen wir, dass es sich dabei um relativistische, magnetisierte Plasmastrahlen handelt, die mit nahezu Lichtgeschwindigkeit aus der unmittelbaren Umgebung eines schwarzen Lochs hinaus geschleudert werden. Auf den kleinsten Skalen erscheint die Radioemission dieser Jets als kompakter Kern mit einem flachen und variablen Radiospektrum. Mit Hilfe der Very Long Baseline Interferometry (VLBI) kann diese Emission meistens in eine Kern-Jet-Struktur aufgelöst werden, die in einigen Quellen scheinbar überlichtschnelle Bewegungen zeigt. Letzteres ist eine optische Täuschung, die durch die relativistische Strömungsgeschwindigkeit verursacht wird.
Man kann allerdings sehr ähnliche Radiokerne auch in einer ganzen Reihe anderer Quelle entdecken, z.B. im Zentrum der Milchstraße (Sgr A*), in galaktischen Röntgen-Doppelsternen (stellare schwarze Löcher oder Neutronensterne) und auch in einigen nahen Galaxien. Obwohl für sich genommen interessant, können diese Quellen doch nicht die unglaublichen Energieausstöße erreichen, wie sie Quasare zeigen. Immerhin geht man auch in diesen Fällen davon aus, dass hier ein schwarzes Loch (in einigen Fällen auch ein Neutronenstern) eine entscheidende Rolle spielt, wobei es scheint, als ob diese schwarzen Löcher auf einem, in absoluten Einheiten, viel niedrigeren Niveau akkretieren.
In dieser Arbeit wird untersucht, ob und in welcher Weise leuchtschwache und radio-leise Radiokerne mit ihren großen Geschwistern in Quasaren, Radiogalaxien und Blazaren verwandt sind. Es wird vorgeschlagen, dass alle Radiokerne in einem einheitlichen Bild beschrieben werden können, bei dem Jet und Scheibe ein symbiotisches System innerhalb eines Akkretionsmodells für schwarze Löcher bilden. Auf irgendeinem, wenn auch noch so kleinen, Niveau wird jedes schwarze

[1]Dieser Abschnitt benutzt die neue deutsche Rechtschreibung.

Loch akkretieren, aber nur eine kleine Minderheit erreicht die enormen Leistungen eines Quasars. Die "schweigende Mehrheit" der schwarzen Löcher arbeitet daher auf einem niedrigen Niveau mit entsprechend leuchtschwachen Radiokernen.

Basierend auf dieser Idee einer "Jet-Scheiben-Symbiose" wird ein allgemeines Emissionsmodell für Radiokerne hergeleitet, das die Radioemission eines kollimierten, relativistischen Plasmastromes beschreibt, der die Kollimationszone – die Düse – verlassen hat und sich frei ausdehnt. Dieser Teil des Jets ist, wegen des großen Überdrucks, mit aller Wahrscheinlichkeit relativ unabängig von Umgebungseinflüssen. Dies führt zu einem relativ homogenen Erscheinungsbild kompakter Radiokerne in unterschiedlichen Quellen, wobei die Leistung im Jet bzw. der Akkretionscheibe der entscheidende freie Parameter ist.

Das Modell wird zunächst benutzt, um einige bekannte und gut bestimmte Radiokerne zu beschreiben. Dabei wird der Bereich von galaktischen Röntgen-Doppelsternen bis hin zu einer nahen Megamaser-Galaxie abgedeckt. Es kann gezeigt werden, dass trotz der sehr unterschiedlichen Skalen bezüglich Akkretionsrate und zentraler Masse das Modell die Eigenschaften des Kernes, d.h. Größe und Fluss als Funktion der Frequenz, sehr gut beschreibt.

Darüberhinaus wird eine detailliertere Untersuchung des Radiokerns und vermutlichen schwarzen Lochs im Zentrum der Milchstraße vorgelegt. Dessen quasisimultanes Radiospektrum wurde in einer internationalen Kampagne bestimmt. Die Beobachtungen bestätigten ein leicht invertiertes Spektrum und die Existenz eines "submm-Buckels". Tägliche Flussdichtemessungen über mehr als zwei Jahre zeigen Variabilität mit charakteristischen Zeitskalen von einigen zehn bis hundert Tagen und Phasen quasi-periodischer Aktivitäten, die wahrscheinlich auf Instabilitäten im Akkretionsfluss zurückzuführen sind. Die Polarisation von Sgr A* ist ausgesprochen ungewöhnlich, mit niedrigen oberen Grenzwerten für die lineare Polarisation und einer überraschenden Entdeckung von zirkularer Polarisation. Das gesamte Radiospektrum kann mit einem Jetmodell im Detail reproduziert werden. Dies schließt auch die neuesten Röntgenmessungen ein und berücksichtigt die oberen Grenzen für die ausgedehnte Emission, die mit VLBI-Beobachtungen im Hochfrequenzbereich bestimmt worden sind. Schließlich wird darauf hingewiesen, dass der submm-Buckel im Spektrum, welcher höchstwahrscheinlich auf den kleinsten räumlichen Skalen produziert wird, eine ideale Hintergrundquelle bildet, gegen den man den Ereignishorizont des schwarzen Lochs abbilden kann. Mit Hilfe von dreidimensionalen allgemeinrelativistischen Ray-Tracing Rechnungen kann gezeigt werden, dass der vom Ereignishorizont produzierte "Schatten" eine Größe von c.a. 30 μ-Bogensekunden haben muss und somit im Auflösungsbereich der nächsten Generation von VLBI-Arrays bei hohen Frequenzen liegt.

Um das Blickfeld noch mehr zu erweitern werden die Ergebnisse einer Suche nach Sgr A*-ähnlichen Radiokernen in einer Stichprobe leuchtschwacher AGN (LLAGN) vorgestellt. Fast die Hälfte aller untersuchten LINER und Seyfert-Galaxien zeigen dabei kompakte, flachspektrum Emission. Durch VLBI-Beobachtungen wird nachgewiesen, dass es sich dabei tatsächlich um Emission von

einem AGN handelt. Dabei zeigen die hellsten Quellen eine Kern-Jet-Struktur. Die gemessenen Spektren sind kompatibel mit den Voraussagen des Jetmodels und zu flach, um von einem advektionsdominierten Akkretionsfluss (ADAF) zu stammen. Die gemessenen Radioflüsse, im Verhältnis zu den optischen Helligkeiten, bewegen sich ebenfalls im Bereich der Voraussagen des Jet-Scheiben-Symbiose-Modells und bestätigen, dass es sich bei diesen Quellen um die leuchtschwachen Gegenstücke zu Quasaren handelt.
Schließlich wird im Rahmen dieser Arbeit auf die Radioemission radio-leiser AGN eingegangen, die den weitaus größten Teil von Quasaren und Seyfert-Galaxien ausmachen. Beobachtungen von Seyfert- und Megamaser-Galaxien mit dem Hubble-Space-Teleskop und dem Very-Large-Array zeigen, dass es auch in radio-leisen AGN Jets gibt, die ihre Umgebung signifikant beeinflussen können. VLBI-Beobachtungen einer speziellen Spiralgalaxie mit hellem Seyfertkern zeigen darüberhinaus zum erstenmal scheinbare Überlichtgeschwindigkeiten in einem Galaxientyp, der normalerweise ausschließlich mit radio-leisen AGN in Verbindung gebracht wird. Die Galaxie war Teil einer Gruppe von sogenannten radio-intermediären Quasaren bei denen man vermutete, dass es sich um relativistisch geboostete radio-leise Quasare oder Seyfert-Galaxien handelte. Die Beobachtungen bestätigen nun, dass es auch in radio-leisen AGN relativistische Jets gibt und somit auch dort das Jetmodell zur Anwendung kommen kann.
Zusammenfassend kann man sagen, dass die Produktion eines relativistischen Jets wahrscheinlich eine unausweichliche Konsequenz akkretierender schwarzer Löcher ist – selbst bei den niedrigsten Akkretionsraten. Daher sind kompakte Radiokerne ein idealer Indikator für schwarze Löcher im nahen und fernen Universum. Mit der sich immer noch steigernden Auflösung und Empfindlichkeit von Radiointerferometern erlauben sie einen genauen Einblick in die Arbeitsweise von schwarzen Löchern auf den verschiedensten Skalen und in den verschiedensten Zusammenhängen. In der Zukunft könnten Radiokerne für kosmologische Fragestellungen und als Referenzpunkte zur genauen Bestimmung extragalaktischer Eigenbewegungen im Rahmen der Suche nach dunkler Materie dienen.

Chapter 9

Bibliography

The material presented in the previous chapters – texts and figures – was taken in part from the publications listed below. The initial number refers to the section number used here, followed by the short references to the original papers. The full reference is given in the "Reference" section. Parts of text from a previous publication were used only where the lead author of the publication and the author of this review were identical. In all cases the text was modified and adapted for this review. Some of the material will become part of a review for "Annual Reviews of Astronomy & Astrophysics".

1.1: Falcke 1998a

1.2: Falcke et al. 2000b

1.3: Falcke & Biermann 1999

2.1: Falcke 1998b

2.2: Falcke 1998b

2.3: Falcke 1998b

2.4: Falcke 1998b

2.5: Falcke 1996a

2.6: Falcke & Biermann 1999

2.7: Falcke & Biermann 1999

2.8: Falcke 1996a

3.2: Falcke 1997; Falcke et al. 1998

3.3: Falcke et al. 1998; Falcke 1996b

3.4: Falcke 1999

3.5: Bower et al. 1999a; Bower et al. 1999b

3.6: Bower, Falcke, & Backer 1999b

3.7: Falcke 1996b

3.8: Falcke & Markoff 2000

3.9: Falcke, Melia, & Agol 2000

4.1: Nagar et al. 2000

4.2: Falcke et al. 2000b

4.3: Falcke et al. 2000b; Falcke et al. 2000a

5.0: Falcke 1998a

5.1: Falcke 1998a; Falcke, Sherwood, & Patnaik 1996; Falcke et al. 1999; Brunthaler et al. 2000

5.2: Falcke 1998a; Falcke, Wilson, & Simpson 1998; Falcke et al. 2000c

Chapter 10

References

REFERENCES

Aharonian, F. A., et al. 1999, A&A, 349, 11

Aitken, D. K., Greaves, J. S., Chrysostomou, A., Holland, W. S., Hough, J. H., Pierce-Price, D., & Richer, J. S. 2000, ApJ Letters, in press

Akujor, C. E., Luedke, E., Browne, I. W. A., Leahy, J. P., Garrington, S. T., Jackson, N., & Thomasson, P. 1994, A&AS, 105, 247

Aller, M. F., Aller, H. D., & Hughes, P. A. 1992, ApJ, 399, 16

Alonso-Herrero, A., Rieke, M. J., Rieke, G. H., & Shields, J. C. 2000, ApJ, 530, 688

Antonucci, R. 1993, ARA&A, 31, 473

Arp, H. 1968, ApJ, 152, 1101

Backer, D. C., & Sramek, R. A. 1999, ApJ, 524, 805

Backer, D. C., Zensus, J. A., Kellermann, K. I., Reid, M., Moran, J. M., & Lo, K. Y. 1993, Science, 262, 1414

Baganoff, F., et al. 1999, in American Astronomical Society Meeting, Vol. 195, 6201

Bahcall, J. N., Kirhakos, S., Saxe, D. H., & Schneider, D. P. 1997, ApJ, 479, 642

Baldwin, J. A., Wilson, A. S., & Whittle, M. 1987, ApJ, 319, 84

Balick, B., & Brown, R. L. 1974, ApJ, 194, 265

Bardeen, J. M. 1973, in Black Holes, ed. C. DeWitt & B. S. DeWitt (New York: Gordon & Breach), 215

Barth, A. J., Ho, L. C., Filippenko, A. V., & Sargent, W. L. W. 1998, ApJ, 496, 133

Baum, S. A., & Heckman, T. 1989, ApJ, 336, 702

Beckert, T., & Duschl, W. J. 1997, A&A, 328, 95

Begelman, M. C., & Cioffi, D. F. 1989, ApJ, 345, L21

Bicknell, G. V. 1994, ApJ, 422, 542

Bicknell, G. V., Dopita, M. A., Tsvetanov, Z. I., & Sutherland, R. S. 1998, ApJ, 495, 680

Biermann, P. L., & Strittmatter, P. A. 1987, ApJ, 322, 643

Biermann, P. L., Strom, R. G., & Falcke, H. 1995, A&A, 302, 429

Bietenholz, M. F., Bartel, N., & Rupen, M. P. 1999, ApJ, in press

Bietenholz, M. F., et al. 1996, ApJ, 457, 604

Black, A. R. S., Baum, S. A., Leahy, J. P., Perley, R. A., Riley, J. M., & Scheuer, P. A. G. 1992, MNRAS, 256, 186

Blandford, R. D., & Königl, A. 1979, ApJ, 232, 34

Blumenthal, G. R., & Gould, R. J. 1970, Reviews of Modern Physics, 42, 237

Blundell, K. M., & Beasley, A. J. 1998, MNRAS, 299, 165

Böhringer, H., Voges, W., Fabian, A. C., Edge, A. C., & Neumann, D. M. 1993, MNRAS, 264, L25

Boroson, T. A., & Green, R. F. 1992, ApJS, 80, 109

Bower, G., Wilson, A., Morse, J. A., Gelderman, R., Whittle, M., & Mulchaey, J. 1995, ApJ, 454, 106

Bower, G. A., Wilson, A. S., Mulchaey, J. S., Miley, G. K., Heckman, T. M., & Krolik, J. H. 1994, AJ, 107, 1686

Bower, G. C., & Backer, D. C. 1998, ApJ, 496, L97

Bower, G. C., Backer, D. C., Zhao, J. H., Goss, M., & Falcke, H. 1999a, ApJ, 521, 582

Bower, G. C., Falcke, H., & Backer, D. C. 1999a, in American Astronomical Society Meeting, Vol. 195, 6203

Bower, G. C., Falcke, H., & Backer, D. C. 1999b, ApJ, 523, L29

Bower, G. C., Wright, M. C. H., Backer, D. C., & Falcke, H. 1999b, ApJ, 527, 851

Braatz, J. A., Wilson, A. S., & Henkel, C. 1994, ApJ, 437, L99

Braatz, J. A., Wilson, A. S., & Henkel, C. 1997, ApJS, 110, 321

Bridle, A. H., Hough, D. H., Lonsdale, C. J., Burns, J. O., & Laing, R. A. 1994, AJ, 108, 766

Bridle, A. H., & Perley, R. A. 1984, ARA&A, 22, 319

Brown, R. L., & Lo, K. Y. 1982, ApJ, 253, 108

Brunthaler, A., Falcke, H., Bower, G. C., Aller, M. F., Aller, H. D., Teräsranta, H., Lobanov, A. P., Krichbaum, T. P., & Patnaik, A. R. 2000, A&A, Letters, submitted

Cannizzo, J. K., Greenhill, L. J., Herrnstein, J. R., Moran, J. M., & Mushotzky, R. F. 1998, in American Astronomical Society Meeting, Vol. 192, 4103

Capetti, A., Axon, D. J., Macchetto, F., Sparks, W. B., & Boksenberg, A. 1996, ApJ, 469, 554

Capetti, A., Macchetto, F., Sparks, W. B., & Boksenberg, A. 1994, ApJ, 421, 87

Cecil, G., Wilson, A. S., & Tully, R. B. 1992, ApJ, 390, 365

Celotti, A., & Fabian, A. C. 1993, MNRAS, 264, 228

Chevalier, R. A. 1992, ApJ, 397, L39

Clark, N. E., Tadhunter, C. N., Morganti, R., Killeen, N. E. B., Fosbury, R. A. E., Hook, R. N., Siebert, J., & Shaw, M. A. 1997, MNRAS, 286, 558

Coker, R., Melia, F., & Falcke, H. 1999, ApJ, 523, 642

Coker, R. F., & Melia, F. 1997, ApJ, 488, L149

Condon, J. J., Condon, M. A., Gisler, G., & Puschell, J. J. 1982, ApJ, 252, 102

Corbin, M. R., Baldwin, J. A., & Wilson, A. S. 1988, ApJ, 334, 584

Cunningham, C. T. 1975, ApJ, 202, 788

Davies, R. D., Walsh, D., & Booth, R. S. 1976, MNRAS, 177, 319

de Bruyn, A. G., & Wilson, A. S. 1978, A&A, 64, 433

de Young, D. S. 1993, ApJ, 405, L13

Dermer, C. D., & Schlickeiser, R. 1993, ApJ, 416, 458

Devereux, N., Ford, H., & Jacoby, G. 1997, ApJ, 481, L71

Dhawan, V., Mirabel, I. F., & Rodriguez, L. F. 1998, in ASP Conf. Ser. 144: IAU Colloq. 164: Radio Emission from Galactic and Extragalactic Compact Sources, 341

di Matteo, T., Fabian, A. C., Rees, M. J., Carilli, C. L., & Ivison, R. J. 1999, MNRAS, 305, 492

Doeleman, S., Rogers, A. E. E., Backer, D. C., Wright, M., & Bower, G. C. 1999, in ASP Conf. Ser. 186: The Central Parsecs of the Galaxy, ed. H. Falcke, A. Cotera, W. J. Duschl, F. Melia, & M.J. Rieke (San Francisco: Astronomical Society of the Pacific), 98

Donea, A. C., & Biermann, P. L. 1996, A&A, 316, 43

Donea, A. C., Falcke, H., & Biermann, P. L. 1999, in ASP Conf. Ser. 186: The Central Parsecs of the Galaxy, ed. H. Falcke, A. Cotera, W. J. Duschl, F. Melia, & M.J. Rieke (San Francisco: Astronomical Society of the Pacific), 162

Dopita, M. A., & Sutherland, R. S. 1995, ApJ, 455, 468

Duschl, W. J., & Lesch, H. 1994, A&A, 286, 431

Eckart, A., & Genzel, R. 1996, Nature, 383, 415

Eckart, A., & Genzel, R. 1997, MNRAS, 284, 576

Eckart, A., Genzel, R., Hofmann, R., Sams, B. J., & Tacconi-Garman, L. E. 1993, ApJ, 407, L77

Eikenberry, S. S., Matthews, K., Morgan, E. H., Remillard, R. A., & Nelson, R. W. 1998, ApJ, 494, L61

Ekers, R. D., Goss, W. M., & Schwarz, U. J. 1975, A&A, 43, 159

Evans, I. N., Ford, H. C., Kinney, A. L., Antonucci, R. R. J., Armus, L., & Caganoff, S. 1991, ApJ, 369, L27

Faber, S. M., Tremaine, S., Ajhar, E. A., Byun, Y. I., Dressler, A., Gebhardt, K., Grillmair, C., Kormendy, J., Lauer, T. R., & Richstone, D. 1997, AJ, 114, 1771

Falcke, H. 1994, Starved Holes and Active Nuclei, PhD thesis (Bonn: University of Bonn)

Falcke, H. 1996a, ApJ, 464, L67

Falcke, H. 1996b, in IAU Symp. 169: Unsolved Problems of the Milky Way, Vol. 169, 169

Falcke, H. 1997, in Accretion Phenomena and Related Outflows; IAU Colloquium 163, ed. D. T. Wickramasinghe, G. V. Bicknell, and L. Ferrario, ASP Conference Series, Vol. 121, 647

Falcke, H. 1998a, in Stars and Galaxies, Review in Modern Astronomy, Vol. 11 (Astronomische Gesellschaft), 245

Falcke, H. 1998b, in Jets from stars and galactic nuclei, Lecture Notes in Physics, ed. W. Kundt, Vol. 11 (Springer), 19

Falcke, H. 1999, in ASP Conf. Ser. 186: The Central Parsecs of the Galaxy, ed. H. Falcke, A. Cotera, W. J. Duschl, F. Melia, & M.J. Rieke (San Francisco: Astronomical Society of the Pacific), 113

Falcke, H., & Biermann, P. L. 1995, A&A, 293, 665

Falcke, H., & Biermann, P. L. 1996, A&A, 308, 321

Falcke, H., & Biermann, P. L. 1999, A&A, 342, 49

Falcke, H., Bower, G. C., Lobanov, A. P., Krichbaum, T. P., Patnaik, A. R., Aller, M. F., Aller, H. D., Teräsranta, H., Wright, M. C. H., & Sandell, G. 1999, ApJ, 514, L17

Falcke, H., Gopal-Krishna, & Biermann, P. L. 1995, A&A, 298, 395

Falcke, H., Goss, W. M., Matsuo, H., Teuben, P., Zhao, J. H., & Zylka, R. 1998, ApJ, 499, 731

Falcke, H., & Heinrich, O. M. 1994, A&A, 292, 430

Falcke, H., Malkan, M. A., & Biermann, P. L. 1995, A&A, 298, 375

Falcke, H., Mannheim, K., & Biermann, P. L. 1993, A&A, 278, L1

Falcke, H., & Markoff, S. 2000, A&A, to be submitted

Falcke, H., & Melia, F. 1997, ApJ, 479, 740

Falcke, H., Melia, F., & Agol, E. 2000, ApJ, 528, L13

Falcke, H., Nagar, N. M., Wilson, A. S., & Ulvestad, J. S. 2000a, in Black Holes in Binaries and Galactic Nuclei, ESO Workshop, ed. P. W. L. Kaper, E.P.J. van den Heuvel (Springer Verlag), in press

Falcke, H., Nagar, N. M., Wilson, A. S., & Ulvestad, J. S. 2000b, ApJ, submitted

Falcke, H., Patnaik, A. R., & Sherwood, W. 1996, ApJ, 473, L13

Falcke, H., Sherwood, W., & Patnaik, A. R. 1996, ApJ, 471, 106

Falcke, H., Wilson, A. S., Henkel, C., Brunthaler, A., & Braatz, J. A. 2000c, ApJ, 530, L13

Falcke, H., Wilson, A. S., & Simpson, C. 1998, ApJ, 502, 199

Falcke, H., Wilson, A. S., Simpson, C., & Bower, G. A. 1996, ApJ, 470, L31

Fanaroff, B. L., & Riley, J. M. 1974, MNRAS, 167, 31P

Fender, R. P., Garrington, S. T., McKay, D. J., Muxlow, T. W. B., Pooley, G. G., Spencer, R. E., Stirling, A. M., & Waltman, E. B. 1999, MNRAS, 304, 865

Fender, R. P., Pooley, G. G., Brocksopp, C., & Newell, S. J. 1997, MNRAS, 290, L65

Ferrarese, L., Ford, H. C., & Jaffe, W. 1996, ApJ, 470, 444

Ferruit, P., Wilson, A. S., Falcke, H., Simpson, C., Pécontal, E., & Durret, F. 1999, MNRAS, 309, 1

Filippenko, A. V., & Terlevich, R. 1992, ApJ, 397, L79

Ford, H. C., Dahari, O., Jacoby, G. H., Crane, P. C., & Ciardullo, R. 1986, ApJ, 311, L7

Franceschini, A., Vercellone, S., & Fabian, A. C. 1998, MNRAS, 297, 817

Gallimore, J. F., Baum, S. A., & O'Dea, C. P. 1997, Nature, 388, 852

Gammie, C. F., Narayan, R., & Blandford, R. 1999, ApJ, 516, 177

Ghez, A. M., Klein, B. L., Morris, M., & Becklin, E. E. 1998, ApJ, 509, 678

Ghez, A. M., Morris, M., & Becklin, E. E. 2000, International Conference of the Astronomische Gesellschaft at Heidelberg, March 20-24, 2000, 16, 28

Ghisellini, G., Guilbert, P. W., & Svensson, R. 1988, ApJ, 334, L5

Greenhill, L. J., Jiang, D. R., Moran, J. M., Reid, M. J., Lo, K. Y., & Claussen, M. J. 1995, ApJ, 440, 619

Gurvits, L. I., Kellermann, K. I., & Frey, S. 1999, A&A, 342, 378

Gwinn, C. R., Danen, R. M., Tran, T. K., Middleditch, J., & Ozernoy, L. M. 1991, ApJ, 381, L43

Haller, J. W., Rieke, M. J., Rieke, G. H., Tamblyn, P., Close, L., & Melia, F. 1996, ApJ, 468, 955

Haniff, C. A., Wilson, A. S., & Ward, M. J. 1988, ApJ, 334, 104

Hazard, C., Mackey, M. B., & Shimmins, A. J. 1963, Nature, 197, 1037

Heckman, T. M. 1980, A&A, 87, 152

Heckman, T. M., van Breugel, W., Miley, G. K., & Butcher, H. R. 1983, AJ, 88, 1077

Herrnstein, J. R., Greenhill, L. J., Moran, J. M., Diamond, P. J., Inoue, M., Nakai, N., & Miyoshi, M. 1998, ApJ, 497, L69

Herrnstein, J. R., Moran, J. M., Greenhill, L. J., Diamond, P. J., Inoue, M., Nakai, N., Miyoshi, M., Henkel, C., & Riess, A. 1999, Nature, 400, 539

Herrnstein, J. R., Moran, J. M., Greenhill, L. J., Diamond, P. J., Miyoshi, M., Nakai, N., & Inoue, M. 1997, ApJ, 475, L17

Hjellming, R. M., & Johnston, K. J. 1988, ApJ, 328, 600

Ho, L. C. 1999, ApJ, 516, 672

Ho, L. C., Filippenko, A. V., & Sargent, W. L. 1995, ApJS, 98, 477

Ho, L. C., Filippenko, A. V., & Sargent, W. L. W. 1996, ApJ, 462, 183

Ho, L. C., Filippenko, A. V., & Sargent, W. L. W. 1997, ApJS, 112, 315

Ho, L. C., Filippenko, A. V., Sargent, W. L. W., & Peng, C. Y. 1997, ApJS, 112, 391

Holloway, A. J., Steffen, W., Pedlar, A., Axon, D. J., Dyson, J. E., Meaburn, J., & Tadhunter, C. N. 1996, MNRAS, 279, 171

Hughes, P. A., Aller, H. D., & Aller, M. F. 1985, ApJ, 298, 301

Hutchings, J. B. 1983, PASP, 95, 799

Hutchings, J. B., & Campbell, B. 1983, Nature, 303, 584

Ishisaki, Y., et al. 1996, PASJ, 48, 237

Jackson, N., & Browne, I. W. A. 1991, MNRAS, 250, 414

Jaroszynski, M., & Kurpiewski, A. 1997, A&A, 326, 419

Jones, T. W., & Hardee, P. E. 1979, ApJ, 228, 268

Jones, T. W., & O'Dell, S. L. 1977, ApJ, 214, 522

Kellermann, K. I., Sramek, R., Schmidt, M., Shaffer, D. B., & Green, R. 1989, AJ, 98, 1195

Kellermann, K. I., Sramek, R. A., Schmidt, M., Green, R. F., & Shaffer, D. B. 1994, AJ, 108, 1163

Kellermann, K. I., Vermeulen, R. C., Zensus, J. A., & Cohen, M. H. 1998, AJ, 115, 1295

Kirhakos, S., Bahcall, J. N., Schneider, D. P., & Kristian, J. 1999, ApJ, 520, 67

Klein, U., Mack, K. H., Strom, R., Wielebinski, R., & Achatz, U. 1994, A&A, 283, 729

Koekemoer, A. M., Henkel, C., Greenhill, L. J., Dey, A., van Breugel, W., Codella, C., & Antonucci, R. 1995, Nature, 378, 697

Köhler, T., Groote, D., Reimers, D., & Wisotzki, L. 1997, A&A, 325, 502

Kollgaard, R. I., Wardle, J. F. C., Roberts, D. H., & Gabuzda, D. C. 1992, AJ, 104, 1687

Kormendy, J., & Richstone, D. 1995, ARA&A, 33, 581

Kraus, A., Witzel, A., Krichbaum, T. P., Lobanov, A. P., Peng, B., & Ros, E. 1999, A&A, 352, L107

Krichbaum, T. 1996, in Science with Large Millimetre Arrays, ESO Astrophysics Symposia (Berlin: Springer), 96

Krichbaum, T., Britzen, S., Standke, K., Witzel, A., Schalinski, C., & Zensus, J. 1995, in Proc. Nat. Acad. Sci., Vol. 92, Quasars and Active Galactic Nuclei: High Resolution Radio Imaging, 11377

Krichbaum, T. P., Graham, D. A., Witzel, A., Greve, A., Wink, J. E., Grewing, M., Colomer, F., de Vicente, P., Gomez-Gonzalez, J., Baudry, A., & Zensus, J. A. 1998, A&A, 335, L106

Krichbaum, T. P., et al. 1993, A&A, 274, L37

Kukula, M. J., Dunlop, J. S., Hughes, D. H., & Rawlings, S. 1998, MNRAS, 297, 366

Kukula, M. J., Pedlar, A., Baum, S. A., & O'Dea, C. P. 1995, MNRAS, 276, 1262

Lasota, J. P., Abramowicz, M. A., Chen, X., Krolik, J., Narayan, R., & Yi, I. 1996, ApJ, 462, 142

Leahy, J. P., Black, A. R. S., Dennett-Thorpe, J., Hardcastle, M. J., Komissarov, S., Perley, R. A., Riley, J. M., & Scheuer, P. A. G. 1997, MNRAS, 291, 20

Leahy, J. P., & Perley, R. A. 1991, AJ, 102, 537

Legg, M. P. C., & Westfold, K. C. 1968, ApJ, 154, 499

Lind, K. R., & Blandford, R. D. 1985, ApJ, 295, 358

Livio, M. 1997, in Accretion Phenomena and Related Outflows; IAU Colloquium 163, ed. D. T. Wickramasinghe, G. V. Bicknell, and L. Ferrario, ASP Conference Series, Vol. 121, 845

Lo, K. Y., Shen, Z. Q., Zhao, J. H., & Ho, P. T. P. 1998, ApJ, 508, L61

Longair, M. 1992, High Energy Astrophysics Vol. I, 2nd edition (Cambridge: Cambridge University Press)

Lüst, R. 1952, Zeitschrift f. Naturf., 7a, 87

Lynden-Bell, D., & Pringle, J. E. 1974, MNRAS, 168, 603

Lynden-Bell, D., & Rees, M. J. 1971, MNRAS, 152, 461

Magorrian, J., Tremaine, S., Richstone, D., Bender, R., Bower, G., Dressler, A., Faber, S. M., Gebhardt, K., Green, R., Grillmair, C., Kormendy, J., & Lauer, T. 1998, AJ, 115, 2285

Mahadevan, R. 1998, Nature, 394, 651

Mannheim, K., & Biermann, P. L. 1992, A&A, 253, L21

Mannheim, K., Schulte, M., & Rachen, J. 1995, A&A, 303, L41

Maoz, D., Filippenko, A. V., Ho, L. C., Macchetto, F. D., Rix, H. W., & Schneider, D. P. 1996, ApJS, 107, 215

Marscher, A. P., & Gear, W. K. 1985, ApJ, 298, 114

Marti, J. M. A., Mueller, E., Font, J. A., Ibanez, J. M. A., & Marquina, A. 1997, ApJ, 479, 151

Mastichiadis, A., & Ozernoy, L. M. 1992, in American Astronomical Society Meeting, Vol. 181, 10904

Melia, F. 1992a, ApJ, 387, L25

Melia, F. 1992b, ApJ, 398, L95

Melia, F. 1994, ApJ, 426, 577

Melia, F., Jokipii, J. R., & Narayanan, A. 1992, ApJ, 395, L87

Menten, K. M., Reid, M. J., Eckart, A., & Genzel, R. 1997, ApJ, 475, L111

Meyer-Hofmeister, E., & Meyer, F. 2000, A&A, in press

Mezger, P. G., Duschl, W. J., & Zylka, R. 1996, A&A Rev., 7, 289

Miller, P., Rawlings, S., & Saunders, R. 1993, MNRAS, 263, 425

Mirabel, I. F., Bandyopadhyay, R., Charles, P. A., Shahbaz, T., & Rodriguez, L. F. 1997, ApJ, 477, L45

Mirabel, I. F., Dhawan, V., Chaty, S., Rodriguez, L. F., Marti, J., Robinson, C. R., Swank, J., & Geballe, T. 1998, A&A, 330, L9

Mirabel, I. F., & Rodriguez, L. F. 1994, Nature, 371, 46

Miyoshi, M., Moran, J., Herrnstein, J., Greenhill, L., Nakai, N., Diamond, P., & Inoue, M. 1995, Nature, 373, 127

Morgan, E. H., Remillard, R. A., & Greiner, J. 1997, ApJ, 482, 993

Morganti, R., Killeen, N. E. B., & Tadhunter, C. N. 1993, MNRAS, 263, 1023

Morris, M., & Serabyn, E. 1996, ARA&A, 34, 645

Nagar, N. M., Falcke, H., Wilson, A. S., & Ho, L. C. 2000, ApJ, submitted

Nagar, N. M., & Wilson, A. S. 1999, ApJ, 516, 97

Napier, P. J., Bagri, D. S., Clark, B., Rogers, A. E. E., Romney, J. D., Thompson, A. R., & Walker, R. C. 1994, in Proc. IEEE, Vol. 82, 658

Narayan, R., Mahadevan, R., Grindlay, J. E., Popham, R. G., & Gammie, C. 1998, ApJ, 492, 554

Narayan, R., & Yi, I. 1994, ApJ, 428, L13

Narayan, R., & Yi, I. 1995a, ApJ, 444, 231

Narayan, R., & Yi, I. 1995b, ApJ, 452, 710

Narayan, R., Yi, I., & Mahadevan, R. 1995, Nature, 374, 623

Narayan, R., Yi, I., & Mahadevan, R. 1996, A&AS, 120, C287

Neufeld, D. A., & Maloney, P. R. 1995, ApJ, 447, L17

Neugebauer, G., Green, R. F., Matthews, K., Schmidt, M., Soifer, B. T., & Bennett, J. 1987, ApJS, 63, 615

O'Connell, R. W., & Dressel, L. L. 1978, Nature, 276, 374

O'Dea, C. P. 1998, PASP, 110, 493

Osterbrock, D. E. 1977, ApJ, 215, 733

Osterbrock, D. E. 1981, ApJ, 249, 462

Owsianik, I., & Conway, J. E. 1998, A&A, 337, 69

Ozernoy, L. 1992, in Testing the AGN Paradigm, AIP Conf. Proc. 254, ed. C. M. U. S. S. Holt, S. G. Neff (New York: AIP), 40

Pacholczyk, A. G. 1977, Radio Galaxies (Oxford: Pergamon)

Perez-Fournon, I., & Biermann, P. 1984, A&A, 130, L13

Perlmutter, S., et al. 1999, ApJ, 517, 565

Pogge, R. W. 1988, ApJ, 332, 702

Pogge, R. W., & de Robertis, M. M. 1995, ApJ, 451, 585

Pomraning, G. C. 1973, The Equations of Radiation Hydrodynamics (Oxford: Pergamon)

Pooley, G. G., & Fender, R. P. 1997, MNRAS, 292, 925

Predehl, P., & Trümper, J. 1994, A&A, 290, L29

Priester, W., Hoell, J., & van de Bruck, C. 1996, in ASP Conf. Ser. 88: Clusters, Lensing, and the Future of the Universe, 286

Ptak, A., Serlemitsos, P., Yaqoob, T., & Mushotzky, R. 1999, ApJS, 120, 179

Rachen, J. P., & Biermann, P. L. 1993, A&A, 272, 161

Ramaty, R. 1969, ApJ, 158, 753

Rawlings, S., & Saunders, R. 1991, Nature, 349, 138

Rees, M. J. 1982, in AIP Conf. Proc. 83: The Galactic Center, 166

Reid, A., Shone, D. L., Akujor, C. E., Browne, I. W. A., Murphy, D. W., Pedelty, J., Rudnick, L., & Walsh, D. 1995, A&AS, 110, 213

Reid, M. J., Readhead, A. C. S., Vermeulen, R. C., & Treuhaft, R. N. 1999, ApJ, 524, 816

Reuter, H. P., & Lesch, H. 1996, A&A, 310, L5

Richstone, D., et al. 1998, Nature, 14

Robertson, D. S. 1991, Reviews of Modern Physics, 63, 899

Rogers, A. E. E., Doeleman, S., Wright, M. C. H., Bower, G. C., Backer, D. C., Padin, S., Philips, J. A., Emerson, D. T., Greenhill, L., Moran, J. M., & Kellermann, K. I. 1994, ApJ, 434, L59

Sanders, R. H. 1983, ApJ, 266, 73

Sault, R. J., & Macquart, J. P. 1999, ApJ, 526, L85

Schlickeiser, R., Campeanu, A., & Lerche, L. 1993, A&A, 276, 614

Schmidt, M. 1963, Nature, 197, 1040

Schmidt, M., & Green, R. F. 1983, ApJ, 269, 352

Schneider, P. 1993, A&A, 278, 315

Seaquist, E. R., Davis, L., & Bignell, R. C. 1978, A&A, 63, 199

Serabyn, E., Carlstrom, J., Lay, O., Lis, D. C., Hunter, T. R., & Lacy, J. H. 1997, ApJ, 490, L77

Serabyn, E., Carlstrom, J. E., & Scoville, N. Z. 1992, ApJ, 401, L87

Shakura, N. I., & Sunyaev, R. A. 1973, A&A, 24, 337

Simpson, C., Wilson, A. S., Bower, G., Heckman, T. M., Krolik, J. H., & Miley, G. K. 1997, ApJ, 474, 121

Slee, O. B., Sadler, E. M., Reynolds, J. E., & Ekers, R. D. 1994, MNRAS, 269, 928

Steiner, J. E. 1981, ApJ, 250, 469

Storchi-Bergmann, T., Mulchaey, J. S., & Wilson, A. S. 1992, ApJ, 395, L73

Strittmatter, P. A., Hill, P., Pauliny-Toth, I. I. K., Steppe, H., & Witzel, A. 1980, A&A, 88, L12

Stüwe, J. A., Schulz, H., & Hühnermann, H. 1992, A&A, 261, 382

Subrahmanyan, R., & Saripalli, L. 1993, MNRAS, 260, 908

Sun, W. H., & Malkan, M. A. 1989, ApJ, 346, 68

Tadhunter, C. N., Morganti, R., di Serego-Alighieri, S., Fosbury, R. A. E., & Danziger, I. J. 1993, MNRAS, 263, 999

Taylor, G. B., & Vermeulen, R. C. 1997, ApJ, 485, L9

Taylor, G. L., Dunlop, J. S., Hughes, D. H., & Robson, E. I. 1996, MNRAS, 283, 930

Terasranta, H., & Valtaoja, E. 1994, A&A, 283, 51

Thompson, A. R., Clark, B. G., Wade, C. M., & Napier, P. J. 1980, ApJS, 44, 151

Trotter, A. S., Greenhill, L. J., Moran, J. M., Reid, M. J., Irwin, J. A., & Lo, K. Y. 1998, ApJ, 495, 740

Turner, J. L., & Ho, P. T. P. 1994, ApJ, 421, 122

Ulvestad, J. S., & Wilson, A. S. 1984, ApJ, 278, 544

Ulvestad, J. S., Wrobel, J. M., Roy, A. L., Wilson, A. S., Falcke, H., Krichbaum, T., Bower, G., & Zensus, A. 1998, in American Astronomical Society Meeting, Vol. 193, 9003

Unger, S. W., Pedlar, A., Axon, D. J., Whittle, M., Meurs, E. J. A., & Ward, M. J. 1987, MNRAS, 228, 671

Urry, C. M., Scarpa, R., O'Dowd, M., Falomo, R., Pesce, J. E., & Treves, A. 2000, ApJ, in press

van Dyk, S. D., & Ho, L. C. 1998, in IAU Symp. 184: The Central Regions of the Galaxy and Galaxies, Vol. 184, 489

van Langevelde, H. J., Frail, D. A., Cordes, J. M., & Diamond, P. J. 1992, ApJ, 396, 686

von Montigny, C., et al. 1995, ApJ, 440, 525

von Weizsäcker, C. F. 1948, Zeitschrift f. Naturf., 3a, 524

Wagner, S. J., & Witzel, A. 1995, ARA&A, 33, 163

Wardle, J. F. C. 1977, Nature, 269, 563

Wardle, J. F. C., Homan, D. C., Ojha, R., & Roberts, D. H. 1998, Nature, 395, 457

Weiler, K. W., & de Pater, I. 1983, ApJS, 52, 293

Whittle, M. 1985, MNRAS, 213, 33

Whittle, M. 1992a, ApJS, 79, 49

Whittle, M. 1992b, ApJ, 387, 109

Whittle, M., Pedlar, A., Meurs, E. J. A., Unger, S. W., Axon, D. J., & Ward, M. J. 1988, ApJ, 326, 125

Wilkes, B. J., Schmidt, G. D., Smith, P. S., Mathur, S., & McLeod, K. K. 1995, ApJ, 455, L13

Wills, B. J., Netzer, H., Brotherton, M. S., Han, M., Wills, D., Baldwin, J. A., Ferland, G. J., & Browne, I. W. A. 1993, ApJ, 410, 534

Wilson, A. S., Braatz, J. A., Heckman, T. M., Krolik, J. H., & Miley, G. K. 1993, ApJ, 419, L61

Wilson, A. S., & Weiler, K. W. 1997, ApJ, 475, 661

Wilson, A. S., & Willis, A. G. 1980, ApJ, 240, 429

Winge, C., Axon, D. J., Macchetto, F. D., & Capetti, A. 1997, ApJ, 487, L121

Wright, M. C. H., & Backer, D. C. 1993, ApJ, 417, 560

Wrobel, J. M., & Heeschen, D. S. 1984, ApJ, 287, 41

Yi, I., & Boughn, S. P. 1998, ApJ, 499, 198

Yusef-Zadeh, F., Cotton, W., Wardle, M., Melia, F., & Roberts, D. A. 1994, ApJ, 434, L63

Yusef-Zadeh, F., & Morris, M. 1987, ApJ, 320, 545

Yusef-Zadeh, F., & Morris, M. 1991, ApJ, 371, L59

Yusef-Zadeh, F., Wardle, M., & Parastaran, P. 1997, ApJ, 475, L119

Zensus, J. A. 1997, ARA&A, 35, 607

Zhao, J., Ekers, R. D., Goss, W. M., Lo, K. Y., & Narayan, R. 1989, in IAU Symp. 136: The Center of the Galaxy, Vol. 136, 535

Zhao, J. H., Goss, W. M., Lo, K. Y., & Ekers, R. D. 1992, in ASP Conf. Ser. 31: Relationships Between Active Galactic Nuclei and Starburst Galaxies, 295

Zweerink, J. A., et al. 1997, ApJ, 490, L141

Zylka, R., Mezger, P. G., & Lesch, H. 1992, A&A, 261, 119

Zylka, R., Mezger, P. G., Ward-Thompson, D., Duschl, W. J., & Lesch, H. 1995, A&A, 297, 83

Danksagungen

Mein ganz besonderer Dank gilt an dieser Stelle meinem Mentor Prof. Peter Biermann. Er hat mir schon früh die notwendige Freiheit und den Ansporn für meine wissenschaftliche Arbeit gegeben und mich immer wieder durch viele Diskussionen, Ratschläge und Ideen begleitet.
Ich danke auch dem Max-Planck-Institut, und insbesondere seinem Direktor Dr. Anton Zensus, für die bereitwillige Unterstützung meiner Arbeit und das hervorragende Arbeitsumfeld.
Von den vielen Kollegen, möchte ich darüberhinaus ganz besonders Prof. F. Melia, Prof. A.S. Wilson, Prof. P.G. Mezger, Prof. K. Menten, Dr. S. Markoff, Dr. G. Bower, Dr. A. Roy, Dr. T. Krichbaum, Dr. A. Lobanov, Dr. E. Agol, Dr. C. Henkel, Dr. A. Patnaik, Prof. Dr. W. Duschl, Dr. R. Zylka, Dr. I. Owsianik, Dr. C. Simpson, Frau G. Pugliese, und Herrn A. Brunthaler hervorheben, von denen ich in intensiven Diskussionen sehr viel gelernt habe.
Schließlich bedanke ich mich bei meiner Familie, insbesondere bei meiner Frau Dagmar und meinen Kindern Jana, Lukas und Niklas für die große Geduld und das Verständnis mir gegenüber, sowie für die fortwährende Erinnerung daran, dass es auch wichtigeres im Leben gibt als die Wissenschaft.

Teile der Arbeit sind bei Aufenthalten an der University of Maryland und der University of Arizona enstanden für deren Gastfreundlichkeit ich mich bedanke.

Viele der gezeigten Beobachtungen sind mit Teleskopen des NRAO[1] und mit dem Hubble-Space-Teleskop[2] gemacht worden.

Diese Arbeit wurde durch ein Habilitationsstipendium und eine Sachbeihilfe der Deutschen Forschungsgemeinschaft (Fa 358/1-1 & 2) unterstützt.

[1] The National Radio Astronomy Observatory is a facility of the National Science Foundation, operated under cooperative agreement by Associated Universities, Inc.

[2] Observations with the NASA/ESA Hubble Space Telescope were obtained at the Space Telescope Science Institute, which is operated by AURA, Inc., under NASA contract NAS 5-26555